UNIVERSITÀ
DI PARMA

Department of Chemistry, Life sciences and Environmental sustainability

Doctoral Programme in Material science and Technology

XXXIII Cycle

Emergence of Chirality in Phenyleneethynylene Based Molecular Assemblies: Experimental and Theoretical Study

Co-ordinator:

Prof. Enrico Dalcanale

Supervisors:

Prof. Cristina Sissa and Prof. K. George Thomas

Ph.D. Student

Swathi

2017-2021

List of Contents

Chapter 1

Supramolecular chirality: An Introduction

1.1 Abstract

A brief description on the concept of chirality both at the molecular and supramolecular level is discussed. An overview of light-matter interaction is presented, including a discussion about chiroptical activity. A section of the chapter indulges in various spectroscopic techniques employed to study chirality in molecular systems. Objectives and scopes of the work are briefly summarized at the end of the chapter.

1.2 Molecular and supramolecular chirality

Chirality is one area which fascinates all branches of science as it exhibits different hierarchical level; from subatomic to molecular to macromolecular and to biological systems. In his Baltimore lectures, Lord Kelvin described any geometrical figure or group of points as chiral if its mirror images are not superimposable on one another.[1] At the molecular level, chirality can be classified into two types: a) point chirality, present in molecule possessing stereocentre; b) axial chirality, present in molecule possessing an axis about which a set of substituents are held in a non-planar arrangement.[2] In both cases, molecules are non-superimposable on their mirror images (Figure 1.1). Chiral molecules are able to rotate the plane of polarised light in a clockwise or anti-clockwise direction (in Section 1.3, an explanation of this phenomenon is briefly introduced). As a result, the isomers are primarily categorized based on the direction to which they rotate the plane of polarised light.[2] If the light is rotated in the clockwise direction, isomers are termed dextrorotatory (+) and those which rotates in the anti-clockwise direction are levorotatory (-) when viewed towards the source.[3] Even though it is possible to recognize one isomer from the other using

A part of the material presented in this chapter is submitted as a tutorial to Chemical Society Reviews and is under revision and acknowledged as Ref. 4

optical rotation, R. S. Cahn, C. K. Ingold, and V. Prelog introduced a reference system allowing the isomers to be identified as *R*- and *S*- forms based on their molecular structure.[3] *R*- or *S*-labels are assigned using two rules: (a) sequence rule and (b) viewing rule.

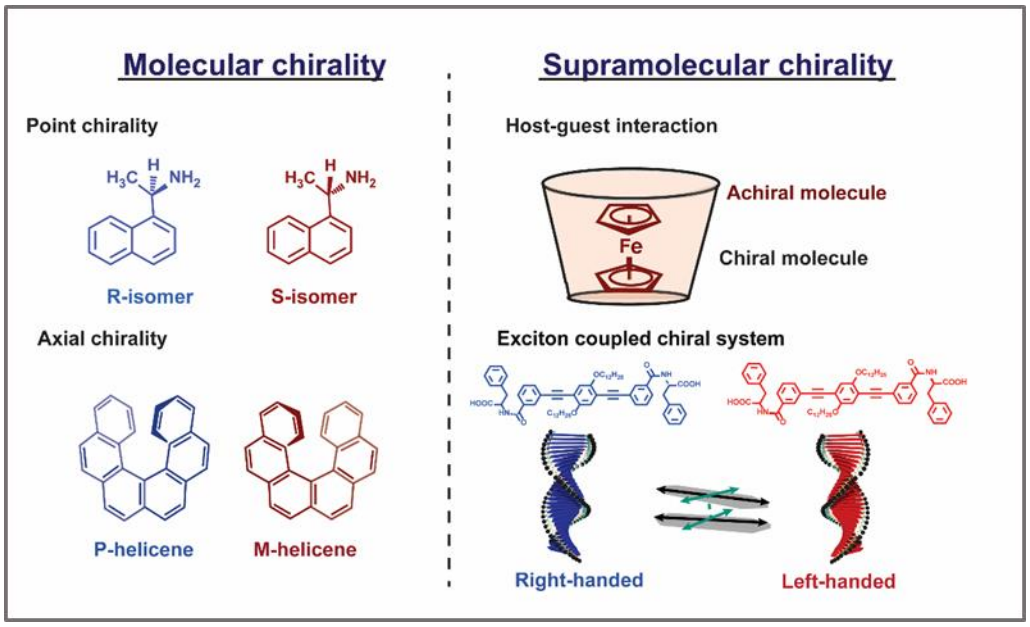

Figure 1.1: *A general description of (a,b) molecular and (c,d) supramolecular chirality.[4] (a,b) Molecular systems showing (a) point chirality: molecule having a stereocentre, represented using R- and S-isomers of 1-(1-naphthyl)ethylamine[5] (b) axial chirality: molecule not having a stereocentre but chirality emerges due to the structure, as in P- and M-helicenes[6] (c,d). Supramolecular chirality arising due to noncovalent interactions: (c) host-guest inclusion complex, represented by ferrocene inside cyclodextrin cavity which shows induced circular dichroism (ICD)[7-8] and (d) self-assembled molecules in a right- and left-handed helix, represented by the helical assemblies of phenylalanine substituted phenyleneethynylene-based molecular systems.[9]*

Sequence rule assigns priorities to the atoms that surrounds the chiral atom. Once the priorities are assigned, the chiral atom needs to be viewed by keeping the lowest priority terminal atom away from the observer. And finally the remaining terminal atoms are traced from higher priority to lower priority, known as the viewing rule. If the tracing constitutes a clockwise rotation, then the enantiomeric molecule is labeled as (*R*), whereas a counterclockwise rotation, indicates the enantiomeric molecule as (*S*). Another method to distinguish between the isomers was assigning a prefix D- or L- to those chemically related to a right-handed or left-handed reference.[3] The D- and

L- designations, referred to as Fischer notation, is based on the arrangement of substituents on the chiral atom of glyceraldehyde. The notation is widely used in labeling carbohydrates and amino acids. In glyceraldehyde, a central carbon atom (or stereocenter) is connected to H, OH, CHO, and CH_2OH groups and can be arranged in two ways as in the Figure 1.2. If in the glyceraldehyde molecule, OH group lies in the right, and H to the left, of the vertical line, then the molecule is labeled as D-glyceraldehyde and in L-glyceraldehyde the H- and OH-group interchanges their position (see Figure 1.2).[3] Here the horizontally aligned bonds are assumed to be pointed above the plane of the paper and that aligned vertically indicates the bonds pointed behind the plane of paper to stereocentre. Further, on viewing the molecule on keeping the H atom pointed away from the observer, the OH, CHO, and CH_2OH groups, represent a clockwise orientation in D-glyceraldehyde and a counterclockwise orientation in L-glyceraldehyde. Configuration of chiral molecules are assigned by comparing their Fischer projection to that of the glyceraldehyde.[3]

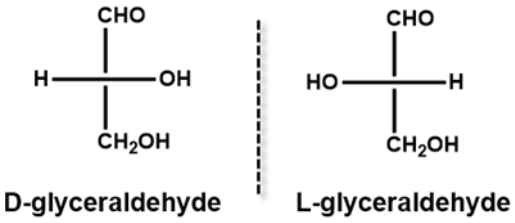

***Figure 1.2**: D/L-glyceraldehyde arranged in Fischer projection.[3]*

In this thesis, attention is primarily focused on supramolecular chiral aggregates. Supramolecular chirality deals with the possibility to form chiral molecular assemblies stitched together by weak noncovalent interactions, thus mimicking nature (Figure 1.1). It is well-known that nature rarely breaks or makes bond for various biological functions, instead rely on the weak and kinetically labile noncovalent interactions.[10] Scientists realized that this strategy is energetically economical, and hence efforts were driven towards understanding of various noncovalent interactions. The higher-order assemblies stitched together using weak noncovalent interactions are called "supermolecules," and the branch of science

dealing with such studies is termed supramolecular chemistry.[11] Compared to monomer, aggregates show non-additive, collective and cooperative properties, making them extremely interesting for different applications.

Supramolecular chiral systems can be classified into two groups: (a) host-guest inclusion complexes where chirality is transferred from one component to the other); and (b) asymmetric arrangement of molecules employing non-covalent interactions to form aggregates (Figure 1.1). In the former case, at least one component (host/guest) should be chiral while in the latter case, it is not necessary that the individual molecule should possess a stereocentre, since helical arrangement of achiral molecules can be achieved by irradiating them with chiral light,[12] using chiral solvent[13] for self assembly, using mechanical methods like vortex-accompanied assembly method[14] etc. The supramolecular organization of molecules results in fascinating dichroic signals such as induced circular dichroism (ICD) and exciton coupled circular dichroism. In the next section, ICD is briefly discussed, while exciton coupled CD is introduced in section 1.4 and is extensively discussed in chapter 2, 3 and 4 for different types of exciton coupled chiral systems.

1.2.1 Induced circular dichroism (ICD) in supramolecular aggregates

Transfer of chirality can occur from non-racemic chiral compound(s) (host; for e.g., cyclodextrin, biomolecular systems, etc.) to achiral molecule(s) (guest; a chromophore) during the molecular or supramolecular organization, as illustrated in Figure 1.3[7-8]. This chirality transfer is observed through the emergence of an exciton coupled CD signal in the spectral region of the absorption of the guest (typically in the visible or near-UV), the phenomenon is termed Induced Circular Dichroism (ICD).[2, 15] The ICD signal emerges mainly due to host-guest interactions resulting in (i) the reduction of the structural symmetry of the achiral guest due to the chiral host in a phenomenon called structurally induced chirality or (ii) the coupling between the transition dipole moments of the host and guest (vide infra) without any major structural perturbation of the guest (Figure 1.3).[7-8] ICD spectra are of great interest,

since they are indicators of the absolute configuration of the chiral component, which is often transparent in the UV-visible region. More importantly, ICD provides information on the relative orientation of the host and guest molecules in the complex.

In ICD, the interacting dipoles correspond to transitions relevant to the host and guest species that typically occur in different spectral regions. Accordingly, the ICD spectrum observed in the spectral region relevant to the guest is not bisignated, but either shows a positive or a negative band. In contrast, in the case of a supramolecular chiral systems where the dipolar coupling between degenerate (or almost so) transitions residing on identical (or very similar) chromophores, the exciton coupling leads to bisignation of the CD band as discussed in detail in Section 1.2.2 and chapter 2 and 4.

A classic example of ICD is the complexation between cyclodextrin (see Figure 1.3A), a host with a specific chirality, and an achiral chromophoric guest, where the dipole-dipole coupling mechanism results in the generation of optical activity for the electronic transitions of the chromophore.[7-8] Here, it is quite evident that the guest molecule does not undergo any structural changes, but an off-resonance coupling between the host and guest leads to the appearance of CD signal. However, at times, structural perturbation of the achiral component is also possible, especially in cases where host is a higher-order molecular systems such as chiral polymers, biomolecules etc.

Linares and co-workers recently reported induction of chirality to an achiral chromophore, 4',6-diamidino-2-phenylindole (DAPI), bound to DNA.[15] The reported study was a curious case as one could see different methods of chirality transfer in the molecular system. With a combination of experimental studies, molecular dynamics simulations and quantum chemical calculations, the authors demonstrated that the ICD of DNA-bound DAPI originates from an intricate interplay between the (i) structurally induced chiral imprint of DNA on DAPI, (ii) off-resonant excitonic

coupling between nucleobases of DNA and DAPI, (iii) charge-transfer and (iv) resonant excitonic coupling between DAPI (Figure. 1.3B).[15]

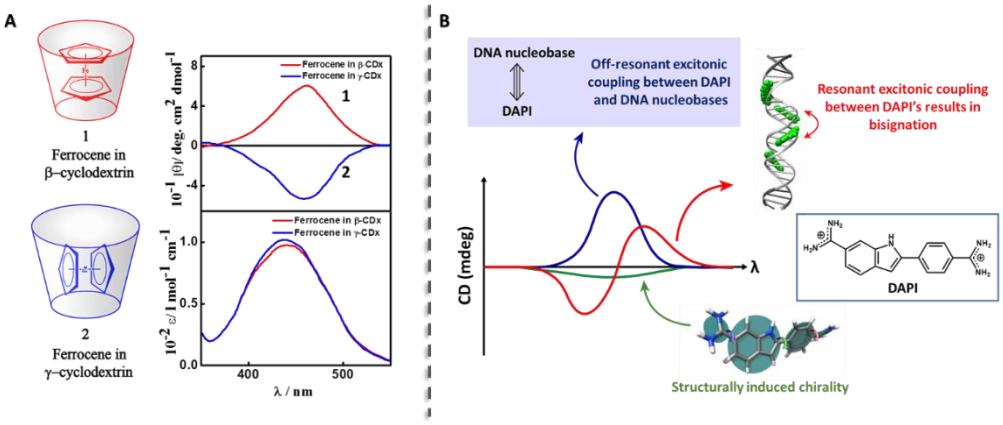

***Figure 1.3**: (A) Inclusion complexes of ferrocene in cyclodextrins and the corresponding induced circular dichroic (ICD) bands showing positive and negative signals.[4] (1) shows the inclusion complex of ferrocene in β- and (2) in γ- cyclodextrin. Absorption and ICD spectra of the complexes are indicated by red trace for complex 1 and blue for complex[7-8] (B) CD spectra of DNA-bound achiral chromophore DAPI with contributions from resonant excitonic coupling between DAPI's resulting in a bisignated CD signal (red trace), off-resonant excitonic coupling between DAPI and DNA nucleobases (blue trace) resulting in a non-bisignated CD signal in the absorption spectral region of DAPI and structurally induced chirality (green trace).[15] Adapted with permission from Ref.[15] Copyright (2017) American Chemical Society.*

1.2.2 Exciton coupled circular dichroism in supramolecular aggregates

Another category of supramolecular chirality (the one we are interested in) originates due to exciton coupling in aggregates. Here the stacking of the molecules due to various non-covalent interactions leads to the coupling of their respective chromophores. As a result, we observe a CD band with cotton effects (bisignated bands) in the chromophoric transition, and the phenomenon is known as exciton coupled circular dichroism.[16] In these systems, CD signals arise from the arrangement of molecules in a chiral fashion. Exciton model developed by Kasha has been extended to chiral systems by Prof. Nakanishi and co-workers to determine the configuration of the molecular assemblies.[17] He observed that if the sign of the CD band in the shorter wavelength region of the exciton coupled CD is positive, molecular assemblies formed

to a right-handed helix (*P*-helix) and if the sign is negative, resulting assembly is left-handed (*M*-helix).[17]

In the literature, many different strategies are reported to obtain exciton coupled chiral aggregates. A classic work from Meijer et al. on optically active poly(3,4-di[(S)-2-methylbutoxy]thiophene) demonstrated that chiral substitution can induce strong chiroptical activity in the π-π* transition of the backbone.[18] However, it is true only in its aggregated state and it is interesting to note that on self-assembly of these chromophoric units conjugated with chiral groups, dichoric behaviour (known as Cotton effects) is dictated by the chiral sense of the substituents. Example for such an instance would be *m*-phenyleneethynylene oligomers containing nonpolar, (S)-3,7-dimethyl-1-octanoxy side chains.[19] On aggregation, the molecule assembled to form left-handed helix alone as evident from the bisignated CD signal.

However, it is not necessary that monomers possess a chiral group: Sang. Y et al used vortex-accompaied assembly method to induce helical arrangement of C_3-symmetric benzene 1,3,5- tricarboxamide molecules with three identical benzoic acid arms (Figure 1.4A).[14] Authors continuously employed vortex mixing during the self-assembly process to create enantiomer-rich assemblies and used the resulting assemblies as seeds for the further induction of chirality in the supramolecular assembly of the achiral molecules. They also co-assembled dyes to these homochiral assemblies to obtain chirality transfer as well.

Another category of chiral supramolecular assembly arises due to co-assembly between more than one molecules in which either one or both the molecules can be c,hiral. An example would be co-assembled aggregation of a chiral rigid molecular linker (1,1′-binaphthyl linked with two imidazolyl ended alkyl chains) and an achiral block copolymer (polystyrene60-block-poly(acrylic acid)120) as in Figure 1.4B[20]. In this case, co-assembly leads to organogel formation due to H-bonding and thus result in cross-linking between the molecular components.[20] In the case of co-assembly, it is again not necessary that we observe a Cotton effects but if the interacting

chromophores have near degenerate energies, it is quite possible to observe an exciton coupled CD.

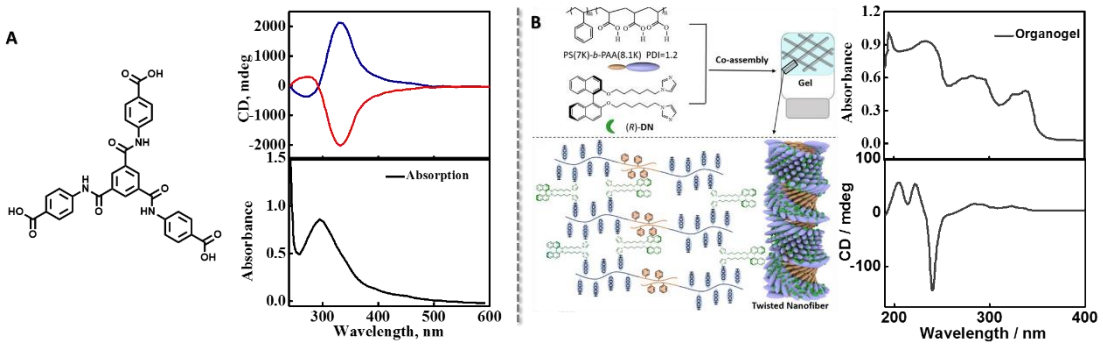

Figure 1.4: *(A) Shows the absorption and CD spectra of the supramolecular chiral assembly formed by the 1,3,5- tricarboxamide molecules after VAA treatment; Reproduced from Ref.*[14] *with permission from the Royal Society of Chemistry. (B) Shows the CD and absorption spectra of a chiral co-assembled assembly by a chiral rigid molecular linker (1,1'-binaphthyl linked with two imidazolyl ended alkyl chains) and an achiral block copolymer (polystyrene60-block-poly(acrylic acid)120). Schematic representation of the hierarchical suprastructure of the twisted nanofibers with a chirality transfer embedded phase segregation is also provided. Adapted with permission from Ref.*[20] *Copyright (2019) American Chemical Society.*

Chiral supramolecular co-assembly not only occurs between organic components but also occurs between organic and inorganic components. For example, chirality is induced in an inorganic nanostructures like quantum dots, nanoparticle etc. by incorporating them onto chiral organic assemblies. One example was reported from our group where we initially synthesized and self-assembled D/L-alanine substituted phenyleneethynylene molecule to form chiral assemblies. Further, gold nanoparticles were grown on these assemblies and the organic assemblies being susceptible to temperature, are destroyed at high temperature: chiral assemblies of gold nanoparticle were obtained, showing an intense CD response in the nanoparticle transition region.[21]

1.3 Light-matter interaction and chiroptical activity: an overview

Interaction of matter with light in a spectral window ranging from microwave to UV is at the heart of various optical spectroscopic methods employed to investigate the structure and properties of matter. The wavelength of light is orders of magnitude

larger than the molecular dimensions, which makes the electric dipole approximation reliable.[22] According to the electric dipole approximation, the oscillating electric field of electromagnetic radiation is responsible for oscillations of the electrons in the molecules and materials. Energy exchange between light and matter is only possible when the frequency of the oscillating field (ω) is close to a transition frequency of the system (ω_{eg}):

$$\omega \simeq \omega_{eg} = (E_e - E_g)/\hbar \qquad (1.1)$$

where E_e and E_g are the energies of the excited *e* state, and the ground *g* state of the molecule, respectively. Under resonance conditions, an absorption band appears in the spectrum. The area under the absorption band defines the intensity of the transition, and is proportional to the oscillator strength, f_{eg} given by:[23]

$$f_{eg} = \frac{2m}{3\hbar e^2}\omega_{eg}\left|\mu_{eg}\right|^2 = \frac{2m}{3\hbar e^2}\omega_{eg}\langle g|\hat{\mu}|e\rangle \cdot \langle e|\hat{\mu}|g\rangle \qquad (1.2)$$

where $\hat{\mu}$ is the dipole moment operator, a vector operator having three components, $\hat{\mu}_x, \hat{\mu}_y, \hat{\mu}_z$, and the dot indicates the scalar product. The transition dipole moment $\langle e|\hat{\mu}|g\rangle$ is a vector whose amplitude is indicated as μ_{eg}. In the prefactor, *m* and *e* are the electron mass and charge, respectively. The oscillator strength is a dimensionless quantity, and is equal to 1 for an elastically bound electron. Under non-resonant conditions ($\omega \neq \omega_{eg}$), energy between light and matter cannot be exchanged and hence the light is not absorbed by the molecule/material. However, the velocity of the transmitted light is slowed down to $c/n(\omega)$, where c is the light velocity in vacuum and $n(\omega)$ is the frequency-dependent refractive index of the medium.

Electromagnetic radiation has an electric and magnetic component which is perpendicular to each other and to the propagation of light. Non-polarized light has electric and magnetic vectors in all directions. However, it is possible to restrict the electric and magnetic vector of light in one direction; such a light is known as plane polarised light. In an isotropic medium, specifically in solution, where the solute molecules are randomly oriented, the induced molecular dipoles can sum up in a non-

vanishing response only along the direction defined by the driving electric field. However, chemists know very well that an aqueous solution of sugar, i.e., an isotropic solution of chiral molecules, rotates the polarization direction of linearly polarized light. Consider a typical experiment as shown in Figure 1.5a, where linearly polarized light propagates along the z-direction with the electric field polarized along the x-direction. On travelling through the sugar solution, a rotation by an angle δ is observed in the polarization direction of light, pointing to the emergence of a component of the oscillating electric field in the y-direction (Figure. 1.5c). However, in an isotropic medium, the driving electric field oscillating along x cannot induce a dipole along y.

To understand this issue, we should consider the nature of light in more detail. Linearly polarized light, propagating along the z-direction, not only has an electric field oscillating along x, but also a magnetic field oscillating along y (Figure 1.5a). The rotation of the polarization of light in a solution of chiral molecules can then be explained if the oscillating magnetic field is able to generate oscillating electric dipoles along the same direction. Such a mixed response, i.e., the electric oscillating dipole generated by the magnetic field of the incident radiation (Figure 1.5c), requires non-vanishing rotational strengths (R_{eg}):[23-24]

$$R_{eg} = Im(\langle g|\hat{\mu}|e\rangle \cdot \langle e|\hat{m}|g\rangle) \qquad (1.3)$$

where, $\hat{m}$ is the magnetic dipole operator (again a vectorial quantity) and *Im* amounts to the imaginary part of the complex number in parenthesis. To have a non-vanishing rotational strength, at least one of the product $\langle g|\hat{\mu}_a|e\rangle\langle e|\hat{m}_a|g\rangle$, with *a=x, y or z*, must be different from zero, or, in other terms, both $\langle g|\hat{\mu}_a|e\rangle$ and $\langle e|\hat{m}_a|g\rangle$ must be different from zero along the same direction. Accordingly, for at least one direction (x, y, or z), the components of the electric and magnetic dipoles must transform as the same irreducible representation in the molecular symmetry group. However, the electric and magnetic dipoles have different symmetry properties with respect to reflection planes (see Figure 1.6). The electric dipole is related to the position of charges, it is a

true vector that changes sign upon reflection on a plane perpendicular to the vector (horizontal mirror) and is invariant upon reflections on a plane parallel to the dipole (longitudinal mirror).

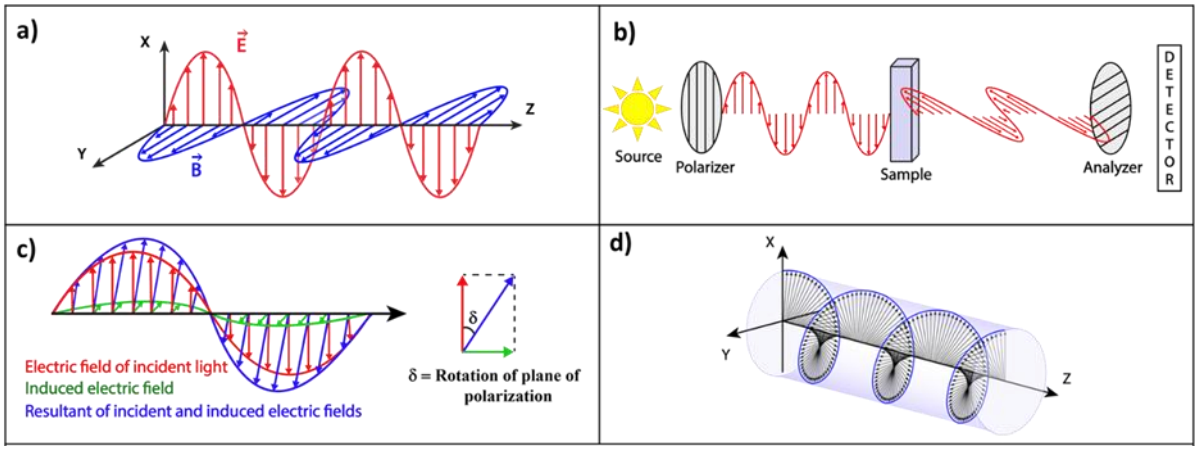

Figure 1.5: *(a) Linearly polarized light having its electric (red) and magnetic (blue) vectors, orthogonal to each other (electric field polarized along x-axis). (b) Optical rotatory dispersion (ORD) experiment: the plane of the polarization of the incident light is rotated in a chiral medium. (c) Rotation of polarization plane in an ORD experiment illustrating the electric field of the incident linearly polarized light (red), the electric field induced by the magnetic field (green) in a chiral medium, and the resultant field (blue). (d) Circularly polarized light: a combination of two linearly polarized light beams (with the same amplitude), with orthogonal polarization and a phase difference of* $\pi/2$.[4]

The magnetic dipole, instead is related to the rotation of charges, it is a pseudovector and does not change sign upon reflection on a horizontal mirror, while it is inverted upon reflection on a longitudinal mirror. Therefore, finite rotational strengths (see Equation. 1.3), and hence the chiral behaviour, are only observed in molecules whose symmetry group does not contain any improper axis of rotation (that includes reflection planes and inversion centres), thus giving a strict, symmetry-based definition of chiral systems.[24]

The intensity of each transition in absorption and CD spectra is proportional to the oscillator strength (Equation 1.2) and to the rotational strength (Equation 1.3), respectively. Of course, signals observed in the absorption spectra are always positive, while CD signals can be positive or negative depending on the sign of the rotational strength. Finally, we observe that accounting for the magnetic field, as needed to

explain chiral effects, requires relaxing the electric dipole (or long-wavelength) approximation that works very well to describe light-matter interaction. Accordingly, chiral spectroscopies typically deal with small responses and are characterized by low sensitivity.

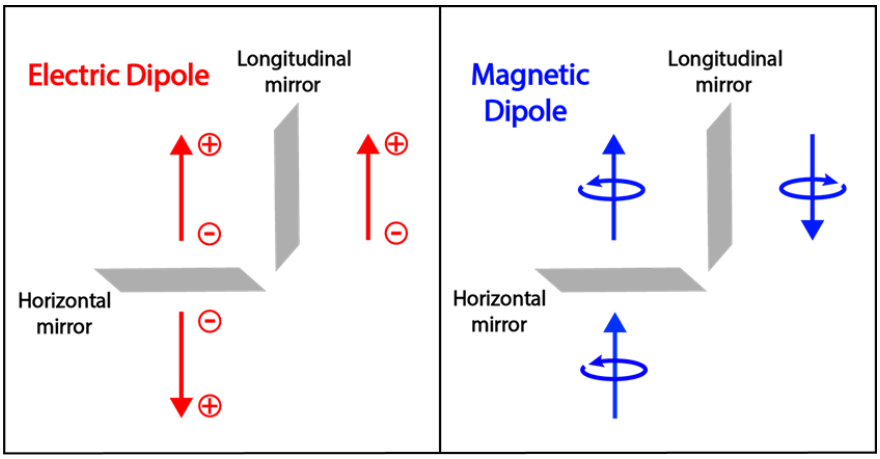

Figure 1.6: *Left panel: the electric dipole is related to the position of positive and negative charges. It is invariant for a reflection on a longitudinal mirror (parallel to the dipole) and changes sign for reflection on a horizontal mirror (perpendicular to the dipole). Right panel: a magnetic dipole is generated by a rotating charge and its sign is defined based on the right-hand rule. Since the rotation direction is reverted upon reflection on a vertical mirror, the magnetic dipole changes its sign upon vertical reflection. On the opposite, the reflection on the horizontal mirror leaves the rotation unaffected and the magnetic dipole is invariant for horizontal reflection.*[4]

1.4 Chiroptical spectroscopic techniques

Several spectroscopic techniques are available to investigate chiroptical properties that exploits the different behaviour of chiral systems interacting with the polarized light. Optical rotatory dispersion (ORD) and electronic circular dichroism (ECD) are the most commonly used spectroscopic methods to probe chiroptical responses. ORD measures the difference between the medium refractive index for left and right circularly polarized light,[7] whereas ECD, reports the difference between extinction coefficients for left and right circularly polarized light.[25] The two measurements are related much in the same way as the refractive index and the extinction coefficient are connected by Kramers-Kröning relation.[26]

An excited molecule can relax to the ground state by emitting light in a process called luminescence. In analogy with ECD spectra, circularly polarized luminescence (CPL) measures the difference between the intensity of the emitted left- and right-circularly polarized light $(I_L\text{-}I_R)$.[27] Two other popular spectroscopic techniques available to analyse the vibrational fingerprints are vibrational circular dichroism (VCD) and Raman optical activity (ROA).[3]

In the next two subsections details are provided for ECD and CPL, the two spectroscopic techniques that were exploited during the thesis work to investigate supramolecular chiral aggregates.

1.4.1 Electronic circular dichroism

ECD measures the differential absorption of left- and right-circularly polarised light. A chiral medium, exposed to a linearly polarised light (resultant of right- and left polarised light with same magnitude), preferentially absorb either left- or right-polarized light more, as a result the light coming out will be elliptically polarised. ECD measures the ellipticity as a function of wavelength. ECD obeys Beer-Lambert law and its chiral absorption is defined as:[7, 25]

$$\Delta A = (\varepsilon_L - \varepsilon_R).c.l, \qquad (1.4)$$

where, ΔA is differential absorption, ε_L and ε_R are the molar extinction coefficient for left- and right-polarized light respectively, c is the concentration of chiral solution and l is the path length of the solution. The instrument measures the ellipticity of the polarized light which is related to the differential absorption and ellipticity (θ; measured in mdeg) by the equation below:[7]

$$\theta = 33000 \times \Delta A, \qquad (1.5)$$

The ECD spectrum for enantiomers of a molecule is always opposite and together they give a mirror image CD spectra. The important parameter in the chiroptical

spectroscopy is g-factor or dissymmetry factor (g_{abs}). For a chiral absorption, g-factor is defined as given below:[2]

$$g_{abs} = \frac{2\Delta A}{A}, \qquad (1.6)$$

where A is the corresponding conventional absorbance for the molecular system. It is important to note that the dissymmetry factor is independent of concentration. The value for g_{abs} usually varies from +2 to -2.

In an ECD spectroscopic instrument, excitation source is an unpolarised light made into a linearly polarised with the help of a linear polarizer. Monochromator regulates the wavelength of the light source. Further, the linearly polarised light pass through a photoelastic modulator (PEM) which converts it into their components: right- and left- polarised light. Thus the chiral media is exposed to a circularly polarised light. The transmitted elliptically polarised light now falls on to a detector, usually a photo multiplier tube to record the spectrum (see Figure 1.7).

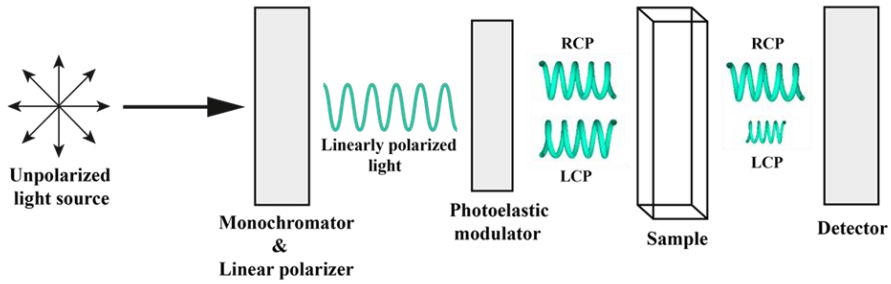

***Figure 1.7**: Shows schematic representation of an electronic circular dichroism spectrometer.*[4]

1.4.2 Circularly polarised luminescence

CPL spectroscopy measures the chiral emission and is defined as the differential emission intensities of left- and right-circularly polarised light. Since the chiral media preferentially absorbs one among the right- or left-polarised light, it is typical that the resulting emission also has a preference for the polarised light. The CPL spectrum gives differential emission intensity as a function of wavelength, where differential emission (ΔI) is defined as:[28]

$$\Delta I = (I_L - I_R), \qquad (1.7)$$

where I_L and I_R are the intensities of the emitted left- and right-polarised light, respectively. The dissymmetry factor in CPL is defined as:[28-29]

$$g_{lum} = \frac{2\Delta I}{I}, \qquad (1.8)$$

where I is the corresponding conventional emission from the same molecular system. Here again the emission dissymmetry factor is independent of concentration and its value usually ranges from -2 to +2. Organic system gives reasonable CPL signal, with a dissymmetry factor ~ 10^{-5} - 10^{-3}.[30]

In a CPL spectrometer on the contrary, chiral media is exposed to an unpolarised light after passing through a monochromator. This is to prevent any stray light from falling on the detector. The emitted elliptically polarised light passes through a PEM and linear polariser to separate the elliptically polarised light into right- and left-polarised light. And finally the detector measures the signal to give the CPL spectrum. Detector in a CPL instrument can also be kept at 90° as well, but at 180° one gets more accurate spectra devoid of birefringence artefacts.[30]

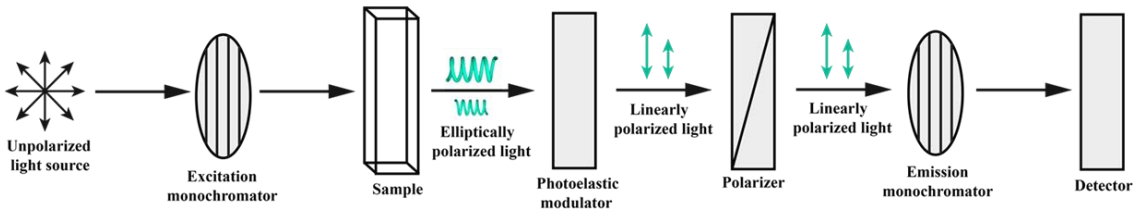

Figure 1.8: *Shows schematic representation of a circularly polarised luminescence (CPL) spectrometer.*[4]

1.5 Scope and applications

Chiral chemical synthesis demands enantiomeric purity, necessitating the development of facile and efficient methods to separate and recognize one form from the other. For example, studies reveals that almost 60% of drugs and 40% of agrochemicals are chiral.[31] Chiral recognition and chiral sensing applications gain

importance in this context, and chiral aggregates become handy in this regard. Among the many spectroscopic techniques reported for high throughput discovery of chiral chemicals for enantiomeric excess, fluorescent based probes were exceptional, especially chiral AIEgens (aggregate induced emission).[32]

Sensors based on Organic Field-Effect Transistors (OFET) are a good example for the industrial application of chiral assemblies. OFET forms the major component of organic integrated circuit and the interest in such materials is due to their low-cost and high tunability for various sensing applications like chemical, biological, temperature, etc. Chiral discrimination is among the area where OFET is reported to be successfully employed. Sun. Y et al recently reported the composition dependent chiral discrimination of D/L-phenylalanine using β-CD sensitized copper hexadecafluorophthalocyanine semiconductive layer as the sensing unit.[33] Yang. Y et al used OFET based on (+)-1-aza[6]helicene and its enantiomer to selectively dictate the right-handed and left-handed light respectively.[34]

'Supramolecular chirogenesis' is another field which is gaining a lot of interest in recent times due to promising applications: (i) catalytic asymmetric synthesis (ii) molecular recognition at nanoscale-level resulting in the formation of intelligent or responsive materials.[35] Generation of chiral sense by means of chirogenesis denotes the chirality transfer to achiral, synthetic molecules by bringing a conformational change in them as a result of an external stimulus like light, pH or additives.[36] Supramolecular interactions are often employed for this purpose thereby mimicking the nature's way of utilizing weak interactions.

Further, chiral emitting supramolecular structures find themselves adept at applications like 3-D display,[37] biological imaging,[38] molecular switch,[39] information storage[40] etc. resulting in the emergence of chiral photonics.[41] So it's very clear that applications of chiral molecules especially chiral assemblies are everlasting and the field remains as active as ever.[42-43] Hence it is essential to understand the underlying principles behind chirality transfer from molecular level to microscopic level. Also

knowledge on the criteria to chirally perturb the chromophoric systems are necessary for the further development of chiral materials for the applications listed above.

1.6 Objective of the thesis

Emergence of chiroptical properties in organic assembled systems, especially the role of transition dipoles of chromophores in dictating the chiral response is not well-explored. The over-all objective of the thesis is to carry out an experimental and theoretical investigation on the nature of chiral response from various phenyleneethynylene based chiral systems. The thesis also aims to explore the role of transition dipole moment in determining the optical and chiral signal exhibited by the molecular assemblies.

In chapter 2, the synthesis of a series of phenyleneethynylene (PE) molecules having linear, bent and tripod shaped geometry, both chiral (attaching phenylalanine) and achiral forms is reported. The investigation of their optical properties in monomeric state is carried out by employing various spectroscopic techniques as well as TD-DFT calculations with the help of achiral PE derivatives. Further studies on their aggregation behaviour is explored using the chiral phenyleneethynylene derivatives. Chapter 3 critically discuss the exciton chirality rule, which is commonly adopted to assign the helicity of supramolecular aggregates based on the sign of ECD spectra. Chapter 4 is focussed on the investigation of the chiroptical response from molecular assemblies of linear phenyleneethynylenes, bearing different sidechains. Here again, the investigation of the aggregation behaviour as well as the resulting chiral response is accomplished with the help of spectroscopic techniques and theoretically using exciton model.

References

1. Barron, L. D., Compliments from Lord Kelvin. *Nature* **2007,** *446* (7135), 505-506.
2. Liu, M.; Zhang, L.; Wang, T., Supramolecular Chirality in Self-Assembled Systems. *Chem. Rev.* **2015,** *115* (15), 7304-7397.

3. Polavarapu, P. L., *Chiroptical spectroscopy: fundamentals and applications*. Crc Press: 2016.
4. Shahana Nizar, N. S. S., M; Swathi, K.; Cissa, C.; Painelli, A.; Thomas, K. G., Emergent chiroptical properties in supramolecular and plasmonic assemblies. *Chem. Soc. Rev* **2021**.
5. Plusquellic, D. F.; Lavrich, R. J.; Petralli-Mallow, T.; Davis, S.; Korter, T. M.; Suenram, R. D., High resolution spectroscopic studies of 1-(1-naphthyl)ethylamine in S0 and S1: exploring the dependence of circular dichroism on conformational structure. *Chem. Phys.* **2002,** *283* (1), 355-370.
6. Nakai, Y.; Mori, T.; Inoue, Y., Theoretical and Experimental Studies on Circular Dichroism of Carbo[n]helicenes. *J. Phys. Chem. A* **2012,** *116* (27), 7372-7385.
7. Chapter 1 Theory of Optical Spectroscopy. In *Circular Dichroism and Magnetic Circular Dichroism Spectroscopy for Organic Chemists*, The Royal Society of Chemistry: 2012; pp 1-41.
8. Kobayashi, N.; Opallo, M., Disposition of ferrocenes in β- or γ-cyclodextrin. *J. Chem. Soc., Chem. Commun.* **1990,** (6), 477-479.
9. Kar, S.; Swathi, K.; Sissa, C.; Painelli, A.; Thomas, K. G., Emergence of Chiroptical Properties in Molecular Assemblies of Phenyleneethynylenes: The Role of Quasi-degenerate Excitations. *J. Phys. Chem. Lett.* **2018,** *9* (16), 4584-4590.
10. Desiraju, G. R., Chemistry beyond the molecule. *Nature* **2001,** *412* (6845), 397-400.
11. Lehn, J.-M., Toward Self-Organization and Complex Matter. *Science* **2002,** *295* (5564), 2400.
12. Castriciano, M. A.; Gentili, D.; Romeo, A.; Cavallini, M.; Scolaro, L. M., Spatial control of chirality in supramolecular aggregates. *Scientific Reports* **2017,** *7*, 44094.
13. Kawagoe, Y.; Fujiki, M.; Nakano, Y., Limonene magic: noncovalent molecular chirality transfer leading to ambidextrous circularly polarised luminescent [small pi]-conjugated polymers. *New Journal of Chemistry* **2010,** *34* (4), 637-647.
14. Sang, Y.; Yang, D.; Duan, P.; Liu, M., Towards homochiral supramolecular entities from achiral molecules by vortex mixing-accompanied self-assembly. *Chem. Sci.* **2019,** *10* (9), 2718-2724.
15. Holmgaard List, N.; Knoops, J.; Rubio-Magnieto, J.; Idé, J.; Beljonne, D.; Norman, P.; Surin, M.; Linares, M., Origin of DNA-Induced Circular Dichroism in a Minor-Groove Binder. *J. Am. Chem. Soc.* **2017,** *139* (42), 14947-14953.
16. Thomas, R.; Kumar, J.; George, J.; Shanthil, M.; Naidu, G. N.; Swathi, R. S.; Thomas, K. G., Coupling of Elementary Electronic Excitations: Drawing Parallels Between Excitons and Plasmons. *J. Phys. Chem. Lett.* **2018,** *9* (4), 919-932.
17. Harada, N.; Nakanishi, K.; Berova, N., Electronic CD Exciton Chirality Method: Principles and Applications. In *Comprehensive Chiroptical Spectroscopy*, 2012; pp 115-166.

18. Langeveld-Voss, B. M. W.; Janssen, R. A. J.; Christiaans, M. P. T.; Meskers, S. C. J.; Dekkers, H. P. J. M.; Meijer, E. W., Circular Dichroism and Circular Polarization of Photoluminescence of Highly Ordered Poly{3,4-di[(S)-2-methylbutoxy]thiophene}. *J. Am. Chem. Soc.* **1996,** *118* (20), 4908-4909.
19. Brunsveld, L.; Prince, R. B.; Meijer, E. W.; Moore, J. S., Conformational Ordering of Apolar, Chiral m-Phenylene Ethynylene Oligomers. *Organic Letters* **2000,** *2* (11), 1525-1528.
20. Yue, B.; Yin, L.; Zhao, W.; Jia, X.; Zhu, M.; Wu, B.; Wu, S.; Zhu, L., Chirality Transfer in Coassembled Organogels Enabling Wide-Range Naked-Eye Enantiodifferentiation. *ACS Nano* **2019,** *13* (11), 12438-12444.
21. George, J.; Kar, S.; Anupriya, E. S.; Somasundaran, S. M.; Das, A. D.; Sissa, C.; Painelli, A.; Thomas, K. G., Chiral Plasmons: Au Nanoparticle Assemblies on Thermoresponsive Organic Templates. *ACS Nano* **2019,** *13* (4), 4392-4401.
22. Schatz, G. C.; Ratner, M. A., *Quantum mechanics in chemistry*. Courier Corporation: 2002.
23. Craig, D. P.; Thirunamachandran, T., *Molecular quantum electrodynamics: an introduction to radiation-molecule interactions*. Courier Corporation: 1998.
24. Condon, E. U., Theories of optical rotatory power. In *Selected Scientific Papers of EU Condon*, Springer: 1991; pp 306-348.
25. Berova, N.; Bari, L. D.; Pescitelli, G., Application of electronic circular dichroism in configurational and conformational analysis of organic compounds. *Chemical Society Reviews* **2007,** *36* (6), 914-931.
26. Moscowitz, A., Theoretical Aspects of Optical Activity Part One: Small Molecules. In *Adv. Chem. Phys.*, 1962; pp 67-112.
27. Brittain, H. G., TECHNIQUES OF CHIROPTICAL SPECTROSCOPY. *Applied Spectroscopy Reviews* **2000,** *35* (3), 175-201.
28. Muller, G., Circularly Polarised Luminescence. In *Luminescence of Lanthanide Ions in Coordination Compounds and Nanomaterials*, 2014; pp 77-124.
29. Nagata, Y.; Mori, T., Irreverent Nature of Dissymmetry Factor and Quantum Yield in Circularly Polarized Luminescence of Small Organic Molecules. *Front. Chem.* **2020,** *8* (448).
30. Blok, P. M. L.; Dekkers, H. P. J. M., Measurement of the Circular Polarization of the Luminescence of Photoselected Samples Under Artifact-Free Conditions. *Appl. Spectrosc.* **1990,** *44* (2), 305-309.
31. Nguyen, L. A.; He, H.; Pham-Huy, C., Chiral drugs: an overview. *Int J Biomed Sci* **2006,** *2* (2), 85-100.
32. Hu, M.; Yuan, Y.-X.; Wang, W.; Li, D.-M.; Zhang, H.-C.; Wu, B.-X.; Liu, M.; Zheng, Y.-S., Chiral recognition and enantiomer excess determination based on emission wavelength change of AIEgen rotor. *Nat. Commun.* **2020,** *11* (1), 161.
33. Sun, Y.; Wang, Y.; Wu, Y.; Wang, X.; Li, X.; Wang, S.; Xiao, Y., A Chiral Organic Field-Effect Transistor with a Cyclodextrin Modulated Copper Hexadecafluorophthalocyanine Semiconductive Layer as the Sensing Unit. *Anal. Chem.* **2018,** *90* (15), 9264-9271.

34. Yang, Y.; da Costa, R. C.; Fuchter, M. J.; Campbell, A. J., Circularly polarized light detection by a chiral organic semiconductor transistor. *Nature Photon* **2013,** *7* (8), 634-638.
35. Escárcega-Bobadilla, M. V.; Kleij, A. W., Artificial chirogenesis: a gateway to new opportunities in material science and catalysis. *Chem. Sci.* **2012,** *3* (8), 2421-2428.
36. Hembury, G. A.; Borovkov, V. V.; Inoue, Y., Chirality-Sensing Supramolecular Systems. *Chem. Rev.* **2008,** *108* (1), 1-73.
37. Schadt, M., Liquid crystal materials and liquid crystal displays. *Annu. Rev. Mater. Sci.* **1997,** *27* (1), 305-379.
38. Chen, Y.; Gao, J.; Yang, X., Chiral Grayscale Imaging with Plasmonic Metasurfaces of Stepped Nanoapertures. *Adv. Opt. Mater.* **2019,** *7* (6), 1801467.
39. Browne, W. R.; Feringa, B. L., Chiroptical Molecular Switches. In *Molecular Switches*, 2011; pp 121-179.
40. Dor, O. B.; Yochelis, S.; Mathew, S. P.; Naaman, R.; Paltiel, Y., A chiral-based magnetic memory device without a permanent magnet. *Nat. Commun.* **2013,** *4* (1), 2256.
41. Nowacki, B.; Oh, H.; Zanlorenzi, C.; Jee, H.; Baev, A.; Prasad, P. N.; Akcelrud, L., Design and Synthesis of Polymers for Chiral Photonics. *Macromolecules* **2013,** *46* (18), 7158-7165.
42. Brandt, J. R.; Salerno, F.; Fuchter, M. J., The added value of small-molecule chirality in technological applications. *Nature Reviews Chemistry* **2017,** *1* (6), 0045.
43. Long, G.; Sabatini, R.; Saidaminov, M. I.; Lakhwani, G.; Rasmita, A.; Liu, X.; Sargent, E. H.; Gao, W., Chiral-perovskite optoelectronics. *Nat. Rev. Mater.* **2020,** *5* (6), 423-439.

Chapter 2

Effect of geometry on the photophysical and chiroptical properties of phenyleneethynylene derivatives

2.1 Abstract

Photophysics of phenyleneethynylene derivatives have always been an intense area of research due to their unique optical and electronic properties and rigid structure making them a versatile candidate for various application. Herein we synthesized three types of phenyleneethynylene derivatives with linear, bent and tripod geometries and performed fluorescence anisotropy measurements to investigate the influence of symmetry on their photophysical properties. Joint experimental and theoretical (TD-DFT) investigations validate a symmetry breaking phenomena in phenyleneethynylene derivatives with bent and tripod geometries, thus indicating strongly influences of geometry on the photophysical properties. Moreover, the phenyleneethynylene core when substituted with phenylalanine, a chiral pendant, induces the formation of chiral aggregates upon self-assembly. These results corroborate that the formation of chiral assemblies is heavily influenced by the geometry of the molecules and the presence of a chiral group does not always guarantee a chiral assembly.

2.2 Introduction

Phenyleneethynylenes are a class of compound comprising alternating benzene and triple bonds thus providing the molecule with rigidity and possible electric conductivity.[1-2] As a result, these compounds are extensively studied since decades, probing them in applications such as conducting wires,[3] sensors,[4] optoelectronics[2] etc. The Sonogashira cross-coupling enabled the efficient and easy synthesis of these compounds and the prospect to perform functionalization with

different substitutions attracts the interest for this class of molecules.[5] Being a π-conjugated system, it possesses a rigid structure and interesting photophysical properties which can be further improved using hydroxyl, amino, carboxyl groups, etc. as substituents. Advantage of such substitution is that it can promote supramolecular assemblies using the weak van der Waals interactions and H-bonding.[6-7] Phenyleneethynylenes can also be attached with chiral pendants to arrange the molecule in helical fashion on self-assembly. Such chiral assemblies always brought about strong chiroptical activities in the π-π* transition of the phenyleneethynylene chromophore.[7-9]

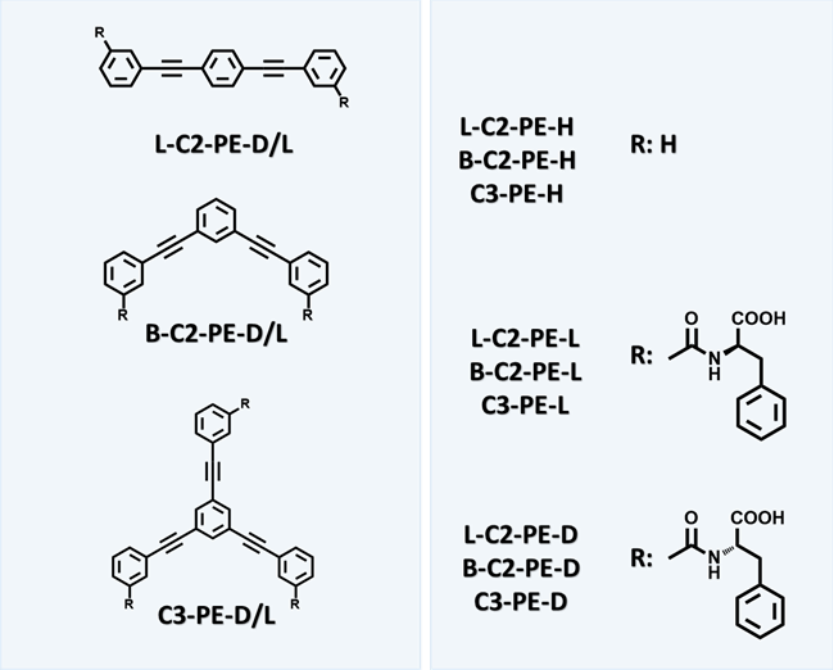

Chart 2.1*: Schematic representation of the molecule of interest. In the case of achiral molecules, R is H while in the case of chiral molecules D and L-isomers of phenylalanine is attached to the core phenyleneethynylene chromophoric unit.*

The objective of this work is to understand the extent to which geometries of the molecule influences their photophysical properties. Hence, three types of phenyleneethynylene derivatives having different geometries i.e. linear, bent and tripod shape (named as **L-C2-PE-H**, **B-C2-PE-H**, and **C3-PE-H**, Chart 2.1) are synthesized**.** Theoretical calculations (DFT and TD-DFT) are performed to understand the photophysical properties exhibited by the molecular systems in its monomeric

form. Chiral variants (named as **L-C2-PE-D/L**, **B-C2-PE-D/L**, and **C3-PE-D/L** respectively) of the derivatives were also synthesized by replacing the *meta-* H- of the terminal benzene group in the latter with D/L- isomers of phenylalanine in the case of chiral derivatives (Chart 2.1). Phenylalanine was chosen as chiral pendant due to the expertise of the host laboratory acquired in the past years with this chiral derivative.[10] Chiral variant of the molecules are synthesized to investigate the self-assembly of the molecules and to understand their chiroptical properties.

Phenyleneethynylene derivatives are synthesized using palladium catalysed Heck-Cassar-Sonogashira-Hagihara cross-coupling reaction.[11] For the achiral molecules, phenylacetylene is coupled to halogenated benzene molecules to obtain the corresponding phenyleneethynylene derivatives using $Pd(PPh_3)_2Cl_2$ and CuI. Phenylalanine is substituted to the 3-iodobenzoic acid via amide coupling[12] using EDC/HOBT as shown in Chart 2.2. Consequently, the coupling of the phenylalanine substituted iodobenzene with corresponding di/triethynylbenzene using $Pd(PPh_3)_2Cl_2$ and CuI gives the corresponding chiral derivatives. Scheme 2.1-2.5 shows the detailed synthesis methodology adopted for the synthesis of the molecules of interest.

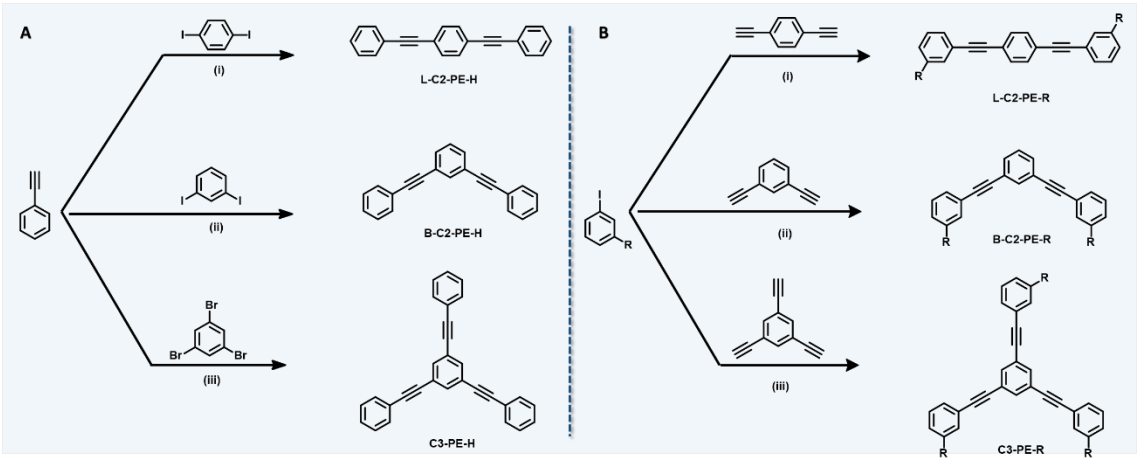

Chart 2.2: *Presented a generalized scheme for the synthesis of chiral and achiral phenyleneethynylene derivatives. (i) and (ii) $Pd(PPh_3)_2Cl_2$, CuI, trimethylamine; (iii) $Pd(PPh_3)_2Cl_2$, CuI, trimethylamine, 60 °C.*

2.3 Photophysical properties of achiral PE derivatives

Detailed synthesis procedure adopted for all the molecules are given in the section 2.6.

The optical spectra of the achiral molecules (**L-C2-PE-H**, **B-C2-PE-H**, **C3-PE-H**) are measured in chloroform. The experiments are performed at a concentration of 2×10^{-5} M and the resulting optical spectra are presented in Figure 2.1 while the photophysical properties are tabulated in Table 2.1. The compounds have an isolated absorption band, and it is interesting to note that all the derivatives show a structured absorption spectrum with partially resolved vibrational features owing to the rigidity of the phenyleneethynylene core.

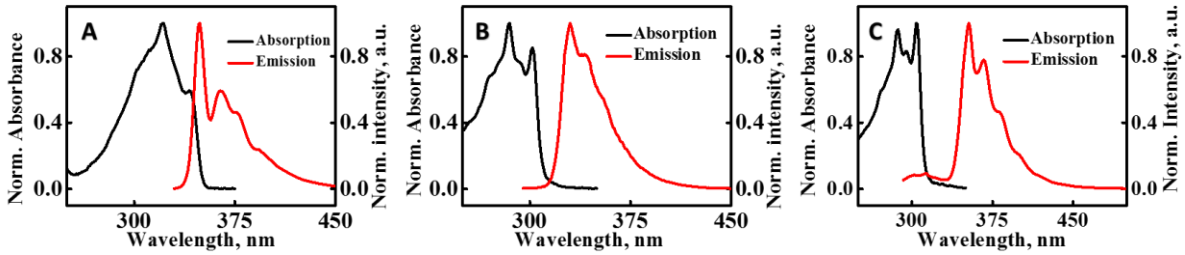

Figure 2.1: *Presented the absorption (black trace) and emission (red trace) spectra of (A)* ***L-C2-PE-H,*** *(B)* ***B-C2-PE-H*** *and (C)* ***C3-PE-H*** *in chloroform*

The absorption spectra of the **L-C2-PE-H** molecule shows a single band with the λ_{max} at 321 nm and a shoulder at 342 nm. Absorption spectra of **B-C2-PE-H** and **C3-PE-H** show a more vibronically resolved structure compared to **L-C2-PE-H**, with the two main peaks: for the **B-C2-PE-H** molecule, the two main peaks come at 285 nm and 302 nm while that of the **C3-PE-H** molecule come at 288 nm and 306 nm. The emission spectrum of all the derivatives also show a single band with partially resolved vibrational features. In the case of **L-C2-PE-H** molecule, vibrational features are more pronounced as indicated by the presence of a sharp and narrow peak at 349 nm. The emission maxima of **B-C2-PE-H** and **C3-PE-H** are observed at 330 nm and 354 nm, respectively. The most fascinating property is the Stokes shift exhibited by the derivatives. It is evident from the spectra that the linear molecule shows minimal shift, and the shoulder at 342 nm is almost superimposed to the 0-0 transition of emission,

that peak at 349 nm, having a Stokes shift (calculated as the energy difference between the 0-0 transition in absorption and in emission) of 587 cm^{-1}. On the other hand, in **B-C2-PE-H** molecule the shift between the 0-0 transition in absorption and emission is 2811.7 cm^{-1}, and it further increases in **C3-PE-H** molecule, being 4459.1 cm^{-1}.

Molar extinction coefficient of the molecule is determined using Beer-Lambert's law.[13] Absorbance of the molecule at three different concentrations are measured and the concentration (c) vs absorbance (A) is plotted. Slope of the plot gives molar extinction coefficient multiplied by path length of the cell (ε×l) and the intercept is set to zero. The molar extinction coefficient is comparable for **L-C2-PE-H** and **B-C2-PE-H**, while it increases for **C3-PE-H**, as expected for a molecule with higher number of arms. The quantum yield of the molecules (Φ_{sample}) are measured using relative method[14] as in Equation 2.1. The reference used is quinine hemisulphate in 0.5 M H_2SO_4 and excited at 330 nm.

$$\phi_{sample} = \phi_{ref} \frac{\eta^2_{sample} \times I_{sample} \times A_{ref}}{\eta^2_{ref} \times I_{ref} \times A_{sample}} \qquad (2.1)$$

where η_{sample}/η_{ref}, I_{sample}/I_{ref}, and A_{sample}/A_{ref} refers to the refractive index of the solvent, emission intensity and absorbance at the excitation wavelength of the molecule (sample) and reference (ref) respectively. ϕ_{ref} is the quantum yield of the reference, 0.546 for quinine sulphate in 0.5 M H_2SO_4.

Table 2.1: *Molar extinction coefficient and quantum yield of the achiral derivatives of the phenyleneethynylenes.*

Molecule	Molar extinction coefficient M^{-1} cm^{-1}	Relative quantum yield
L-C2-PE-H	5.84×10^4 (321 nm)	0.94±0.01
B-C2-PE-H	5.38×10^4 (284 nm)	0.15±0.03
C3-PE-H	10.68×10^4 (287 nm)	0.19±0.02

The **L-C2-PE-H** molecule shows the very high quantum yield with **B-C2-PE-H** and **C3-PE-H** molecules showing reasonably good luminescence.

2.3.1 Fluorescence anisotropy studies

Fluorescence anisotropy measures the average angular displacement between the absorption and emission transition dipole moments of the fluorophore. It is a dimension-less quantity independent of the concentration and total intensity of the sample. Experimentally, for the measurement of anisotropy, the sample is excited with linearly polarized light, and the intensity of emission is collected through another polarizer. The emission collected when the emission polarizer is parallel to the polarized excitation is $I_{\parallel}$ and the one collected perpendicular to excitation is $I_{\perp}$. The anisotropy is defined as follows:[15-16]

$$r = \frac{I_{\parallel} - I_{\perp}}{I_{\parallel} + 2\, I_{\perp}} \qquad (2.2)$$

Fluorescence anisotropy of a molecule having β as the angular displacement between absorption and emission transition dipoles is defined as follows:[15]

$$r_0 = \frac{3\, cos^2\, \beta - 1}{5} \qquad (2.3)$$

The term r_0 is used to indicate the intrinsic value of anisotropy, i.e. the anisotropy measured in the absence of any other depolarising process like rotational diffusion or energy transfer. The value of fluorescence anisotropy ranges from -0.2 (for β=90°) to 0.4 (for β=0°). Since the rotational diffusion is one of the major source of depolarization, for small molecules, anisotropy measurements are performed in highly viscous solvents or at low temperatures in glassy solvent. However, anisotropy does not tell the orientation of the dipole within the molecule. Theoretical calculation or studies using the ordered systems are essential to such an understanding. Excitation anisotropy is dependent on the excitation wavelength, as dipole orientation varies from one absorption band to another. Nevertheless, a constant anisotropy value throughout the excitation spectral region points to a single absorbance band.

Anisotropy is usually independent of the emission wavelength as emission always occur from the lowest excited state.

Excitation and emission anisotropy spectra of phenyleneethynylene derivatives are collected in propylene glycol at 190 K, ensuring the formation of glass that suppresses rotational diffusion. Emission and excitation spectra collected at 190K are reported in Figure 2.2, and are qualitatively similar to those collected at room temperature, apart from being more resolved due to a reduced inhomogeneous broadening.

L-C2-PE-H molecule shows a flat excitation anisotropy spectrum in the excitation spectral region, indicating that a single transition dipole is responsible for the transition (Figure 2.2A). Anisotropy value is found to be 0.38, which is very close to the limiting value for anisotropy, proving that the same state is responsible for both absorption and emission processes (Figure 2.2B).

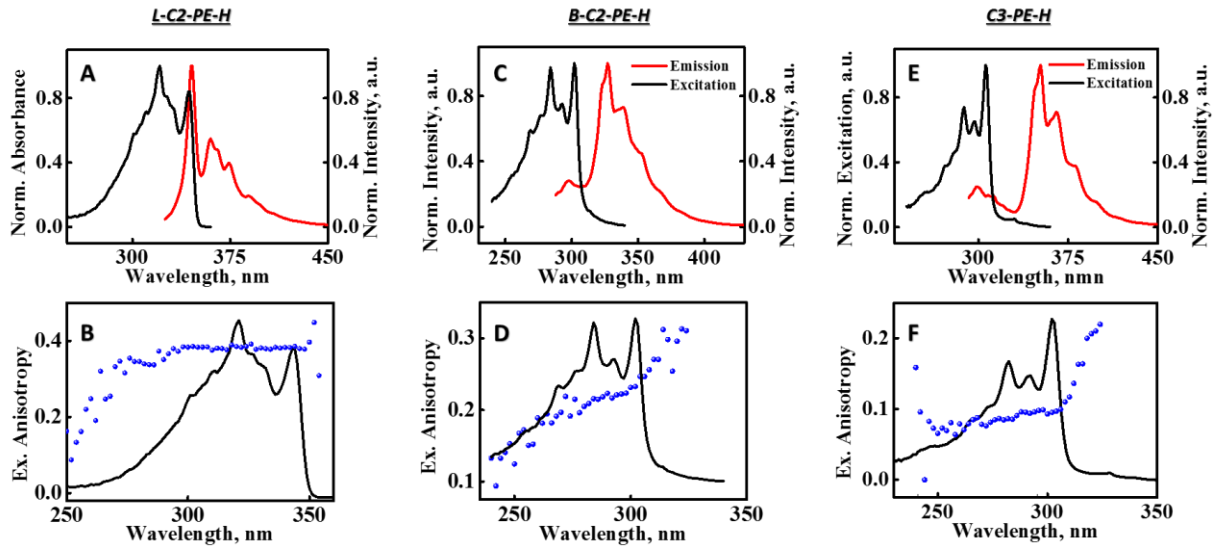

Figure 2.2: *Top panels: Excitation (black trace) and emission (red race) at low temperature, 190 K of (A)* ***L-C2-PE-H****, (C)* ***B-C2-PE-H*** *and (E)* ***C3-PE-H*** *respectively. Bottom panels: Anisotropy spectra are shown (blue trace) along with excitation spectra (black trace) measured in propylene glycol at 190 K of (B)* ***L-C2-PE-H****, (D)* ***B-C2-PE-H*** *and (F)* ***C3-PE-H*** *respectively.*

Studies with **C3-PE-H** also show a flat spectrum in the excitation region, and an abrupt increase in the red-region of the band (red-edge effect).[17-19] For this molecules, the

anisotropy value is 0.1 (Figure 2.2 F). It was interesting to note that fluorescence anisotropy experiments on **B-C2-PE-H** molecule show a gradual increase in the anisotropy on increasing the wavelength (Figure 2.2D) suggesting the presence of more than one excited state contributing to the absorption band, with transition dipole moments polarized along different directions. A classic example for a similar molecular system is 9-anthroyloxy stearic acid.[20]

2.3.2 Theoretical investigation

DFT/TD-DFT calculations using Gaussian 16[21] suite of programs are performed for theoretical investigation. All the calculations are carried out at the DFT level using the CAM-B3LYP functional and 6-31G(d) as basis set in the gas phase. The ground state as well as the excited states of all the different phenyleneethynylene are optimized before performing the vertical transition calculations.

TD-DFT calculations are very useful in this context to understand the role of multiple degenerate (or quasi-degenerate) electronic states, which are expected in the multi-branched systems, in determining the photophysical properties.

2.3.2.1 Vertical transitions from optimized ground-state geometries

The optimized ground state of **L-C2-PE-H** has a planar geometry. The low-energy transition is only one and is located at 3.96 eV (313.38 nm), is in reasonable agreement with the experiment (the blue shift of calculated transition can be assigned to the choice of functional, and to the absence of solvation effects). The transition dipole moment is polarized along the main molecular axis (x-axis) and has an oscillator strength of 1.91. The second transition is located at 4.93 eV, and has vanishing transition dipole moment: the energy gap of ≈1 eV between the two transitions is very high, and for this reason can be safely disregarded for the analysis of photophysical properties presented in the previous section. The main orbitals involved in the transition are the HOMO-1, HOMO, LUMO and LUMO+1, whose shape are reported in Table 2.3.

Table 2.2: *Calculated transitions for* ***L-C2-PE-H****, the Cartesian coordinates are defined in Table 2.3*

Transition	Energy (eV)	Oscillator strength	Orbitals involved in the transition*	Transition dipole moment component (a.u.)
1	3.9563	1.91	72→75; -0.16262 73→74; 0.67488	x: 4.4402 y: 0.0000 z: 0.0000
2	4.9300	0.00	69→74; -0.46197 73→76; 0.48103	x: 0.0000 y: 0.0295 z: 0.0000

*The coefficients are obtained from Gaussian output, and correspond to the normalized wavefunction coefficients (only the largest are reported)

Table 2.3: *Orbitals involved in first transition (0-1) of* ***L-C2-PE-H.*** *x-axis=red; y-axis=green, z-axis=blue, isosurface value=0.02*

Orbital	Energy (eV)	Shape
HOMO−1(72)	-7.756	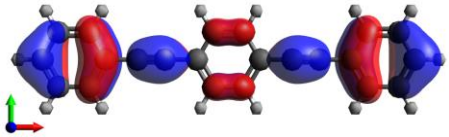
HOMO(73)	-6.717	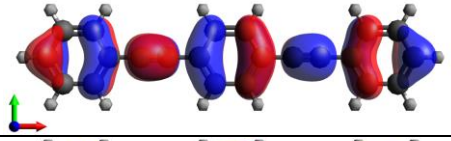
LUMO(74)	-0.547	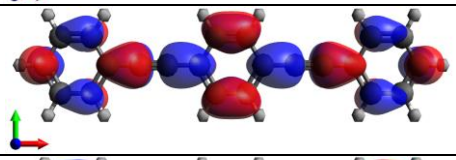
LUMO+1(75)	0.665	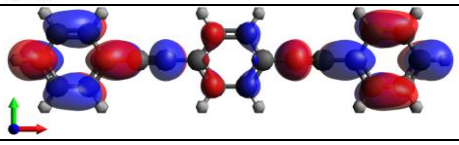

The optimized ground state of **B-C2-PE-H** is planar, and the molecule belongs to the C_{2v} point group. At low energy, two excited states are reported, which are close in energy (energy gap: 0.07eV). In agreement with experiment, both transitions are blue-shifted compared to the first transition of **L-C2-PE-H**. The lowest transition has a sizeable oscillator strength (1.66), and is polarized along the main molecular axis, while the oscillator strength of the second transition is reduced, and the transition dipole moment is polarized perpendicularly with respect to the first transition. The

orbitals involved in the transition are the HOMO-1, HOMO, LUMO and LUMO+1 and their shapes are reported in Table 2.5. The third transition has a negligible dipole moment, while the fourth is dark. These two transitions should not influence the photophysical properties analysed in the previous section, and will not be further discussed. It is noteworthy to notice that the sum of the oscillator strength of the two transition compares well with the calculated oscillator strength of the first transition of **L-C2-PE-H**. In an oversimplified excitonic picture, **L-C2-PE-H** and **B-C2-PE-H** can be considered as dimers of diphenylacetylene. Due to symmetry, only the low-energy transition of L-C2-PE-H is bright, and it bears all the oscillator strength, while for B-C2-PE-H both transitions have non-vanishing transition dipole moments, and the total intensity is distributed between the two transitions.

The optimized geometry of **C3-PE-H** is planar, and the molecule belong to the D3h point group. TD-DFT results for **C3-PE-H** are reported in Table 2.6: four excited states are calculated in the spectral range 4.34 eV-4.59 eV. In agreement with the experiment, calculated transition for **C3-PE-H** are in the same spectral region as the transition of **B-C2-PE-H** (and blue shifted with respect to **L-C2-PE-H**). The lowest state is a dark state, having vanishing oscillator strength, as well as the fourth state. The second and the third state are degenerate, with equivalent oscillator strength and perpendicular transition dipole moments: these two states can be safely assigned to E-symmetry states of the D3h point group (all calculations are run without imposing any symmetry to the system. D3h point group is determined from the analysis of the optimized ground state geometry, and the symmetry of excited states is inferred from the analysis of excited state energies and orbitals exploiting group theory). Six orbitals (from HOMO-2 to LUMO+2) are mainly involved in the transition, and their shapes are reported in Table 2.7: HOMO and HOMO+1 as well as LUMO and LUMO+1 are degenerate. Relevant results of the calculations of vertical transitions from the optimized ground state are summarized in the Table 2.8.

Table 2.4: *Calculated transitions for* ***B-C2-PE-H.*** *The definition of Cartesian axis is reported in table 2.5*

Transition	Energy (eV)	Oscillator strength	Orbitals involved in the transition	Transition dipole moment component (a.u.)
1	4.5032	1.66	72→74; 0.51774 73→75; 0.44804	x: 3.8822 y: 0.0000 z: 0.0001
2	4.5723	0.36	72→75; 0.29203 73→74; 0.61329	x: 0.0000 y: -1.7905 z: -0.0002
3	4.7008	0.01	67→75; -0.12843 67→78; 0.10053 69→74; 0.23391 72→74; -0.36998 72→79; -0.13272 73→75; 0.44317 73→78; 0.23219	x: 0.2422 y: 0.0000 z: 0.0000
4	5.2099	0.00	66→75; -0.39814 66→85; -0.11957 68→74; 0.55838	x: 0.0000 y: 0.0000 z: -0.0008

Table 2.5*: Orbitals involved in the first transition (0-1) of* ***B-C2-PE-H.*** *x-axis=red; y-axis=green; z-axis=blue. Isosurface value=0.02*

Orbital	Energy (eV)	Shape
HOMO−1(72)	-7.292	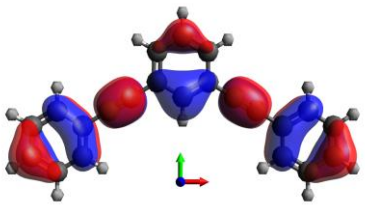
HOMO(73)	-6.982	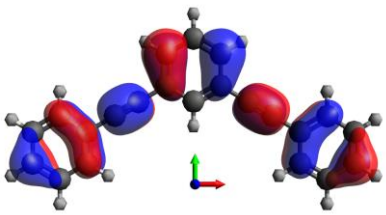

LUMO(74)	-0.232	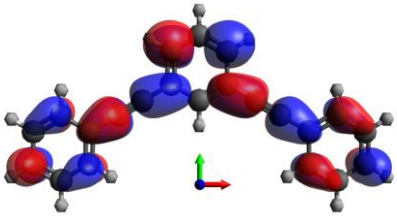
LUMO+1(75)	0.124	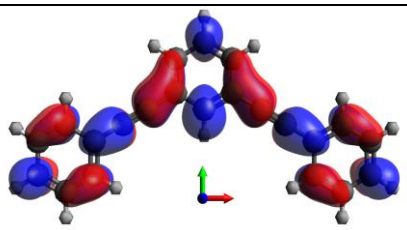

Table 2.6: *Calculated transitions for* ***C3-PE-H.*** *Cartesian axis are defined in table 2.7.*

Transition	**Energy (eV)**	**Oscillator strength**	**Orbitals involved in the transition**	**Transition dipole moment component (a.u.)**
1	4.3372	0.00	91 →101; -0.11285 92 →100; 0.11286 98 →100; -0.38001 98 →101; -0.24495 98 →106; 0.13718 99 →100; -0.24534 99 →101; 0.38040 99 →101; 0.13717	x: 0.0009 y: 0.0034 z: 0.0000
2	4.4704	1.61	97 →100; 0.22309 97 →101; -0.22121 98 →100; 0.37558 98 →101; 0.10140 98 →102; -0.26068 99 →100; -0.10103 99 →101; 0.37524	x: 0.8912 y: 3.7727 z: 0.0000
3	4.4704	1.61	97 →100; 0.22131 97 →101; 0.22311 98 →100; 0.10081 98 →101; -0.37506 99 →100; 0.37574 99 →101; 0.10161 99 →102; 0.26059	x: 3.7770 y: -0.8901 z: -0.0000
4	4.5911	0.00	97 →102; 0.15687 98 →100; -0.25143 98 →101; 0.39008 99 →100; 0.38938 99 →101; 0.25115	x: -0.0060 y: 0.0003 z: -0.0000

Table 2.7: *Orbitals involved in the first transition (0-1) of* ***C3-PE-H****. x-axis=red; y-axis=green, z-axis=blue. Isosurface value=0.02*

Orbital	Energy (eV)	Shape
HOMO−2(97)	-7.573	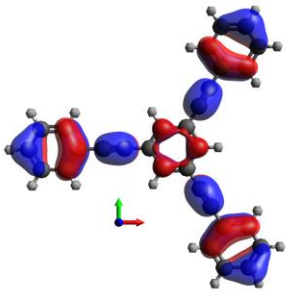
HOMO−1(98)	-7.013	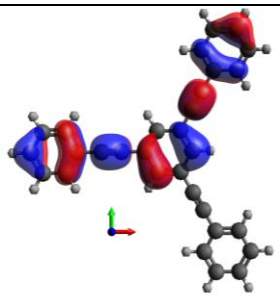
HOMO(99)	-7.013	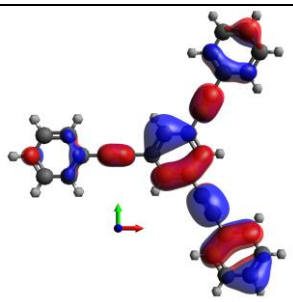
LUMO(100)	-0.362	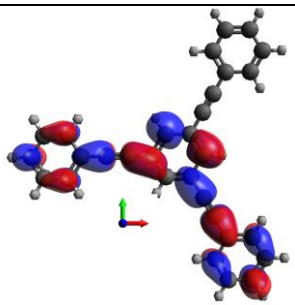
LUMO+1(101)	-0.362	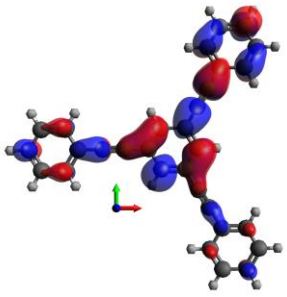

LUMO+2(102)	0.343	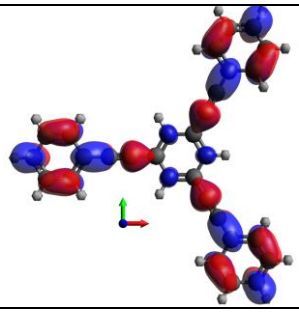

Table 2.8: *Presented the results of theoretical calculations: transition energy, oscillator strength and the orientation as well as the magnitude of the transition dipole for the relevant transitions in* ***L-C2-PE-H, B-C2-PE-H, C3-PE-H***

Molecule	**L-C2-PE-H**	**B-C2-PE-H**		**C3-PE-H**		
Transition	(0-1)	(0-1)	(0-2)	(0-1)	(0-2)	(0-3)
λ_{calc} (nm)	313.33	275.3	271.2	292.24	283.72	283.72
Oscillator strength (f)	1.92	1.66	0.36	0.0000	1.6089	1.6121
Transition dipole (a.u.)	x= -4.4398 y= -0.0 z= 0.0	x= 3.8822 y= 0.0052 z= 0.00	x= 0.0108 y=-1.7905 z=0.0000	x= -0.0009 y= 0.0034 z= 0.00	x=0.8912 y=3.7727 z=0.0	x=3.7770 y=--0.8901 z=-0.0

2.3.2.2 Vertical transitions from optimized excited-state geometries

In order to understand the origin of the Stokes shift, and to rationalize the emissive properties of the family of molecules, a deep investigation of the low-energy excited states is required. For this purpose, we optimized the geometry of the molecule in their excited state(s) and calculated the vertical transition to the ground state. Results for the **L-C2-PE-H** molecule show that the transition from the first excited state is allowed and the geometry of the molecule is similar to that of the ground state except for a slight elongation of the molecule on both sides of the central benzene ring (Figure 2.3). Also, the transition dipole is calculated to be 4.44 au aligned along x-direction.

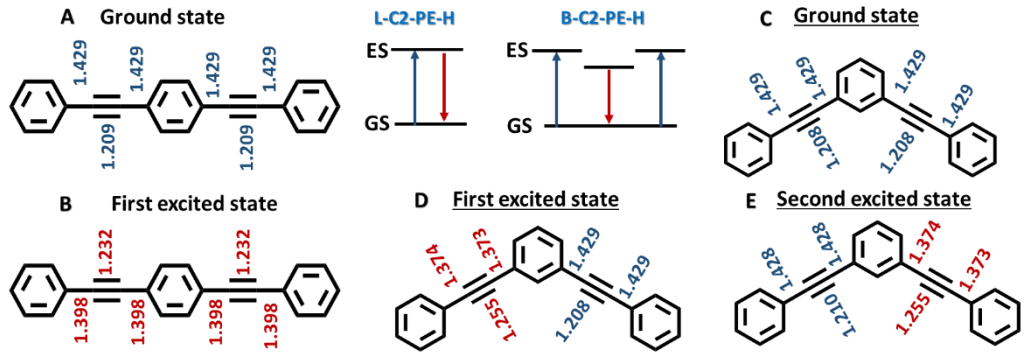

Figure 2.3: *Presented the bond length between benzene and ethylene groups in the phenyleneethynylene derivatives: (A-B) and (C-E) in their ground state and excited state. (A) show the ground and (B) shows the excited state geometry of L-C2-PE-H. On the other hand, (C) shows the ground, (D) and E shows the first and second excited state of B-C2-PE-H. Also provided the schematic representation of the transition possible for both the molecule.*

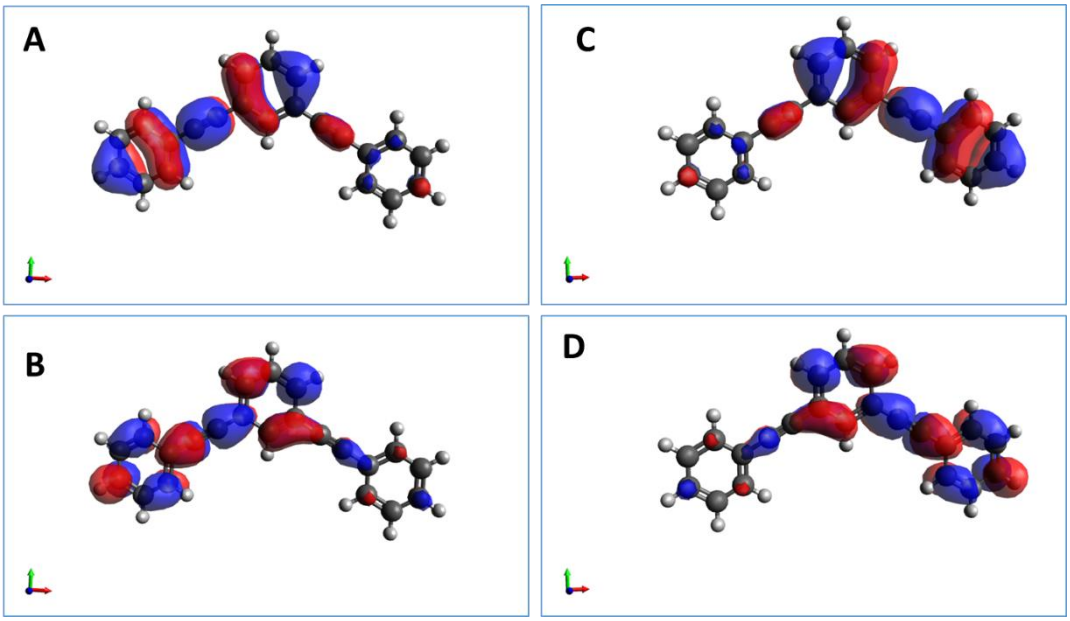

Figure 2.4*: The molecular orbitals of the HOMO and LUMO of the excited states of the bent molecule is shown: (A,B) shows the HOMO and LUMO of the first excited state and (C,D) shows the HOMO and LUMO of the second excited state.*

For **B-C2-PE-H** molecule, we observed that the transition from the optimized ground-state to the first and second excited states are close in energy. The optimization of the first and second excited state gives analogous results: the two arms of the molecule become non-equivalent, one arm of the molecule is slightly shortened compared to that of the ground state (Figure 2.3). The two minima are equivalent (i.e. have the same energy), suggesting to the bistability of the first excited state.

Localization of the excitation on one of the two arm occurs, as observed from HOMO and LUMO orbitals (the main orbitals involved in the transition) obtained from the relaxed states (Figure2.4). The relaxed excited state is bright, with sizeable oscillator strength, but reduced compared to the oscillator strength of the relaxed state of **L-C2-PE-H**. The transition dipole moment of the relaxed state is aligned along one molecular arm.

The **C3-PE-H** molecule also show similar trend as of **B-C2-PE-H**. TD-DFT results on the first optimized excited states reveal that the geometry of this state is very similar to the geometry of the ground state, and it remains a dark state. However, the optimization of the second and the third states gives a very interesting results: the energy of these states becomes lower in energy compared to that of the first optimized excited state. The energies of the second and third relaxed states are equivelant (Table 2.9), and similar to as observed for **B-C2-PE-H,** one arm of the molecule is shortened (the other two arms remain equivalent, Figure 2.5). The symmetry breaking observed in the relaxed excited states is interpreted as a Jahn-Teller distortion, that removes the degeneracy of excited states (of E-symmetry) imposed by symmetry.

***Table 2.9**: Shows the results from TD-DFT excited state calculation of **L-C2-PE-H**, **B-C2-PE-H** and **C3-PE-H**.*

Molecule	**L-C2-PE-H**	**B-C2-PE-H**		**C3-PE-H**		
Excited state	First state	First state	Second state	First state	Second state	Third state
Transition	(1-0)	(1-0)	(2-0)	(1-0)	(2-0)	(3-0)
λ_{calc} (nm)	362.76	319.4	319.4	304.73	320.71	320.70
Oscillator strength (f)	1.9853	1.13	1.13	0.00	1.2372	1.2372
Transition dipole (a.u.)	x= -4.8693 y= -0.0 z= 0.0	x= 3.1830 y= 1.3057 z= 0.0001	x=3.1830 y=-1.3052 z=0.0002	x= 0.00 y= -0.0001 z= 0.00	x=-3.6142 y=0.0183 z=0.0	x=-3.6141 y=-0.0298 z=-0.0

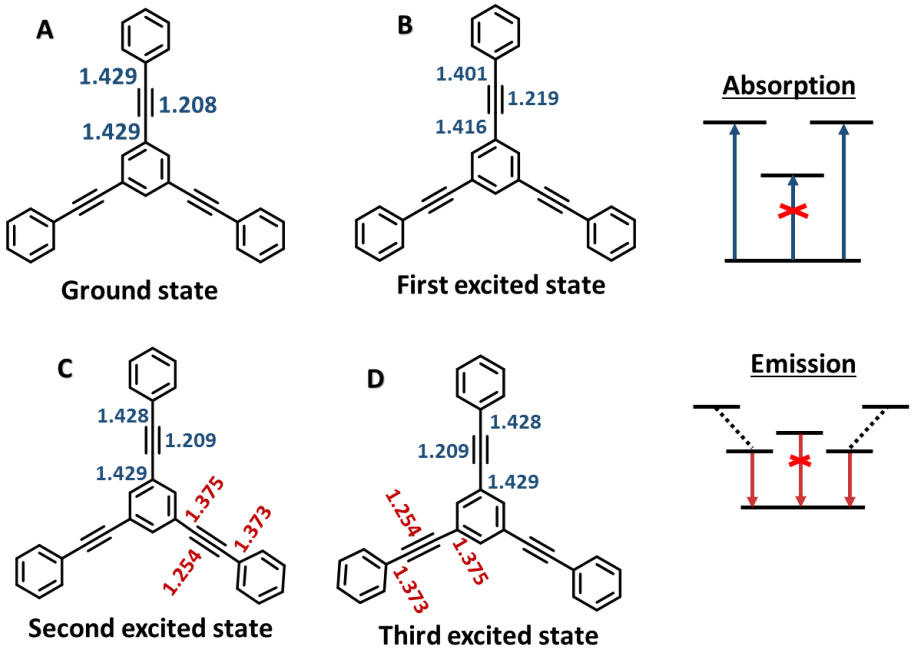

Figure 2.5: *Presented the bond length between benzene and ethylene groups in the* ***C3-PE-H*** *in their ground (A) and first, second and third excited (B, C, D respectively) state. Also provided the schematic representation of the transition possible for the molecule in their ground and excited state.*

2.3.3 Understanding photophysical properties through calculations

Experimental absorption, emission and fluorescence anisotropy of the linear **L-C2-PE-H** molecule points to the presence of a single electronic transition in the low-energy region, which is responsible for the absorption (250-355 nm) and the emission (330-450 nm) bands, for the flat excitation anisotropy and for a reduced Stokes shift. TD-DFT calculations confirm that a single excited state is present at low energy, with sizeable oscillator strength, having the transition dipole moment polarized along the main molecular axis.

B-C2-PE-H molecule has a similar absorption and emission properties compared to **L-C2-PE-H**, but a different excitation anisotropy profile. Excitation anisotropy is high in the red edge of the excitation band and decreases at higher energies, suggesting the contribution of different excited states to the low-energy absorption band. This experimental observation is confirmed by TD-DFT calculations: two excited states, very close in energy, are revealed, having perpendicular transition dipole moments.

In this case, the contribution of each state to anisotropy should be weighted considering its oscillator strength.[15] The detailed calculation requires a deconvolution of spectra, which is not trivial, but the behaviour of experiments is qualitatively well reproduced by theoretical calculations. Emission comes from a symmetry-broken state, where the length of the two arms of the molecule is different. The large Stokes shift observed in **B-C2-PE-H** can be attributed to the change in geometry of the relaxed excited state.

C3-PE-H is a highly symmetric molecule, having a C_3 axis of symmetry that ensures the presence of degenerate (E-symmetry) states. Absorption shows apparently a single band, and emission is red-shifted compared to absorption, with a sizeable Stokes shift (4459.1 cm^{-1}). Anisotropy is flat within the absorption band, except for an increase in the red-edge: the value of anisotropy is 0.1. The anisotropy value is explained by TD-DFT results: the second and third excited state are perfectly degenerate, having the same oscillator strength and perpendicular transition dipole moments. These two states contribute to anisotropy in an equivalent way, and their contributions can be averaged: the state polarized in the same direction as emission will contribute to anisotropy with a value of 0.4, while the state polarized perpendicularly will contribute with a value of -0.2. The average of 0.4 and -0.2 gives exactly 0.1, in agreement with the experiment. Even more interesting is the detailed investigation of the origin of the Stokes shift. The first calculated excited state of **C3-PE-H** is dark, pointing to a non-emissive molecule. However, experimental fluorescent quantum yield indicates that the molecule has good emission. The optimized first excited state remains a dark state. Hence the issue is solved by optimizing the second (or equivalently the third) excited state: the second and the third relaxed excited states becomes lower in energy compared to the first optimized excited state, and this is the reason for the observation of emission, which is sizeably red-shifted compared to the absorption. The Stokes shift is related to a symmetry-broken geometry (Jahn-Teller

distortion) of the relaxed emissive excited states compared to the symmetric excited state responsible for absorption.

2.4 Aggregation studies for chiral molecules

For the purpose of investigating the influence of geometry on the chiroptical and photophysical properties of the aggregates, we synthesized the chiral linear, bent and tripod phenyleneethynylene derivatives substituted with D/L-phenylalanine (Chart 2.2). Before performing the solvent-dependent photophysical studies, we carried out studies with their monomer as well. The results showed that in the case of monomer, the results are similar to their achiral counter parts as shown in Figure 2.6. The experiments are performed by dissolving the molecule in methanol and the concentration used is 20×10^{-6} M.

Solvent-dependent studies for linear molecule **L-C2-PE-D/L** are carried out in methanol-water mixture. On the other hand, bent, **B-C2-PE-D/L** and tripod, **C3-PE-D/L** molecules are studied in chloroform-methyl cyclohexane solvent mixture. A series of solvent-dependent studies are performed to find out the solvent composition that is optimal for aggregation studies. It was observed that at lower composition of poor solvent (upto 20 % water in methanol for **L-C2-PE-D/L**), the aggregation is very weak and further increase in the water percentage results increased aggregation as evident from the CD and absorption spectrum. At very high percentage of poor solvent (above 75% water in the case of **L-C2-PE-D/L**) precipitation occurs.

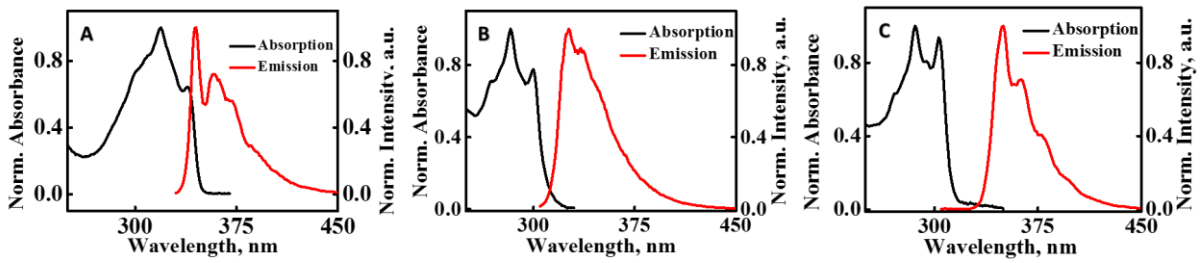

Figure 2.6: *Absorption (black trace) and emission (red trace) spectra of (A)* ***L-C2-PE-L*** *(B)* ***B-C2-PE-L*** *and (C)* ***C3-PE-L*** *I their molecularly dissolved form in methanol.*

75%(v/v) water in methanol is the solvent composition used for the **L-C2-PE-D/L** molecule and the experiments reveal that the molecule form aggregates as marked by the presence of a red shifted peak in the absorption spectrum (Figure 2.7A). In the case of emission spectrum, apart from a reduction in the intensity, the aggregate did not show much change in the spectral features compared to the monomer (Figure 2.7B).

***Table 2.10**: Molar extinction coefficient and quantum yield of the different chiral phenyleneethynylene derivatives.*

Molecule	L-C2-PE-L	L-C2-PE-D	B-C2-PE-L	B-C2-PE-D	C3-PE-L	C3-PE-D
Molar extinction coefficient $M^{-1}cm^{-1}$	4.7×10^4 (319 nm)	4.15×10^4 (319 nm)	5.431×10^4 (283 nm)	5.035×10^4 (283 nm)	8.59×10^4 (286 nm)	8.84×10^4 (286 nm)
Relative Quantum yield	0.93±0.02	0.95±0.02	0.20±0.02	0.22±0.01	0.22±0.02	0.23±0.02

C3-PE-D/L derivatives also show similar trend and the solvent composition used is 70% (v/v) methyl cyclohexane in chloroform (see Figure 2.7E,F). Here again, we observe that the aggregate formation is indicated by a red-shifted peak in the absorption peak and a reduction in the emission intensity with the spectral features remaining almost intact. It was interesting to note that on aggregation the absorbance of the λ_{max} also comes down in the absorption spectrum. It was speculated that the absence of shift in emission spectrum may be due to a drastic reduction in the emission for aggregates.

However, in the case of **B-C2-PE-D/L** molecule, aggregation of the molecule was very difficult. We found that though the molecule aggregates in 95% (v/v) methyl cyclohexane in chloroform, apart from a loss of partial vibrational features and a slight bathochromic shift, we could not observe marked difference in the absorption spectrum (Figure 2.7C). On the other hand, fluorescence spectrum showed a broad, structureless emission along with a decrease in intensity (Figure 2.7D). In the case of **B-C2-PE-D/L** molecules, other than chloroform-methyl cyclohexane, we also checked the aggregation of the molecule in methanol-water, THF-water and acetonitrile-water

mixtures as well. In all the cases, we observed that molecule aggregates at 95% (v/v) in poor solvent as indicated by the presence of slight turbidity. However, apart from a small reduction in the absorbance of λ_{max} and a loss of partially resolved vibrational features in absorption spectrum we could not see any shift in the absorption spectrum.

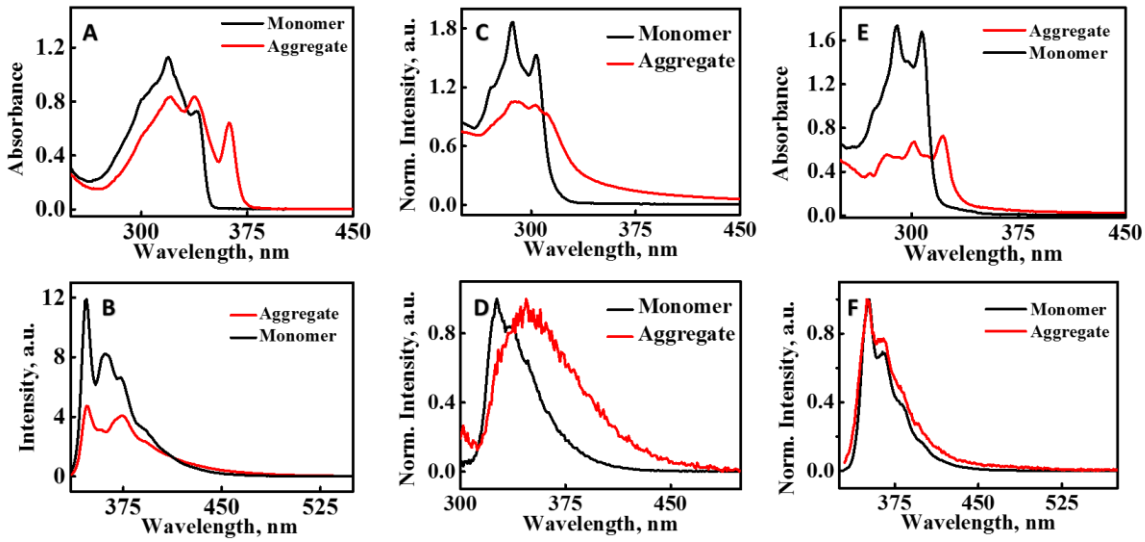

Figure 2.7: *Absorption and emission spectra of monomer (black trace) and aggregate (red trace) of the different chiral phenyleneethynylene derivatives. A,C and E shows the absorption and B, D and F shows the emission spectra of* ***L-C2-PE-L****,* ***B-C2-PE-L****, and* ***C3-PE-L*** *respectively. For all the experiment, the concentration used is 2 × 10^{-5} M. Solvent used for the measurement for the monomer of L-C2-PE-D/L is methanol and aggregate is 75% water in methanol. In the case of B-C2-PE-D/L and C3-PE-D/L, monomer experiments are carried out using chloroform as the solvent. In the case of aggregates, a mixture 95 %(v/v) methyl cyclohexane in chloroform for the former and 70% (v/v) methyl cyclohexane in chloroform for the latter.*

Further we carried out investigation of the chiroptical properties of the aggregates formed by different phenyleneethynylene derivatives using electronic circular dichroism (ECD) and is presented in Figure 2.8. In most cases, self-assembly of molecules where a chiral group is attached to a chromophore is marked by split CD bands in the chromophore absorption region. This arises due to the chiral arrangement of chromophores leading to exciton coupling.

In the case of the linear molecule **L-C2-PE-D/L**, CD shows a positive and negative bands indicating that the chiral assembly indeed leads to exciton coupling. Moreover, it was interesting to note that the CD band in the longer wavelength region have

partially resolved vibrational features as well. The D-isomer showed a negative band in the longer wavelength region followed by a positive band in the shorter wavelength region. The g-factor of the CD absorption maxima are calculated to be -7.8×10^{-3} at 361 nm and 2.9×10^{-3} at 313 nm. While, the L-isomer showed a negative, followed by a positive CD band. The g-factor of the CD absorption maxima are calculated to be 7.8×10^{-3} at 361 nm and -2.9×10^{-3} at 313 nm. In all these cases, we assumed that the NH-CO linkages in the molecule is primarily responsible for dictating the chiral assembly and employed the exciton chirality method to predict the handedness of assembly. On applying the Exciton chirality method proposed by Prof. Koji Nakanishi and co-workers,[22-23] we concluded that on self-assembly, the **L-C2-PE-D** formed a left-handed assembly while it's L-isomer, **L-C2-PE-L** formed a right-handed assembly. For the tripod molecules as well, we obtained an exciton coupled CD for both the isomers. In this case, we noted that the molecular aggregates show a sharp and narrow band at the longer wavelength followed by a broad band at the shorter wavelength.

For the **C3-PE-D** we observed a positive CD band in the longer wavelength region followed by a negative band in the shorter wavelength. On the other hand, **C3-PE-L** showed reverse, i.e. first negative and then positive cotton effects in the phenyleneethynylene absorption region. Hence we concluded that in the case of tripod molecules, L-isomer arranged to a left-handed while the D-isomer arranged to a right-handed chiral assembly. Here g_{abs} is found to be -0.45 ×10^{-3} for L-isomer and 0.54 ×10^{-3} for D-isomer at 323 nm.

For the aggregates of **B-C2-PE-L/D**, CD spectrum showed very weak signal, indicating the absence of well-developed aggregates. Schanze and co-workers have also reported similar results in a bent phenyleneethynylene derivative substituted with an L-alanine group: the authors claim that this happens as a result of the inability of the chiral centre in the alanine group to induce measurable chiral response in the conjugated chromophore.[24] Further, they polymerised the molecule to obtain the chiral response from the molecular system and observed an increase in the chiral absorption on

increasing the percentage of water in the methanol-water solvent system. Hence, we conclude that in the case of bent molecules **B-C2-PE-D/L** we do not observe chiral response since the attached phenylalanine group is insufficient in dictating a chiral self-assembly for the molecular system.

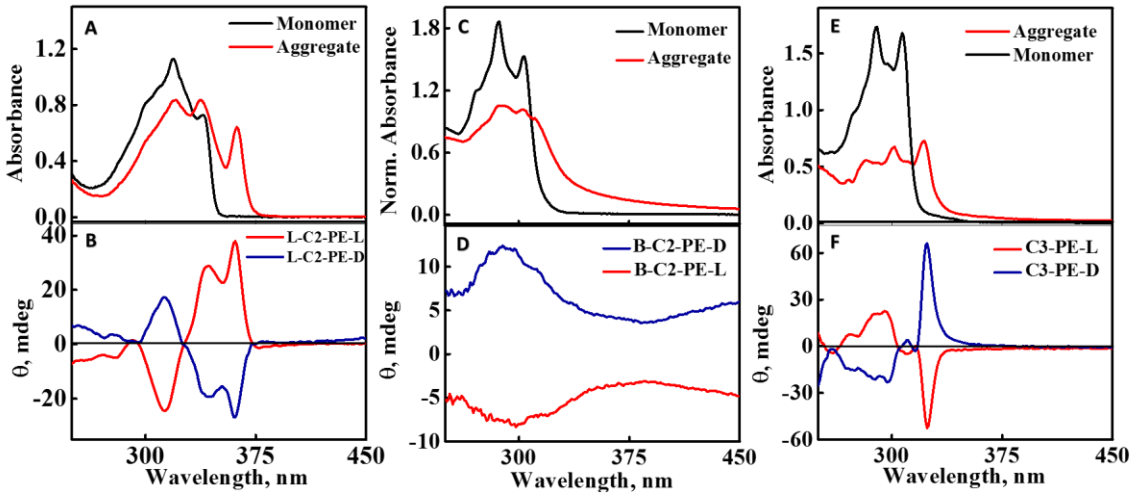

Figure 2.8: *Top panels: Absorption spectra of monomer (black trace) and molecular aggregate (red trace) of (A)* ***L-C2-PE-L*** *(B)* ***B-C2-PE-L*** *and (C)* ***C3-PE-L****, respectively. Bottom panels: CD spectra of D-isomer (blue trace) and L-isomer (red trace) of (B)* ***L-C2-PE-D/L*** *(D)* ***B-C2-PE-D/L*** *and (F)* ***C3-PE-D/L****, respectively.*

2.4.1 Microscopic analysis

Scanning electron microscopy (SEM) is employed to investigate the morphological nature of the molecular aggregates. For this purpose, we dropcasted few drops of the sample (concentration is same as that used for other studies) to a clean silicon wafer and left it overnight undisturbed for the solvent to evaporate. Even though the helical sense of the aggregates cannot be seen using this technique, one can understand very clearly the nature of the morphology of the aggregate in thin films (the morphology of aggregates formed in thin films strongly depends on the deposition technique and post deposition steps, so that the aggregates formed in films could be not equivalent to aggregates in solvent/non solvent mixtures).

The SEM analysis of the aggregates of **L-C2-PE-D/L** as well as **C3-PE-D/L** indicates the formation of highly interlocked fibre. Interestingly, we noted that in the case of **L-C2-**

PE-D/L, the fibres further bundled to form higher order structures. While in the case of **B-C2-PE-D/L**, SEM analysis reveals that the aggregates formed have mostly sheet-like morphology. However, in small domains we also observed few fibres as well, as seen in Figure 2.9.

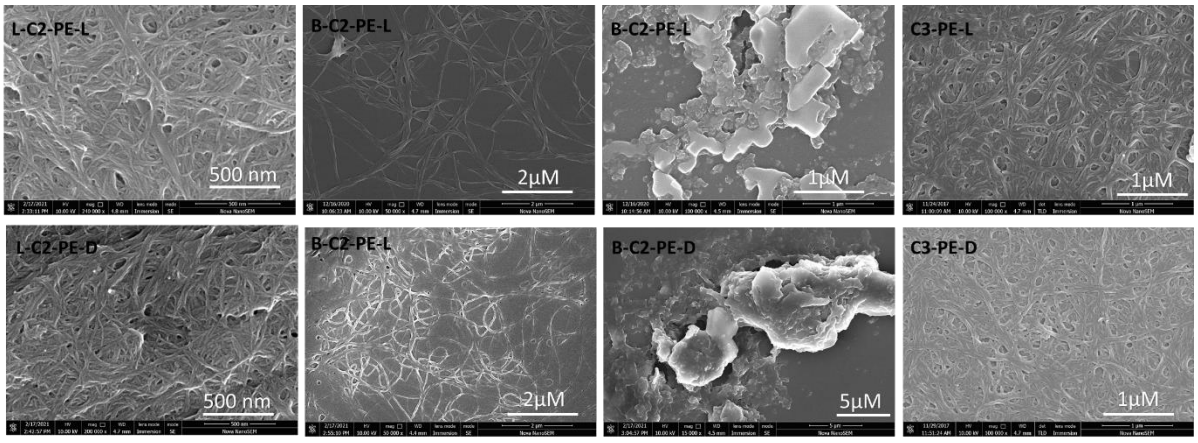

Figure 2.9: *SEM images of the molecular assemblies formed by* ***L-C2-PE-D/L****,* ***B-C2-PE-D/L*** *and* ***C3-PE-D/L****.*

2.5 Conclusions

In conclusion, three types of phenyleneethynylene derivatives having different geometry are synthesized and a thorough investigation of their photophysical properties using spectroscopic techniques as well as TD-DFT calculations are carried out. It was fascinating to note that when the geometry changes from linear to a bent or tripod, the number of states involved in the transition increases. Fluorescence anisotropy is high and flat in **L-C2-PE-H**, due to the presence of a single excited state. The presence of multiple excited states involved in the transition influences fluorescence anisotropy. For **B-C2-PE-H**, two states with slightly different energy, different oscillator strength and perpendicular transition dipole moments determine the wavelength dependence of experimental fluorescence anisotropy. On the other hand, in **C3-PE-H** the presence of two degenerate excited states, with equal oscillator strength but perpendicular transition dipoles is responsible for the flat and low value (0.1) of anisotropy. In the presence of degenerate (**C3-PE-H**) or quasi-degenerate (**B-**

C2-PE-H) excited states symmetry breaking is observed in their relaxed excited state. The symmetry breaking is reflected in an increased experimental Stokes shift.

On self-assembly, the molecules formed aggregates in suitable solvent composition. However, pronounced influence of the geometry is again visible in the chiroptical and microscopic analysis of them. Thus, it is expected that this fundamental work on the optical properties of the phenyleneethynylene derivatives comes handy when designing phenyleneethynylene based molecular system for various applications.

2.6 Synthesis and characterization

2.6.1 Methods and materials

All solvents used for the synthesis are purchased from commercial sources and used as such without much purification. All the precursors for the synthesis of the various phenyleneethynylene derivatives are purchased from Sigma Aldrich. Silica gel of 200-400 mesh size is used to perform flash column chromatography. Appropriate eluent is selected with the help of TLC prior to column chromatography by trial and error method. Intermediate compounds are purified by passing through recycling HPLC manufactured by Japan Analytical Industry Co., Ltd. All melting points are uncorrected and determined using Stuart SMP30 melting point apparatus. IR spectra are recorded on Shimadzu IR prestige-21 FT-IR spectrophotometer as KBr pellets in the case of solids. ^{1}H and ^{13}C NMR spectra are recorded on Bruker Avans 500 MHz DPX spectrometer using 1,1,1,1-tetramethyl silane (TMS) as an internal standard. Elemental analysis is carried out on Elementar vario MICRO cube Elemental Analyser. Electronic absorption spectra are recorded using quartz cuvette of 1 cm path length on a Shimadzu UV-3600 Vis-NIR Spectrophotometer. Steady state fluorescence spectra are recorded on Horiba Jobin Yvon Fluorimeter equipped with thermostat peltier cell holder, in a quartz cuvette of 1 cm path length.

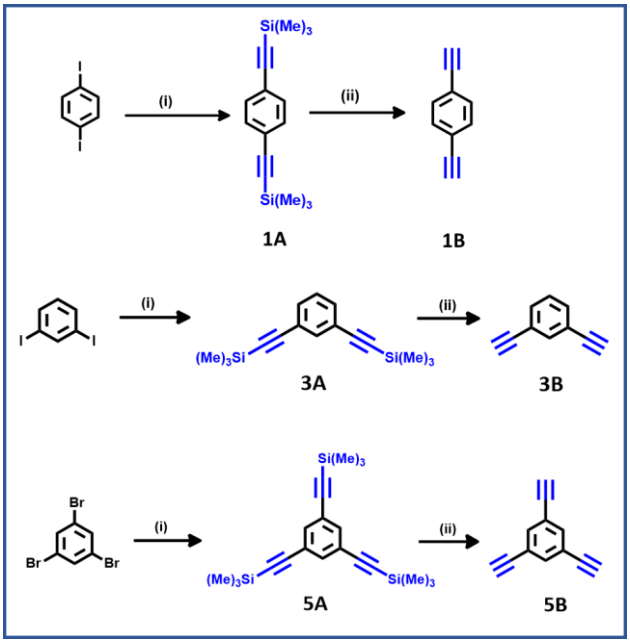

Scheme 2.1: *(i) $Pd(PPh_3)_2Cl_2$, TMSA, Et_3N, CuI, THF (ii) K_2CO_3, MeOH. 6*

Synthesis of 1A: A pressure tube (100 mL) is evacuated, and N_2 is passed. A solution of 1,4-diiodobenzene (4 g, 12.1 mmol), CuI (0.46 g, 2.43 mmol), $Pd(PPh_3)_2Cl_2$ (1.71 g, 2.43 mmol) in dry triethylamine 60 mL) and dry THF (35 mL) is added. The reaction mixture is raised to a temperature of 60 °C and added trimethylsilylacetylene (TMSA) (3.6 mL, 28 mmol) to the flask under N_2 flow. The reaction mixture is stirred overnight. After the completion of reaction, the excess solvent is removed under pressure and resulting residue is dissolved in $CHCl_3$ followed by a flash column chromatography. Further, the excess solvent is again removed under reduced pressure and the residue obtained is chromatographed over silica (100-200 mesh) using a petroleum ether as eluent to yield 2.3 g of **1A** (70%) as white thin flakes. ^1H NMR ($CDCl_3$, 500 MHz): δ 7.41 (s, 4H, Ar), 0.27 (s, 18H, $SiCH_3$).

Synthesis of 1B: To a solution of 1A (2.0 g, 7.39 mmol) in dry THF (75 mL), a mixture of methanol (55 mL) and dry potassium carbonate (8.17 g, 59.12 mmol) is added and stirred overnight in a 250 mL two-neck RB flask. The solvent is evaporated; the residue is poured into water and extracted with chloroform (×3 times). The organic layer is repeatedly washed with water (3 x 25 mL) and dried over anhydrous Na_2SO_4. The crude product thus obtained is further purified using column chromatography with

silica (100-200 mesh) and using petroleum ether as the eluent. We obtained 0.76 g (82%) of **1B** as a pale yellow solid. ^{1}H NMR ($CDCl_3$, 500 MHz): δ 7.37 (s, 4H, Ar), 3.10 (s, 2H, acetylenic).

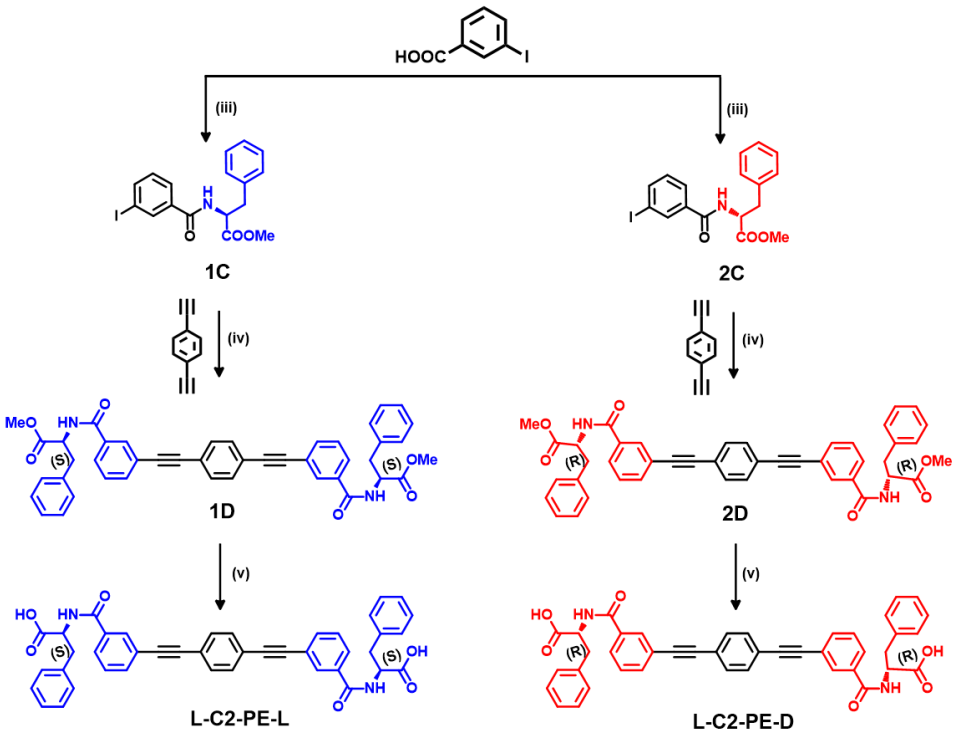

Scheme 2.2: *Provided the detailed scheme on the synthesis of* ***L-C2-PE-L/D****. (iii) L-Phenylalanine methyl ester hydrochloride, EDC, HOBT, N.N-diisopropylethylamine (DIPEA) ; (iv)D- Phenylalanine methyl ester hydrochloride, EDC, HOBT, N.N-diisopropylethylamine (DIPEA) ; (v) Pd(PPh$_3$)$_2$Cl$_2$, CuI, trimethylamine, PPh$_3$; (vi) LiOH, MeOH*

Synthesis of 1C, 2C: Under N_2 atmosphere, to a mixture of 3-iodobenzoic acid (2.77 g, 11.16 mmol) and D/L-phenylalanine methyl ester hydrochloride (3 g, 16.74 mmol) in 10 mL dry DMF, 1-ethyl-3-(dimethylaminopropylamine)carbodiimide hydrochloride (EDCI.HCl) (2.57 g, 13.4 mmol), hydroxybenzotriazole (HOBT) (1.8 g, 13.4 mmol) in 10 mL dry N,N-diisopropylethylamine are added and stirred for 24 h at room temperature. Then the reaction mixture is poured into cold water and extracted with ethyl acetate. Organic layer is repeatedly washed with water, finally, combined and dried over anhydrous Na_2SO_4. After removal of the solvent under reduced pressure the crude product is purified by column chromatography over silica gel (100-200 mesh) using ethyl acetate/hexane (1:5) as eluent to obtain 3.2 g of white solid of **1C/2C**

both with ~70% yield. ^{1}H NMR (500 MHz, $CDCl_3$, TMS): δ 7.98 (s, 1H, aromatic), 7.76-7.74 (m, 1H, aromatic), 7.58-7.56 (m, 1H, aromatic), 7.25-7.17 (m, 3H, aromatic), 7.09-7.04 (m, 3H, aromatic), 6.45 (d, *J* = 7.3 Hz, 1H, NH), 5.01-4.97 (m, 1H, CH), 3.70 (s, 3H, OCH_3), 3.25-3.12 (m, 2H, CH_2).

Synthesis of 1D, 2D: A mixture of 1,4-diethynylbenzene (250 mg, 1.98 mmol) and **1C**/**2C** (2.15 g, 4.76 mmol), CuI (75 mg, 0.4 mmol), $Pd(PPh_3)_2Cl_2$ (0.28 g, 0.4 mmol), triphenylphosphine (51 mg, 0.2 mmol) was added to a degassed solution of triethylamine (25 mL), and the mixture was stirred at room temperature overnight. The reaction mixture was diluted with chloroform and passed through a short flash column. After removal of the solvent under reduced pressure, the crude product was purified by column chromatography over silica gel (100-200 mesh) using chloroform as the eluent. The product was further purified by HPLC to obtain 0.7 g of white solid of **1D/2D** both with ~ 52% yield. The compound is further purified using recycling HPLC with chloroform as the eluent. ^{1}H NMR (500 MHz, $CDCl_3$, TMS): δ 7.81 (s, 2H, aromatic), 7.64-7.58 (m, 4H, aromatic), 7.47-7.43 (m, 7H, aromatic), 7.38-7.35 (t, *J = 7.75* Hz, 2H, aromatic), 7.25-7.21 (m, 5H, aromatic), 7.08 (d, *J* = 7.1 Hz, 4H, aromatic), 6.53 (d, *J* = 6.95 Hz, 2H, NH), 5.05-5.02 (m, 2H, CH), 3.72 (s, 6H, OCH_3) 3.26-3.15 (m, 4H, CH_2).

Synthesis of L-C2-PE-L, L-C2-PE-D: To a solution of **1D/2D** (140 mg, 0.2 mmol) in THF (10 mL), $LiOH.H_2O$ (0.5 g, 20.8 mmol), MeOH (10 mL) were added. The mixture was refluxed for 5 h. Then reaction mixture was quenched using 1M HCl and the desired product precipitate out**.** The precipitate thus obtained is further washed with water and chloroform to yield 0.17 g of **L-C2-PE-L/L-C2-PE-D** both with ~85% yield. ^{1}H NMR (500 MHz, DMSO, TMS): δ 8.86 (d, *J* = 8.5 Hz, 2H, NH), 7.98 (s, 2H, aromatic), 7.83 (d, *J* = 7.8 Hz, 2H, aromatic), 7.68 (d, *J* = 7.75 Hz, 2H, aromatic), 7.53 (t, *J* = 7.8 Hz, 2H, aromatic), 7.48 (s, 2H, aromatic), 7.33-7.25 (m, 8H, aromatic), 7.18 (t, *J* = 7.25 Hz, 2H, aromatic), 4.66-4.62 (m, 2H, CH), 3.23-3.05. 0.81 (t, *J* = 6.85 Hz, 6H, aliphatic). ^{13}C NMR (500 MHz, DMSO, TMS): 172.53, 166.02, 138.08, 134.75, 134.59, 132.32, 130.61,

129.57, 129.52, 128.77, 128.56, 127.03, 122.86, 122.54, 91.19, 89.93, 54.79, 52.51, 36.68. Anal. Calcd for $C_{42}H_{32}N_2O_6$: C, 76.35; H, 4.88; N, 4.24; O, 14.53. Found for **L-C2-PE-D**: C, 75.86; H, 5.01; N, 3.99.

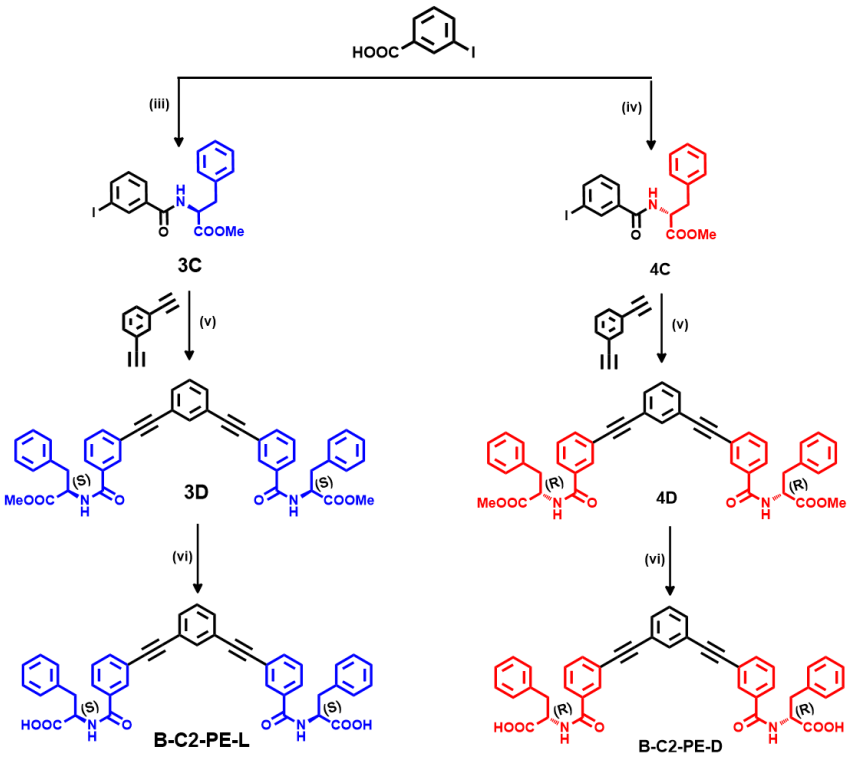

Scheme 2.3: *Provided the detailed scheme on the synthesis of* ***B-C2-PE-L/D****. (iii) L-Phenylalanine methyl ester hydrochloride, EDC, HOBT, (DIPEA); (iv)D- Phenylalanine methyl ester hydrochloride, EDC, HOBT, (DIPEA); (v) $Pd(PPh_3)_2Cl_2$, CuI, trimethylamine, PPh_3; (vi) LiOH, MeOH.*

Synthesis of 3A: A pressure tube (100 mL) is evacuated, and N_2 is passed. A solution of 1,3-diiodobenzene (6 g, 18.2 mmol), CuI (0.35 g, 1.82 mmol), $Pd(PPh_3)_2Cl_2$ (1.28 g, 1.82 mmol) in dry triethylamine (50 mL) and dry THF (35 mL) is added. The reaction mixture is raised to a temperature of 60 °C and added TMSA (6.0 mL, 45.5 mmol) to the flask under N_2 flow. The reaction mixture is stirred overnight. After the completion of reaction, the excess solvent is removed under pressure and resulting residue is dissolved in $CHCl_3$ followed by a flash column chromatography. Further, the excess solvent is again removed under reduced pressure and the residue obtained is chromatographed over silica (100-200 mesh) using petroleum ether as eluent to yield 2.5 g of 1A (51%) as white solid. mp 74-75 °C; ^{1}H NMR ($CDCl_3$, 500 MHz): δ 7.61 (s,

1H, aromatic), 7.43-7.41 (m, 2H, aromatic), 7.27 (t, *J=7.8* Hz, 1H, aromatic) 0.27 (s, 18H, $SiCH_3$).

Synthesis of 3B: To a solution of **3A** (2 g, 7.4 mmol) in dry THF (60 mL), a mixture of methanol (40 mL) and dry potassium carbonate (5.12 g, 37.02 mmol) is added and stirred for 4 h in a 250 mL two-neck RB flask. The solvent is evaporated; the residue is poured into water and extracted with chloroform. The organic layer is repeatedly washed with water (3 x 25 mL) and dried over anhydrous Na_2SO_4. Evaporation of solvent yielded 0.75 g (80 %) of **3B** as a pale yellow solid. ^1H NMR ($CDCl_3$, 500 MHz): δ 7.55 (s, 1H, aromatic), 7.4-7.38 (m, 2H, aromatic), 7.22-7.20 (m, 1H, aromatic) 3.02 (s, 2H, acetylenic).

Synthesis of 3C, 4C: Under N_2 atmosphere, to a mixture of 3-iodobenzoic acid (2.77 g, 11.16 mmol) and D/L-phenylalanine methyl ester hydrochloride (3 g, 16.74 mmol) in 10 mL dry DMF, 1-ethyl-3-(dimethylaminopropylamine)carbodiimide hydrochloride (EDCI.HCl) (2.57 g, 13.4 mmol), hydroxybenzotriazole (HOBT) (1.8 g, 13.4 mmol) in 10 mL dry N,N-diisopropylethylamine are added and stirred for 24 h at room temperature. Then the reaction mixture is poured into cold water and extracted with ethyl acetate. Organic layer is repeatedly washed with water, finally, combined and dried over anhydrous Na_2SO_4. After removal of the solvent under reduced pressure the crude product is purified by column chromatography over silica gel (100-200 mesh) using ethyl acetate/hexane (1:5) as eluent to obtain 3.2 g of white solid of **1C/2C** both with~70% yield. ^1H NMR (500 MHz, $CDCl_3$, TMS): δ 7.98 (s, 1H, aromatic), 7.76-7.74 (m, 1H, aromatic), 7.58-7.56 (m, 1H, aromatic), 7.25-7.17 (m, 3H, aromatic), 7.09-7.04 (m, 3H, aromatic), 6.45 (d, J = 7.3 Hz, 1H, NH), 5.01-4.97 (m, 1H, CH), 3.70 (s, 3H, OCH_3), 3.25-3.12 (m, 2H, CH_2).

Synthesis of 3D, 4D: A mixture of 1,3-diethynylbenzene (300 mg, 2.37 mmol) and **3C**/**4C** (2.7 g, 5.7 mmol), CuI (90 mg, 0.48 mmol), $Pd(PPh_3)_2Cl_2$ (0.36 g, 0.48 mmol), and triphenylphosphine (60 mg, 0.24 mmol) was added to dry THF (30 mL) and dry triethylamine (30 mL) in a 100 mL two-neck RB. The resulting mixture was stirred at

60 °C overnight. Once the reaction is completed, the reaction mixture was diluted with chloroform and passed through a short flash column. After the removal of the solvent under reduced pressure, the crude product was purified by column chromatography over silica gel (100-200 mesh) using chloroform as an eluent. The product was further purified by recycling HPLC to obtain 0.77 g, white solid of **3D/4D** both with~47% yield. ^{1}H NMR (500 MHz, $CDCl_3$, TMS): δ 7.82 (s, 2H, aromatic), 7.67 (s, 1H, Ar) 7.64-7.59 (m, 4H, aromatic), 7.46-7.44 (m, 2H, aromatic), 7.38-7.35 (t, *J* = *8* Hz, 2H, aromatic), 7.32-7.29 (t, J= Hz, 1H), 7.25-7.21 (m, 6H, aromatic), 7.08 (d, *J* = 6.75 Hz, 4H, aromatic), 6.53 (d, *J* = 7.35 Hz, 2H, NH), 5.05-5.02 (m, 2H, CH), 3.71 (s, 6H, OCH_3) 3.27-3.15 (m, 4H, CH_2).

Synthesis of B-C2-PE-L, B-C2-PE-D: To a solution of **3D/4D** (200 mg, 0.29 mmol) in THF (15 mL), $LiOH.H_2O$ (35 mg, 1.5 mmol), MeOH (20 mL) were added in a 50 mL two-neck RB. The mixture was refluxed for 5 h. Then reaction mixture was quenched using 1M HCl and the desired compound precipitate out. The precipitate thus obtained is washed with water to yield 0.15 g **B-C2-PE-L/B-C2-PE-D** both with~78% yield. ^{1}H NMR (500 MHz, DMSO, TMS): δ 8.88 (d, *J* = 8.15 Hz, 2H, NH), 8.31 (s, 1H, aromatic), 8.01 (s, 2H, aromatic), 7.84 (d, *J* = 7.9 Hz, 2H, aromatic), 7.78 (s, 1H, aromatic), 7.73 (d, *J* = 7.7 Hz, 2H, aromatic), 7.64-7.63 (m, 2H, aromatic), 7.54-7.51 (m, 3H, aromatic), 7.32-7.25 (m, 8H, aromatic), 7.19 (t, *J* = 7.25 Hz, 2H, aromatic), 4.67-4.62 (m, 2H, CH), 3.22-3.05 (m, 4H, CH_2). ^{13}C NMR (500 MHz, DMSO, TMS): 173.5, 165.93, 138.60, 134.84, 134.63, 134.52, 132.29, 130.65, 130.05, 129.5, 128.68, 128.5, 126.86, 123.18, 122.46, 89.94, 89.27, 79.68, 54.74, 36.69. Anal. Calcd for $C_{42}H_{32}N_2O_6$: C, 76.35; H, 4.88; N, 4.24; O, 14.53. Found for **B-C2-PE-D**: C, 74.67; H, 5.13; N, 3.99.

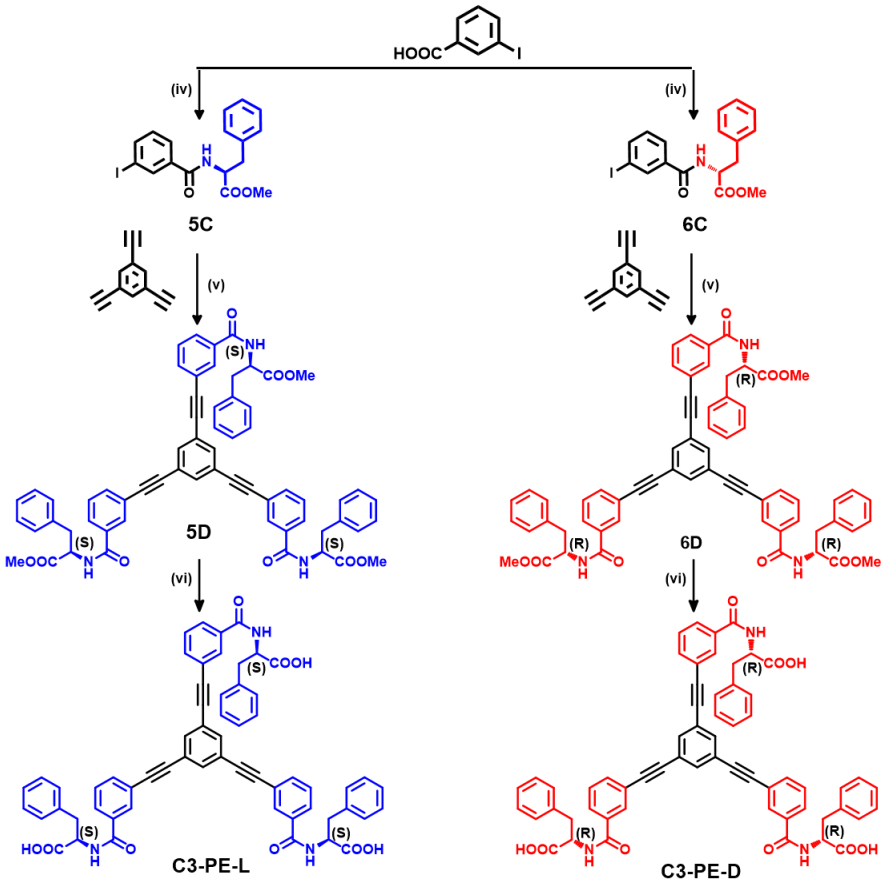

Scheme 2.4: *Provided the detailed scheme on the synthesis of* ***C3-PE-L/D****. (iii) L-Phenylalanine methyl ester hydrochloride, EDC, HOBT, (DIPEA); (iv)D- Phenylalanine methyl ester hydrochloride, EDC, HOBT, (DIPEA) ; (v)* $Pd(PPh_3)_2Cl_2$*, CuI, triethylamine,* PPh_3 *; (vi) LiOH, MeOH*

Synthesis of 5A: A pressure tube (100 mL) is evacuated, and N_2 is passed. A solution of 1,3,5-tribromobenzene (3 g, 9.53 mmol), CuI (0.54 g, 2.86 mmol), $Pd(PPh_3)_2Cl_2$ (2.0 g, 2.86 mmol) in dry triethylamine (30 mL) and dry THF (30 mL) is added. The reaction mixture is raised to a temperature of 60 °C and added TMSA (4.7 mL, 34.3 mmol) to the flask under N_2 flow. The reaction mixture is stirred overnight. After the completion of reaction, the excess solvent is removed under pressure and resulting residue is dissolved in $CHCl_3$ followed by a flash column chromatography. Further, the excess solvent is again removed under reduced pressure and the residue obtained is chromatographed over silica (100-200 mesh) using petroleum ether as the eluent to yield 2.5 g of **5A** (72%) as white solid.

Synthesis of 5B: A solution of **5A** (2 g, 5.45 mmol) in dry THF (60 mL), is added to a mixture dry potassium carbonate (11.0 g, 81.8 mmol) in methanol (75 mL) and stirred for 4 h in a 250 mL two-neck RB flask. Once the reaction is completed, the solvent is evaporated; the residue is poured into water and extracted with chloroform. The organic layer is repeatedly washed with water (3 x 25 mL) and dried over anhydrous Na_2SO_4. The crude product is purified using column chromatography using silica (100-200 mesh) employing petroleum ether as the eluent to yield 0.63 g (77 %) of **5B** as a white solid. ^{1}H NMR (500 MHz, $CHCl_3$, TMS): δ 7.45 (s, 3H, aromatic), 2.97 (s, 3H, acetylenic).

Synthesis of 5C, 6C: Under N_2 atmosphere, to a mixture of 3-iodobenzoic acid (2.77 g, 11.16 mmol) and D/L-phenylalanine methyl ester hydrochloride (3 g, 16.74 mmol) in 10 mL dry DMF, EDC.HCl (2.57 g, 13.4 mmol), HOBT (1.8 g, 13.4 mmol) in 10 mL dry N,N-diisopropylethylamine are added and stirred for 24 h at room temperature. Then the reaction mixture is poured into cold water and extracted with ethyl acetate. Organic layer is repeatedly washed with water, finally, combined and dried over anhydrous Na_2SO_4. After removal of the solvent under reduced pressure the crude product is purified by column chromatography over silica gel (100-200 mesh) using ethyl acetate/hexane (1:5) as eluent to obtain 3.2 g of white solid of **5C/6C** both with ~ 70% yield. ^{1}H NMR (500 MHz, $CDCl_3$, TMS): δ 7.98 (s, 1H, aromatic), 7.76-7.74 (m, 1H, aromatic), 7.58-7.56 (m, 1H, aromatic), 7.25-7.17 (m, 3H, aromatic), 7.09-7.04 (m, 3H, aromatic), 6.45 (d, J = 7.3 Hz, 1H, NH), 5.01-4.97 (m, 1H, CH), 3.70 (s, 3H, OCH_3), 3.25-3.12 (m, 2H, CH_2).

Synthesis of 5D, 6D: To a 100 mL two-neck RB, 1,3,5-triethynylbenzene (0.3 g, 2 mmol), **5C/5D** (2.8 g, 6.6 mmol), CuI (0.11 g, 0.66 mmol), $Pd(PPh_3)_2Cl_2$ (0.43 mg, 0.6 mmol), triphenylphosphine (16 mg, 0.6 mmol) was added and degassed. To the RB flask, dry triethylamine (20 mL), and dry THF (20 mL) is added and the mixture was stirred at room temperature overnight. The reaction mixture was diluted with chloroform and passed through a short flash column. After removal of the solvent

under reduced pressure, the crude product was purified by column chromatography over silica gel (100-200 mesh) using chloroform as the eluent. The product was further purified by recycling HPLC to obtain 1.3 g of white solid as **5D/6D** both with ~65% yield. . ^{1}H NMR (500 MHz, $CDCl_3$, TMS): δ 7.82 (s, 3H, aromatic), 7.66-7.60 (m, 9H, aromatic), 7.39 (t, *J= 7.8*, 4H, aromatic), 7.26-7.20 (m, 9H, aromatic), 7.08 (d, *J=6.8* Hz, 6H, aromatic), 6.54 (d, *J* = 7.5 Hz, 3H, NH), 5.06-5.02 (m, 3H, CH), 3.72 (s, 9H, OCH_3), 3.27-3.15 (m, 6H, CH_2).

Synthesis of C3-PE-L, C3-PE-D: To a solution of **5D/6D** (0.5 g, 0.5 mmol) in THF (20 mL) in a 100 mL two-neck RB, $LiOH.H_2O$ (96 mg, 4.02 mmol), and MeOH (30 mL) were added. The mixture was refluxed for 5 h. Then reaction mixture was quenched using 1M HCl and the desired product precipitate out. The precipitate is further washed with water and chloroform to yield 0.38 g of **C3-PE-L/C3-PE-D** as white powder both with ~79% yield. ^{1}H NMR (500 MHz, DMSO, TMS): ^{1}H NMR (500 MHz, DMSO, TMS): δ 8.9 (d, *J* = 8.15 Hz, 3H, NH), 8.06 (s, 3H, aromatic), 7.88 (m, 6H, aromatic), 7.78 (d, *J* = 7.7 Hz, 3H, aromatic), 7.59 (t, *J* = 7.8 Hz, 3H, aromatic), 7.34-7.27 (m, 12H, aromatic), 7.21-7.18 (m, 3H, aromatic), 4.69-4.64 (m, 3H, CH), 3.24-3.07 (m, 4H, CH_2). ^{13}C NMR (500 MHz, DMSO, TMS): 173.48, 165.90, 138.61, 134.88, 134.74, 134.57, 130.80, 130.65, 129.51, 128.68, 128.5, 126.85, 124.03, 122.22, 90.78, 88.35, 54.77, 36.69. Anal. Calcd for $C_{60}H45N_3O9$: C, 75.70; H, 4.76; N, 4.41; O, 15.13. Found for **C3-PE-D**: C, 73.94; H, 5.00; N, 3.96.

Synthesis of L-C2-PE-H: To a 100 mL two-neck RB, 1,4-diiodobenzene (0.5 g, 1.5 mmol) and phenylacetylene (387 mg, 3.8 mmol), CuI (58 mg, 0.3 mmol), $Pd(PPh_3)_2Cl_2$ (213 mg, 0.3 mmol) was added and degassed. Further, to the RB, dry THF (5mL) and triethylamine (10 mL) was added and the reaction mixture is stirred at room temperature overnight. The reaction mixture was diluted with chloroform and passed through a short flash column. After removal of the solvent under reduced pressure, the crude product was purified by column chromatography over silica gel (100-200 mesh) using chloroform/hexane (1:3) as an eluent. The product was further purified

by recycling HPLC to obtain 0.3 g of white solid as **L-C2-PE-H** (~72%). ^{1}H NMR (500 MHz, $CDCl_3$, TMS) δ (ppm) 7.47–7.45 (m, 4H), 7.44 (s, 4H), 7.31-7.25 (m, 6H). ^{13}C NMR ($CDCl_3$, 125 MHz, TMS): δ (ppm) 131.65, 131.55, 128.48, 128.41, 123.12, 123.06, 91.24, 89.12. m/z (EI-MS) Calcd for $C_{22}H_{14}$, 278.11; Found, 278.15 $[M]^+$. Anal. Calcd for $C_{22}H_{14}$: C, 94.93; H, 5.07. Found: C, 96.07; H, 5.13.

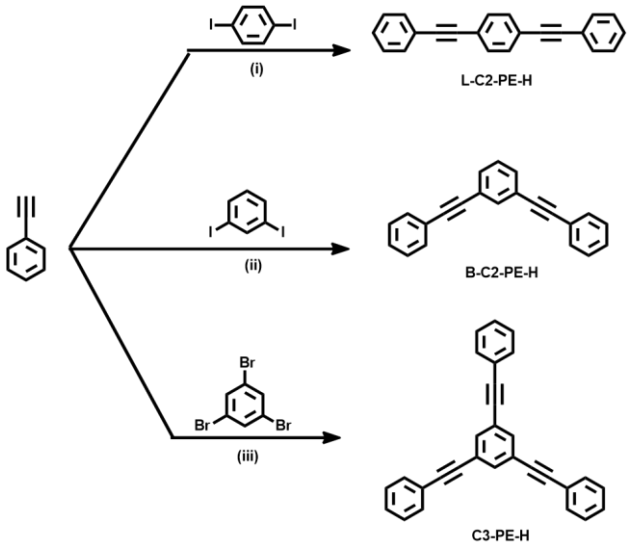

Scheme 2.5: *Provided the detailed scheme on the synthesis of* ***L-C2-PE-H, B-C2-PE-H*** *and* ***C3-PE-H****. (i), (ii), (iii) $Pd(PPh_3)_2Cl_2$, CuI, triethylamine.*

Synthesis of B-C2-PE-H: A mixture of 1,3-diiodobenzene (0.5 g, 1.5 mmol) and phenylacetylene (387 mg, 3.8 mmol), CuI (58 mg, 0.3 mmol), $Pd(PPh_3)_2Cl_2$ (213 mg, 0.3 mmol), was degassed, followed by the addition of dry triethylamine (10 mL) and dry THF (10mL). The reaction mixture was stirred at room temperature overnight. The reaction mixture was diluted with chloroform and passed through a short flash column. After removal of the solvent under reduced pressure, the crude product was purified by column chromatography over silica gel (100-200 mesh) using chloroform/hexane (1:3) as an eluent. The product was further purified by recycling HPLC to obtain 0.28 g white solid of **B-C2-PE-H** (~67%). ^{1}H NMR (500 MHz, $CDCl_3$, TMS) δ (ppm) 7.65 (s, 1H), 7.48-7.46 (dd, 4H), 7.43-7.41 (dd, 2H), 7.31-7.25 (m, 7H). ^{13}C NMR ($CDCl_3$, 125 MHz, TMS): δ (ppm) 133.58, 130.63, 130.25, 127.44, 127.42, 127.36,

122.61, 121.99, 88.94, 87.51. m/z (EI-MS) Calcd for $C_{22}H_{14}$, 278.11; Found, 278.15 $[M]^+$. Anal. Calcd for $C_{22}H_{14}$: C, 94.93; H, 5.07. Found: C, 93.85; H, 5.21.

Synthesis of C3-PE-H: A mixture of 1,3,5-tribromobenzene (1.0 g, 3.2 mmol) and phenylacetylene (1.2 g, 11.4 mmol), CuI (181 mg, 0.95 mmol), $Pd(PPh_3)_2Cl_2$ (0.67 g, 0.95 mmol), was added to a degassed and added with dry triethylamine (20 mL) and dry THF (20 mL). Further the reaction mixture was stirred at room temperature for overnight. The reaction mixture was diluted with chloroform and passed through a short flash column. After removal of the solvent under reduced pressure, the crude product was purified by column chromatography over silica gel (100-200 mesh) using chloroform/hexane (1:3) as an eluent. The product was further purified by HPLC to obtain 0.82 g of white solid of **C3-PE-H** (~69%). ^{1}H NMR (500 MHz, $CDCl_3$, TMS) δ (ppm) 7.59 (s, 3H), 7.48-7.46 (dd, 6H), 7.31-7.28 (m, 9H), 7.31-7.25 (m, 9H). ^{13}C NMR ($CDCl_3$, 125 MHz, TMS): δ (ppm) 133.02, 130.69, 127.59, 127.39, 123.02, 121.79, 89.49, 86.80. m/z (EI-MS) Calcd for $C_{30}H_{18}$, 378.14; Found, 378.15 $[M]^+$. Anal. Calcd for $C_{30}H_{18}$: C, 95.21; H, 4.79. Found: C, 94.95; H, 5.29.

References

1. James, P. V.; Sudeep, P. K.; Suresh, C. H.; Thomas, K. G., Photophysical and Theoretical Investigations of Oligo(p-phenyleneethynylene)s: Effect of Alkoxy Substitution and Alkyne−Aryl Bond Rotations. *J. Phys. Chem. A* **2006,** *110*, 4329-4337.
2. Weder, C.; Voskerician, G., Electronic Properties of PAEs. In *Poly(arylene etynylene)s: From Synthesis to Application*, Weder, C., Ed. Springer Berlin Heidelberg: Berlin, Heidelberg, 2005; pp 209-248.
3. Hu, W.; Zhu, N.; Tang, W.; Zhao, D., Oligo(p-phenyleneethynylene)s with Hydrogen-Bonded Coplanar Conformation. *Org. Lett.* **2008,** *10*, 2669-2672.
4. Chen, Z.; Xue, C.; Shi, W.; Luo, F.-T.; Green, S.; Chen, J.; Liu, H., Selective and Sensitive Fluorescent Sensors for Metal Ions Based on Manipulation of Side-Chain Compositions of Poly(p-phenyleneethynylene)s. *Anal. Chem.* **2004,** *76*, 6513-6518.
5. Sonogashira, K.; Tohda, Y.; Hagihara, N., A convenient synthesis of acetylenes: catalytic substitutions of acetylenic hydrogen with bromoalkenes, iodoarenes and bromopyridines. *Tetrahedron Lett.* **1975,** *16*, 4467-4470.

6. Zalake, P.; Thomas, K. G., Role of Hydrogen Bonding on the Self-Organization of Phenyleneethynylenes on Surfaces. *Langmuir* **2013,** *29*, 2242-2249.
7. Wang, F.; Gillissen, M. A. J.; Stals, P. J. M.; Palmans, A. R. A.; Meijer, E. W., Hydrogen Bonding Directed Supramolecular Polymerisation of Oligo(Phenylene-Ethynylene)s: Cooperative Mechanism, Core Symmetry Effect and Chiral Amplification. *Chem. Eur. J.* **2012,** *18*, 11761-11770.
8. Fernández, Z.; Fernández, B.; Quiñoá, E.; Freire, F., The Competitive Aggregation Pathway of an Asymmetric Chiral Oligo(p-phenyleneethynylene) Towards the Formation of Individual P and M Supramolecular Helical Polymers. *Angew. Chem. Int. Ed.* **2021**, *60*, 9919 .
9. Fiesel, R.; Scherf, U., A chiral poly(para-phenyleneethynylene) (PPE) derivative. *Macromol. Rapid Commun.* **1998,** *19*, 427-431.
10. Kar, S.; Swathi, K.; Sissa, C.; Painelli, A.; Thomas, K. G., Emergence of Chiroptical Properties in Molecular Assemblies of Phenyleneethynylenes: The Role of Quasi-degenerate Excitations. *J. Phys. Chem. Lett.* **2018,** *9*, 4584-4590.
11. Bunz, U. H. F., Poly(aryleneethynylene)s: Syntheses, Properties, Structures, and Applications. *Chem. Rev.* **2000,** *100*, 1605-1644.
12. Bodanszky, M.; Bodanszky, A., Activation and coupling. In *The Practice of Peptide Synthesis*, Springer: 1984; pp 87-150.
13. Valeur, B.; Berberan-Santos, M. N., Absorption of Ultraviolet, Visible, and Near-Infrared Radiation. In *Molecular Fluorescence*, Valeur, B.; Berberan-Santos, M. N., Eds. 2012; pp 31-51.
14. Brouwer, A. M., Standards for photoluminescence quantum yield measurements in solution (IUPAC Technical Report). *Pure Appl. Chem.,* **2011,** *83*, 2213-2228.
15. J.R., L., Fluorescence Anisotropy. In *Principles of Fluorescence Spectroscopy*, Lakowicz, J. R., Ed. Springer US: Boston, MA, 2006; pp 353-382.
16. Ameloot, M.; vandeVen, M.; Acuña, A. U.; Valeur, B., Fluorescence anisotropy measurements in solution: Methods and reference materials (IUPAC Technical Report). *Pure Appl. Chem.,* **2013,** *85*, 589-608.
17. Demchenko, A. P., Weber's Red-Edge Effect that Changed the Paradigm in Photophysics and Photochemistry. In *Perspectives on Fluorescence: A Tribute to Gregorio Weber*, Jameson, D. M., Ed. Springer International Publishing: Cham, 2016; pp 95-141.
18. Lakowicz, J. R., Dynamics of Solvent and Spectral Relaxation. In *Principles of Fluorescence Spectroscopy*, Springer US: Boston, MA, 1999; pp 211-236.
19. Sissa, C.; Painelli, A.; Blanchard-Desce, M.; Terenziani, F., Fluorescence Anisotropy Spectra Disclose the Role of Disorder in Optical Spectra of Branched Intramolecular-Charge-Transfer Molecules. *J. Phys. Chem. B* **2011,** *115*, 7009-7020.
20. Vincent, M.; De Foresta, B.; Gallay, J.; Alfsen, A., Nanosecond fluorescence anisotropy decays of n-(9-anthroyloxy) fatty acids in

dipalmitoylphosphatidylcholine vesicles with regard to isotropic solvents. *Biochemistry* **1982,** *21*, 708-716.

21. Frisch, M. J.; Trucks, G. W.; Schlegel, H. B.; Scuseria, G. E.; Robb, M. A.; Cheeseman, J. R.; Scalmani, G.; Barone, V.; Petersson, G. A.; Nakatsuji, H.; Li, X.; Caricato, M.; Marenich, A. V.; Bloino, J.; Janesko, B. G.; Gomperts, R.; Mennucci, B.; Hratchian, H. P.; Ortiz, J. V.; Izmaylov, A. F.; Sonnenberg, J. L.; Williams; Ding, F.; Lipparini, F.; Egidi, F.; Goings, J.; Peng, B.; Petrone, A.; Henderson, T.; Ranasinghe, D.; Zakrzewski, V. G.; Gao, J.; Rega, N.; Zheng, G.; Liang, W.; Hada, M.; Ehara, M.; Toyota, K.; Fukuda, R.; Hasegawa, J.; Ishida, M.; Nakajima, T.; Honda, Y.; Kitao, O.; Nakai, H.; Vreven, T.; Throssell, K.; Montgomery Jr., J. A.; Peralta, J. E.; Ogliaro, F.; Bearpark, M. J.; Heyd, J. J.; Brothers, E. N.; Kudin, K. N.; Staroverov, V. N.; Keith, T. A.; Kobayashi, R.; Normand, J.; Raghavachari, K.; Rendell, A. P.; Burant, J. C.; Iyengar, S. S.; Tomasi, J.; Cossi, M.; Millam, J. M.; Klene, M.; Adamo, C.; Cammi, R.; Ochterski, J. W.; Martin, R. L.; Morokuma, K.; Farkas, O.; Foresman, J. B.; Fox, D. J. *Gaussian 16 Rev. C.01*, Wallingford, CT, 2016.
22. Harada, N.; Chen, S.-M. L.; Nakanishi, K., Quantitative definition of exciton chirality and the distant effect in the exciton chirality method. *J. Am. Chem. Soc.* **1975,** *97*, 5345-5352.
23. Harada, N.; Nakanishi, K.; Berova, N., Electronic CD Exciton Chirality Method: Principles and Applications. In *Comprehensive Chiroptical Spectroscopy*, Berova, N.; Polavarapu, P. L.; Nakanishi, K.; Woody, R. W., Eds. 2012; pp 115-166.
24. Zhao, X.; Schanze, K. S., Meta-Linked Poly(phenylene ethynylene) Conjugated Polyelectrolyte Featuring a Chiral Side Group: Helical Folding and Guest Binding. *Langmuir* **2006,** *22*, 4856-4862.

Chapter 3

Supramolecular chirality: A caveat in assigning the handedness of chiral aggregates

3.1 Abstract

The handedness of a supramolecular chiral aggregates is often assigned based on the sign of the circular dichroism spectra, adopting the exciton chirality method (ECM) proposed by Nakanishi and Harada.[1] However, the method does not properly account for the nature of intermolecular interactions. In this work, the ECM is re-examined, considering different chiral aggregates, having repulsive or attractive intermolecular interactions. CD spectra of chiral aggregates are calculated in the framework of the exciton model, and results are supported by TD-DFT calculations.

3.2.1 Interactions in aggregates

Molecules come together by invoking various types of interactions such as hydrogen bonding, van der Waals interaction, π-π interactions, hydrophobic interactions etc. to form aggregates. Theoretical and experimental studies of the supramolecular organization of molecules in aggregates and macroscopic structures have substantially contributed to our understanding of their intriguing photophysical properties. In the 1930s, Kuhn proposed the coupled oscillator theory which was later extended by Davydov to treat excitonic effects in molecular crystals.[2] Kasha and McRae related the sign of the interaction energy to their dipole arrangement leading to the development of the exciton model.[3] According to the arrangement of the monomeric units in these aggregates, they are broadly divided into three groups: (i) H-aggregate and (ii) J- aggregate, aligned aggregates, which are symmetric and (iii) twisted aggregates which are asymmetric in nature.[4-5] In H-aggregates, monomers are arranged in a head-to-head fashion whereas in J-aggregate they are arranged in a

head-to-tail fashion such that the angle between the dimers (θ) is 0° in former and 180° in the latter case respectively (Figure 3.1).[4] The intermolecular interaction energy acting on H-aggregates is repulsive (V>0), while on J-aggregates, it is attractive in nature (V<0).[4]

Excitonic interaction between two or more molecules in a crystal or aggregate results in the splitting of their excited state, known as Davydov splitting.[6] This happens because the degeneracy of the excited state of the identical molecules in the crystal/aggregate is lost due to excitonic interactions. Such non-degenerate excited states bring about interesting optical properties in aggregates.

The exciton model considers a single excited state per molecule and only accounts for intermolecular interactions between degenerate states. In the dipolar approximation, the interaction between transition dipole moments on nearby molecules is the driving force for the delocalization of the molecular excitation and the redistribution of oscillator strength (exciton coupling). In a dimer composed of two equivalent molecules, the two degenerate excited states where either one of the two molecules is excited, recombine due to intermolecular interactions into two new states, corresponding to the in-phase and out of phase combination of the two original states. The new states are separated by an energy gap equal to twice the interaction energy (V) between the transition dipoles (Figure 3.1). For aggregates of perfectly aligned molecules, optical transitions are only allowed towards states where all dipoles oscillate in phase, resulting in (i) a red-shift (bathochromic shift) of absorption and fluorescence bands in J-aggregates and (ii) a blue-shift (hypsochromic shift) of the absorption band in H-aggregates, as shown in Figure 3.1. In H-aggregates, a large suppression of fluorescence intensity is also observed.

Our interest is mainly focused on twisted aggregates: here, the molecules are arranged at an angle between the 0° and 180°, and the chiral aggregates fall into this category (Figure3.1). The advantage here is that unlike H- and J-aggregate, transitions to both the exciton coupled states are electronically allowed. In the absorption spectra,

such an aggregate provides two electronic transitions (even if apparently a single absorption band is observed).

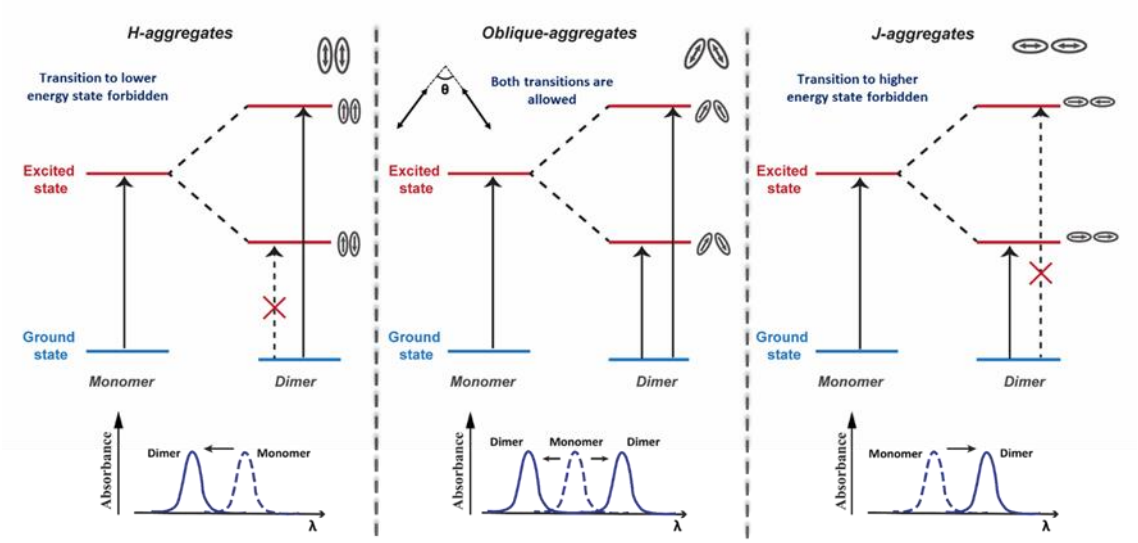

***Figure 3.1**: Spectral shift and arrangement of transition dipoles in an exciton coupled dimer of identical chromophores is presented. The excited states split on exciton coupling. Transitions are only allowed if the vectorial sum of transition dipoles is different from zero. Allowed and forbidden transitions are represented in solid and broken arrows, respectively. The different types of aggregates include aligned (H- and J-) and twisted and are differentiated by the sign of the interaction, V, in the case of aligned dimers. Absorption spectra, highlighting the exciton shifts, are sketched in the bottom panels. Left column: H-aggregates have repulsive interactions (V>0), the bright state is formed in the short wavelength region (blue shift) with respect to the monomer; Middle column: for twisted geometry, V can be either positive or negative, depending on geometrical details, and both exciton states are optically allowed (leading to the formation of two absorption peaks on both sides of the monomer absorption whose relative intensity depends on the geometry); Right column: J-aggregates have attractive interactions (V<0) and the bright state is formed in the long wavelength region (red shift) with respect to the monomer.*

3.2.2 The exciton chirality method

Nakanishi and Harada brought out the implications of exciton coupling in chiral aggregates, providing the basis of the exciton chirality (EC) rule.[1, 7-8] The rule relates the sign of the states to the handedness of the assembly. The simplicity and effectiveness of the exciton model are exploited by Nakanishi and Harada in their classic work of 1969 to develop the dibenzoate chirality rule, which later became the basis for the exciton chirality rule.[1, 7] The rule states that states "if the exciton circular dichroism (CD) shows a positive (negative) first and a second negative (positive)

cotton effect, then the two electric transition dipole moments constitute a clockwise (anti-clockwise) screw sense."[8] Another method available to determine the absolute configuration (AC) of the bichromophoric molecular system was the X-ray Bijvoet method.[9] The method was first used to study the AC of (+)-tartaric acid, employing the anomalous scattering effect of heavy atoms in X-ray crystallographic diffraction experiments. But the ease of using the exciton model made it popular among scientists.

Despite caution that the rule does not have general validity, the EC rule became the method of choice for chemists and biologists to experimentally determine the absolute handedness of chiral supramolecular and nanoscopic structures.[10-11] Recently, a few exceptions to the EC rule were highlighted: they were ascribed to conformational disorder or strong transition magnetic dipoles.[12] Pescitelli showed using Laucysteinamide A as an example that when the molecule does not possess axial symmetry and exists in more than one conformation, the EC rule should be applied with caution.[13] In fact, the presence of multiple conformers demands the exciton-coupled CD to be a weighted average of all possible conformers. Moreover, in the case of chromophores like thiazoline ring, the transition dipole can be aligned in any plane, thus making the application of the EC rule further difficult. In another example, Mennucci and co-workers showed that in the molecule (1,1'-bis-phenanthrenes) with a high value of magnetic dipoles, it is essential to consider their influence as well.[12] The exciton chirality rule for vibrational circular dichroism has been recently discussed by Polavarapu and co-workers to highlight its limitations and potentials.[14-15] From these above articles, the authors remind the scientific community against the usage of the EC rule without ensuring the nature of chromophore, and the CD signal

The objective of the work carried out herein is to re-examine the EC rule for electronic circular dichroism, focusing on the relation between the sign of ECD spectra and the absolute chirality of the supramolecular system. For this purpose, two different types of chiral dimers, namely simple helix and creeper-helix (Figure 3.2) are

chosen and their chiroptical properties are explored using the exciton model and TD-DFT calculations. In addition, the applicability of the exciton model to predict the properties of bigger chiral aggregates is also investigated.

3.3 Theoretical details

In order to reassess the EC rule, exciton model results are compared with the state-of-the-art quantum chemical calculations. A linear phenyleneethynylene dye (PE, Figure 3.2A), which is a rigid-rod-like molecule characterized by a single low-lying excited state, is selected as the molecular building block for the supramolecular structure. The details of both the exciton model and TD-DFT calculation are provided below.

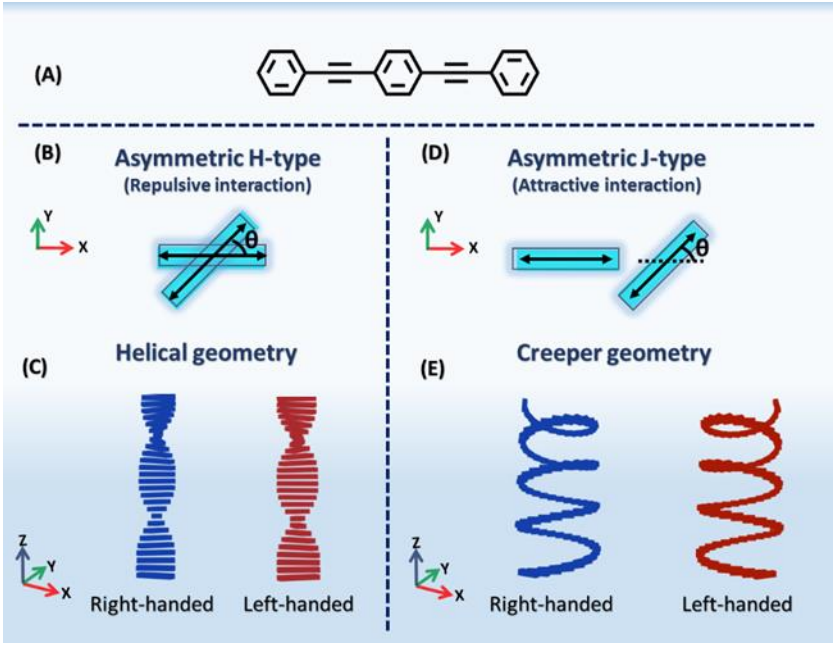

***Figure 3.2**: (A) Molecular structure of phenyleneethynylene (PE) used for creating helical and creeper geometries. PE possesses one transition dipole (TD) along its longitudinal axis, represented by a double-sided arrow. A top view of different chiral dimers with tilt angle θ (B,D) and three-dimensional sketch of larger aggregates (C,E). In all cases, both right- and left-handed geometries are shown. (B,C) denote asymmetric H-type stacking with repulsive interactions, and (D,E) denote asymmetric J-type stacking with attractive interactions.*[16]

3.3.1 Exciton model for a dimer

The monomer of the molecule is modeled taking into account only 2 states: a ground and an excited state, $|\boldsymbol{g}\rangle$ and $|\boldsymbol{e}\rangle$ respectively, separated by a transition energy E. The

model is applied to the phenyleneethynylene (PE) molecule reported in Figure 3.2A. Both states are non-polar, so that the only matrix element of the dipole moment is:

$$\vec{\mu} = \langle g|\hat{\vec{\mu}}|e\rangle \qquad (3.1)$$

In a dimer composed of two equivalent molecules (A and B in the following), we, consider four basis states:

- $|\boldsymbol{g_A g_B}\rangle$ where the two molecules are in the ground state. The energy of this state is set to be 0

- $|\boldsymbol{e_A g_B}\rangle$, $|\boldsymbol{g_A e_B}\rangle$, where one of the molecules is in the ground state and the other is in the excited state. These basis states are degenerate, and their energy is E

- $|\boldsymbol{e_A e_B}\rangle$, where both the molecules are in the excited state. The energy of this state is 2E

The Hamilton matrix can be expressed as:

$$H = \begin{bmatrix} 0 & 0 & 0 & 0 \\ 0 & E & V & 0 \\ 0 & V & E & 0 \\ 0 & 0 & 0 & 2E \end{bmatrix}$$

where V represents the intermolecular interaction energy. In the exciton model we only account for the mixing due to electrostatic intermolecular interactions between the two degenerate states$|e_A g_B\rangle$, $|g_A e_B\rangle$. Upon diagonalization, two states stay unmixed, the ground state$|G\rangle = |g_A g_B\rangle$ and the doubly excited state, $|E_E\rangle = |e_A e_B\rangle$. The two degenerate states are mixed in the symmetric (in-phase) $|E_+\rangle = \frac{1}{\sqrt{2}}(|e_A g_B\rangle + |g_A e_B\rangle)$ and antisymmetric (out-of-phase) $|E_-\rangle = \frac{1}{\sqrt{2}}(|e_A g_B\rangle - |g_A e_B\rangle)$ combinations.[17] The eigenvalues derived from the above Hamiltonian, H, corresponds to the energy of the dimeric states: the energy of the ground state stays 0, as well as the energy of the doubly excited state, remains 2E, since they are both unmixed. The energy of the singly excited states is $E \pm V$: the coupling between two monomers results in two new states, lowered and raised in energy by a factor, V, corresponding to the interaction

energy. As schematically shown in Figure 3.3, the relative energy of the in-phase and out-of-phase states depends on the sign of the electrostatic interaction between the transition dipole moments on the two molecules, with the in-phase state lying lower (higher) in energy for the attractive (repulsive) interactions. Consequently, we observe different optical properties from the two aligned aggregates which are explained in the previous sections.

In the point-dipole approximation, valid for intermolecular distances larger than the molecular dimension, the intermolecular interaction energy V is estimated as the interaction energy between two transition dipoles located at monomers A and B. V is derived as:

$$V = \frac{\overrightarrow{\mu_A}.\overrightarrow{\mu_B}}{4\pi\varepsilon_0\eta^2 r^3} - \frac{3(\overrightarrow{\mu_A}.\hat{r})(\overrightarrow{\mu_B}.\hat{r})}{4\pi\varepsilon_0\eta^2 r^5} \qquad (3.2)$$

where ε_0 is the vacuum permittivity, n is the medium refractive index and $\vec{r}$ is the vector that connects the two molecular centres. Finally, $\mu_{A/B}$ is the transition dipole moment for the two molecules.

In exciton model calculations, the monomer transition energy E and $\mu_{A/B}$ are set to the value calculated in TD-DFT (see Section 3.3.2 for details) for an isolated PE molecule. Simultaneously, the squared refractive index (η^2) is fixed to reproduce the exciton splitting calculated in TD-DFT for the aligned dimer. The resulting values (2.48 and 2.31 for helix and creeper, respectively) are in line with typical values for organic materials.[18] In the exciton model calculations, the refractive index is needed to account for the screening effects of the electrons, which are not involved in the transitions (they are not accounted for in the exciton picture, while they are present in TD-DFT calculations). Moreover, this procedure allows to phenomenologically correct the inaccuracies of the dipolar approximation.

For a dimer, the dipole moment operator is the vectorial sum of the two dipole moments and is given by:

$$\hat{\vec{\mu}} = \widehat{\vec{\mu_A}} + \widehat{\vec{\mu_B}} \qquad (3.3)$$

Accordingly, the transition dipole moment in the dimer can be written as the vectorial sum of the transition dipole moments associated with the two dyes:

$$\langle G|\hat{\vec{\mu}}|E_-\rangle = \langle G|\widehat{\vec{\mu_A}}|E_-\rangle + \langle G|\widehat{\vec{\mu_B}}|E_-\rangle \qquad (3.4)$$

$$\langle G|\hat{\vec{\mu}}|E_+\rangle = \langle G|\widehat{\vec{\mu_A}}|E_+\rangle + \langle G|\widehat{\vec{\mu_B}}|E_+\rangle \qquad (3.5)$$

$$\langle G|\hat{\vec{\mu}}|E_E\rangle = \langle G|\widehat{\vec{\mu_A}}|E_E\rangle + \langle G|\widehat{\vec{\mu_B}}|E_E\rangle \qquad (3.6)$$

The orthogonality of the |g> and |e> states of the monomer guarantees for a vanishing $\langle G|\hat{\vec{\mu}}|E_E\rangle$ transition dipole moment.

Explicit expressions of the transition dipole moments read:

$$\vec{\mu}_{-,A} = \langle G|\widehat{\vec{\mu_A}}|E_-\rangle = \frac{1}{\sqrt{2}}\overrightarrow{\mu_A} \qquad (3.7)$$

$$\vec{\mu}_{-,B} = \langle G|\widehat{\vec{\mu_B}}|E_-\rangle = -\frac{1}{\sqrt{2}}\overrightarrow{\mu_B} \qquad (3.8)$$

$$\vec{\mu}_{+,A} = \langle G|\widehat{\vec{\mu_A}}|E_+\rangle = \frac{1}{\sqrt{2}}\overrightarrow{\mu_A} \qquad (3.9)$$

$$\vec{\mu}_{+,B} = \langle G|\widehat{\vec{\mu_B}}|E_+\rangle = \frac{1}{\sqrt{2}}\overrightarrow{\mu_B} \qquad (3.10)$$

where $\vec{\mu}_A = \langle g_A|\widehat{\vec{\mu_A}}|e_A\rangle$ and $\vec{\mu}_B = \langle g_B|\widehat{\vec{\mu_B}}|e_B\rangle$

3.3.2 TD-DFT calculations

The TD-DFT calculations are performed using the Gaussian 16[19] suite of programs. All the calculations at the DFT level are carried out using the CAM-B3LYP functional and 6-31G(d) as the basis set in the gas phase. To investigate the chiroptical properties of the aggregates using TD-DFT calculation, the ground state of the monomer is optimized first. Further calculations were performed by simply arranging the monomers in a helical and creeper arrangement without optimizing the geometry of dimers or other higher assemblies. For the helix geometry, the intermolecular distance along z is fixed as 10 Å, maintaining the molecular centre at x=y=0. In the

creeper geometry, the intermolecular distance along Z-axis is set to be 5 Å, and the molecular centre is displaced by 12 Å along X. In the helix, repulsive interactions among transition dipole moments make the E_- state lower in energy (Figure 3.2). On the contrary, in the creeper, the X-displacement is large enough to guarantee attractive interactions and the E_+ state becomes the lower energy state.

3.3.3 Chiral Dimer: calculation of CD spectra

Interestingly, the twisted arrangement of the molecules gives rise to chiral responses, and spectral features are dictated by the rotational strength, which is analogous to the oscillator strength in the absorption spectrum (see Section 1.3). The exciton model is instrumental in understanding the basic features of circular dichroic (CD) signals exhibited by twisted aggregates. Rotational strengths associated with the different singly excited states, E_i is:[20]

$$R_i = -\frac{\omega_i}{2}\,\vec{r}\cdot\left(\vec{\mu}_{i,A}\times\vec{\mu}_{i,B}\right) \qquad (3.11)$$

where i counts on the two excitonic states, i= -,+, and ω_i is the corresponding transition frequency. For E+ and E- states, the rotational strength results:

$$R_- = +\frac{\omega_-}{4}\,\vec{r}\cdot(\vec{\mu}_A\times\vec{\mu}_B) \qquad (3.12)$$

$$R_+ = -\frac{\omega_+}{4}\,\vec{r}\cdot(\vec{\mu}_A\times\vec{\mu}_B) \qquad (3.13)$$

CD spectra are calculated assigning a Gaussian band shape to the two transitions (with standard deviation σ = 0.35 eV) using equation 3.14,[21]

$$\Delta\varepsilon(\tilde{\nu}) = \sum_{i=1}^{n}\left(\frac{R_i\,\tilde{\nu}_i}{2.296\times10^{-39}\sqrt{\pi}\,\sigma}\exp\left[-\left\{\frac{\tilde{\nu}-\tilde{\nu}_i}{\sigma}\right\}^2\right]\right), \qquad (3.14)$$

where i count the electronic excitations, R_i is the corresponding rotational strength and $\tilde{\nu}_i$ is the transition wavenumber in nm^{-1} (for TD-DFT calculation, the same expression is used to calculate the CD spectra, where the rotational strength is derived from the output of calculation).

3.4 Results and discussion

The monomeric characteristics of the PE molecule were investigated employing DFT/TD-DFT calculations. The ground state of the molecule is optimized at the DFT level (details are given above), and we performed a TD-DFT calculation to obtain the transition energies and the dipole moment of the monomer. The lowest energy transition is calculated at 313.13 nm with a transition dipole moment of 11.28 Debye, adopted for the exciton model calculation in studying the chiral aggregates.

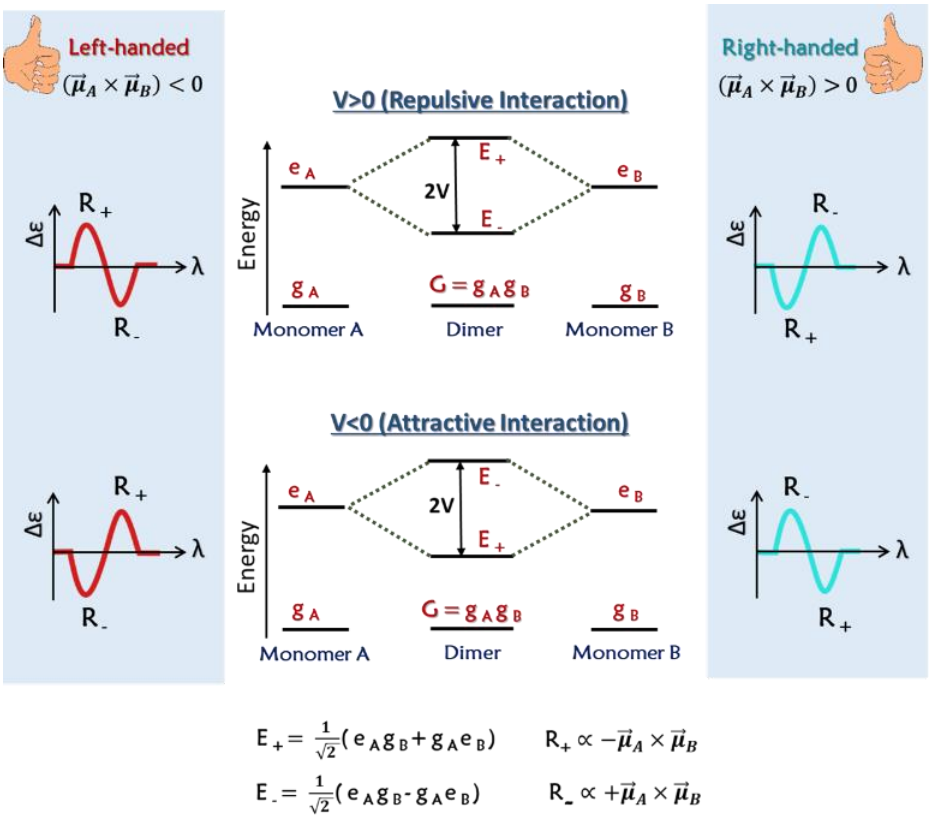

Figure 3.2: *Schematic representation of the energy diagram for dimers with repulsive and attractive interactions using exciton model and corresponding bisignated circular dichroic (CD) spectrum for right- and left-handed dimers. The shaded left and right columns show the bisignated CD of the dimeric structures, organized in left- and right-handed fashion, respectively. The central column shows the energy level diagram for dimers with repulsive (V>0; top panel) and attractive (V<0; bottom panel) interactions.*[16]

PE does not have a chiral centre but can be designed to form chiral supramolecular assemblies (Figure 3.2). Specifically, two different supramolecular assemblies are considered where PEs (frozen ground state geometry is calculated for the isolated dye)

are arranged in a simple-helix (asymmetric H-type) and creeper-helix geometry (asymmetric J-type) as in Figure 3.2C,E. Henceforth simple-helix and creeper-helix geometries are denoted as helix and creeper, respectively. In both geometries, the twist angle between the monomers (θ, see Figure 3.2B,D) is varied from 10° to 80° (at 0° and 90°, the system is non-chiral and CD signals vanish). As a representative example, Table 3.1 and 3.2 show the transition energy, oscillator strength (f), and rotational strength (R) calculated using TD-DFT and exciton model for right-handed helical and creeper dimers with various tilt angles, respectively.

Table 3.1 *Oscillator strength (f) and rotational strength (R) of electronic transition in dimer at angles 10° - 90° in helical and creeper-helical geometry calculated using TD-DFT calculations.*

Right-handed helix: TD-DFT calculations						
Angle	Helical geometry			Creeper-helical geometry		
	Trans. Energy eV	f	R ($\times 10^{-54}$) $C^2m^3s^{-1}$	Trans. Energy eV	f	R ($\times 10^{-54}$) $C^2m^3s^{-1}$
10 °	3.93	0.03	359.85	3.93	3.85	-185.02
	3.99	3.66	-358.05	3.98	0.03	174.31
20°	3.93	0.11	708.77	3.93	3.76	-363.23
	3.99	3.58	-705.24	3.97	0.11	345.07
30 °	3.93	0.25	1036.18	3.94	3.61	-528.50
	3.98	3.45	-1030.86	3.97	0.25	506.59
40 °	3.93	0.43	1331.98	3.94	3.41	-675.78
	3.98	3.26	-1325.33	3.97	0.43	654.04
50 °	3.94	0.66	1586.88	3.94	3.16	-801.50
	3.98	3.04	-1579.81	3.97	0.67	782.23
60 °	3.94	0.93	1793.22	3.95	2.89	-901.09
	3.97	2.78	-1786.53	3.96	0.94	898.72
70 °	3.95	1.22	1944.50	3.95	2.58	-968.97
	3.97	2.49	-1939.47	3.96	1.24	958.57
80 °	3.95	1.22	1944.50	3.95	2.58	-968.97
	3.97	2.49	-1939.47	3.96	1.24	958.57
90 °	3.95	1.53	2036.46	3.95	2.25	-980.73
	3.96	2.18	-2033.70	3.96	1.57	974.88

For small twist angles in the helix arrangement, the oscillator strength is mainly concentrated in the high energy state, while the opposite occurs for the creeper dimer.

This is in line with the exciton model for aligned molecules (θ=0°), which predicts that only a transition from the ground state to the E_+ state is allowed. Upon increasing θ, the oscillator strength redistributes between E_+ and E_- states. TD-DFT results in Figure 3.4A,C,G,E demonstrate that the absolute sign of CD spectra in the long-wavelength region is positive for right-handed in helix and left-handed in creeper, confirming that the sign of the CD spectra indeed changes with the sign of the interaction energy. These results clearly indicate that the chirality rule holds for aggregates with repulsive interactions (helix); however, it fails for aggregates with attractive interactions (creeper).

Table 3.2: *Calculated the oscillator strength (f) and rotational strength (R) of the electronic transitions possible in a dimer at various twist angles (10° - 80°) in helical and creeper geometry using exciton model.*

Right-handed helix: Exciton model						
Angle	Helical			Creeper		
	Trans. energy eV	f	R ($\times 10^{-54}$) $C^2m^3s^{-1}$	Trans. energy eV	f	R ($\times 10^{-54}$) $C^2m^3s^{-1}$
10°	3.93	0.03	366.65	3.94	3.79	-183.68
	3.99	3.83	-372.55	3.98	0.03	185.92
20°	3.93	0.12	722.43	3.94	3.7	-361.88
	3.99	3.75	-733.50	3.98	0.12	366.09
30°	3.93	0.26	1056.75	3.94	3.56	-529.27
	3.99	3.61	-1071.68	3.98	0.26	534.95
40°	3.94	0.45	1359.64	3.94	3.37	-680.84
	3.99	3.41	-1376.61	3.98	0.45	687.29
50°	3.94	0.68	1621.98	3.94	3.13	-812.01
	3.98	3.17	-1638.96	3.98	0.69	818.46
60°	3.94	0.96	1835.81	3.95	2.87	-918.80
	3.98	2.89	-1850.74	3.97	0.96	924.47
70°	3.95	1.26	1994.53	3.95	2.57	-997.93
	3.97	2.58	-2005.61	3.97	1.26	1002.14
80°	3.95	1.58	2093.14	3.96	2.25	-1046.92
	3.97	2.25	-2099.04	3.96	1.59	1049.17

Figure 3.5 shows the CD spectra of dimer in the helical and creeper arrangement, but having a left-handed assembly and the tilt angle is again varied from 10° - 80°: as expected, we obtain exactly the same results as for right-handed helix (Figure 3.4), but

with opposite sign. The intensity of calculated CD signals increases from 10° to 40°, then it decreases and vanishes at 90°, wherein the system becomes achiral. The sizable rotational strengths calculated in the θ = (50°- 80°) range are indeed associated with weak CD signals (Figure 3.3 and 3.4, E-H) due to the mutual cancellation of positive and negative CD signals from two states coming very close in energy. In order to have a quantitative comparison of TD-DFT results with the exciton model, squared refractive index (η^2) are fixed to values (2.48 and 2.31 for helix and creeper, respectively) which are in line with typical values for organic materials.[22] Results obtained from the exciton model (Figure 3.4 and 3.5 B,D,F,H) are in line with TD-DFT calculations, and confirm that the chirality rule as commonly defined only applies to chiral aggregates with repulsive interactions and cannot be generalized.

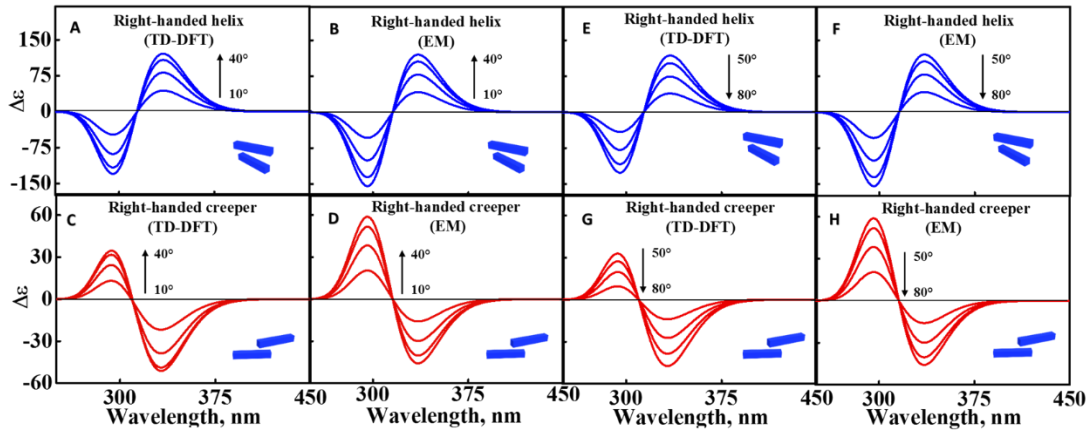

Figure 3.3: *Calculated CD spectra of the right-handed dimer with repulsive (A,B,E,F) and attractive interactions (C,D,G,H). Spectra are shown for twist angle varying from 10° - 40° (A-D) and 50° - 80° (E-H) in 10° increment. Panels (A,C) and (E,G) show TD-DFT while panels (B,D) and (F,H) show exciton model results, respectively.*

Further investigations on the CD response of a trimeric assembly in helical and creeper geometry (Figure 3.6) are also carried out. These results are again in line with the previous discussions, proving that the exciton model is fully consistent with TD-DFT results.

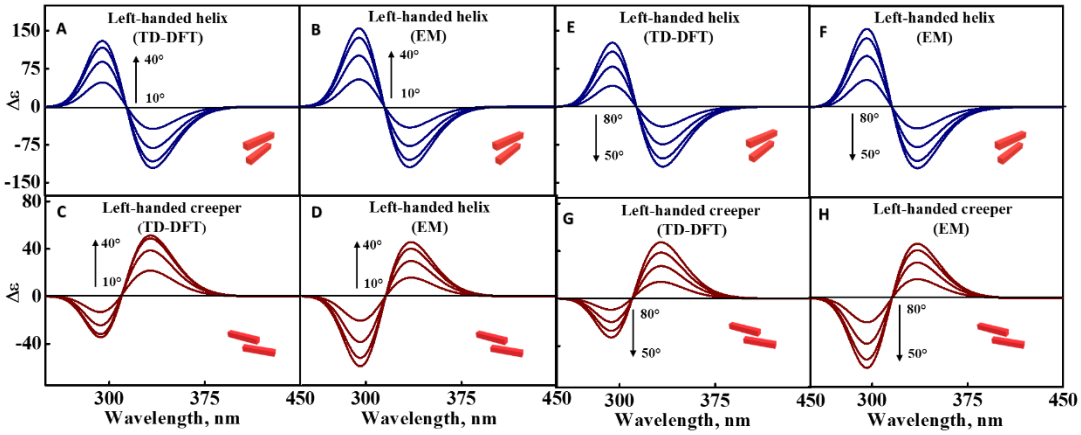

Figure 3.4: *Calculated CD spectra of the left-handed dimer with repulsive (A,B,E,F) and attractive interactions (C,D,G,H). Spectra are shown for twist angle varying from 10° - 40° (A-D) and 50° - 80° (E-H) in 10° increment. Panels (A,C) and (E,G) show TD-DFT while panels (B,D) and (F,H) show exciton model results, respectively.*

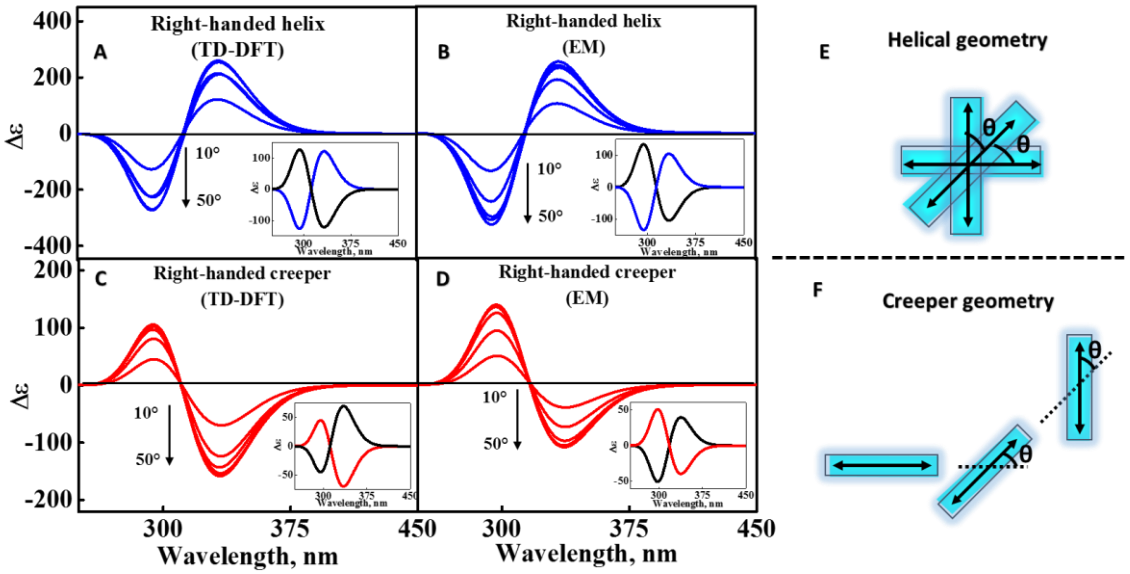

Figure 3.5: *Calculated the CD spectra of right-handed helical (A,B) and creeper (C,D) trimer at θ (10° - 50°) using TD-DFT (A,C) and exciton model (B,D) calculations. For simplicity, only the CD spectra from right-handed arrangement is provided but in the inset of all the graphs the CD spectra for a trimer at a tilt angle of 10° in the right-handed fashion (blue trace for helix and red trace for creeper) and left-handed fashion (black trace) is presented. The tilt angle (θ) between the interacting dipoles are defined in the helical (E) and creeper (F) trimeric assembly in a two-dimensional arrangement. The intermolecular distance between molecules along z is 10 Å for the helix and 5 Å for the creeper.*

Having validated the exciton model against TD-DFT results for small aggregates, the exciton model is now exploited to study the chiroptical response of larger aggregates.

Figure 3.7 reports the results for an aggregate constituted by ten molecules arranged in helix and creeper structures using the same geometrical parameters as defined for the dimer. Once again, the exciton chirality rule is obeyed in the helix geometry and is broken in the creeper geometry. Of course, when ten molecules are put together, the exciton model predicts ten excited states. Nevertheless, Figure3.7 confirms that only two transitions mainly contribute to the CD spectrum, while the remaining transitions have negligible rotational strengths. In helical geometry, the main contribution to the CD spectra is associated with states lying at higher energies (shorter wavelength). In contrast, states lying at lower energies (longer wavelength) are the dominant contributors to the creeper geometry. Thus, for a supramolecular assembly even if there are 'n' number of molecules and consequently 'n' number of higher energy states, the CD spectrum gives only a single CD couplet (provided there is single transition dipole moment, and exciton coupling is possible).

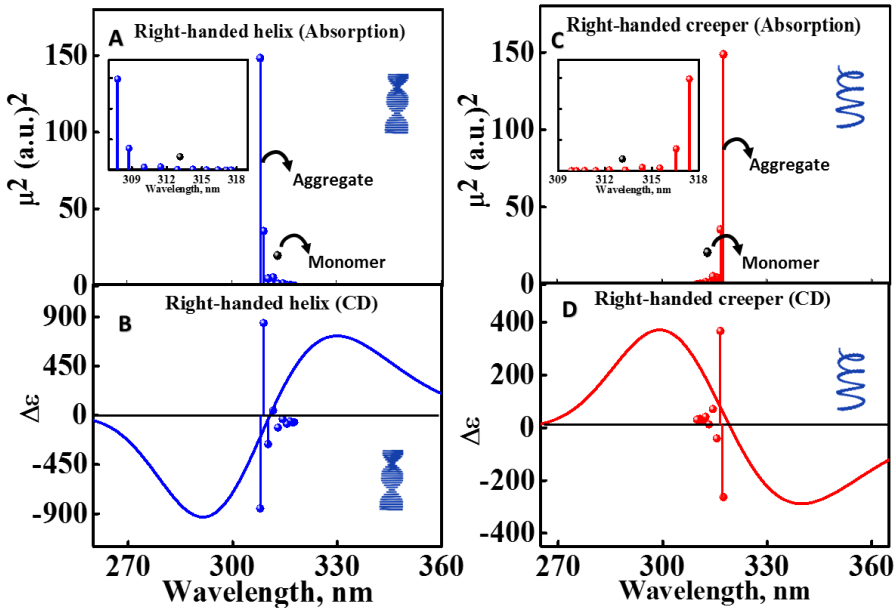

Figure 3.6: *Exciton model calculations for a molecular aggregate of ten molecules (twist angle: 10°). Top panels (A,C): squared transition dipole moment of the monomer (black sphere) and the molecular aggregate (blue for helix and red for creeper). Insets show the same data on a zoomed scale. Bottom panels (B,D): CD spectrum of the molecular aggregate. Rotational strengths are shown as spheres (blue for helix and red for creeper) for each individual transition*

on the aggregate. Left panels (A,B) and right panels (C,D) refer to right-handed helix and creeper, respectively.

The calculations are repeated for different twist angles like 45° and 80°; the results are consistent, and the corresponding figures are provided (Figure 3.8). Moreover, change in the sign of the bisignated CD spectrum (also referred to as the crossover point) of a chiral aggregate is observed in the spectral region where the absorption of the aggregate is maximum, i.e., to the blue (shorter wavelength) and the red (longer wavelength) of the monomer absorption band for the helix and creeper, respectively.

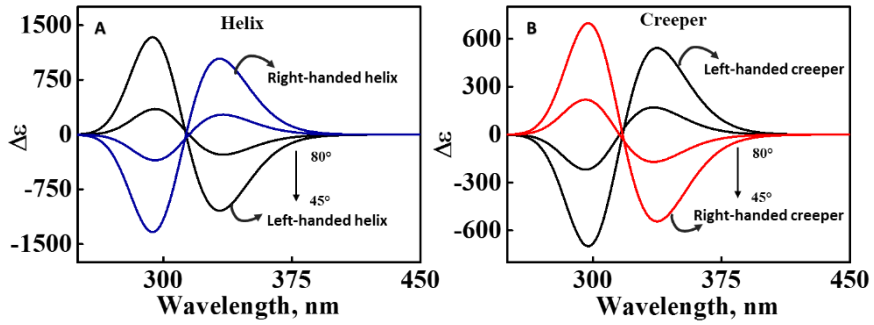

Figure 3.7: *Estimated the CD spectra of a chiral aggregate in helical (A) and creeper (B) geometry arranged in right-handed (blue trace for helical and red trace for creeper) and left-handed (black trace) fashion with a tilt angle of 45° and 80°.*

3.5 Conclusions

From the above studies, it is well established that in supramolecular chiral aggregates, the sign of the CD couplet depends not only on the handedness of the aggregate but also on the sign of the interaction energy between neighboring dipoles. The exciton chirality rule does not account for the sign of interactions and is valid only for aggregates in which adjacent dipoles have repulsive interaction energy. Hence, when assigning the handedness of a chiral assembly based on the sign of the CD couplet, care should be given to understand the nature of interaction energy before employing the exciton chirality rule. It can be seen in the literature that incorrect reports on the absolute configuration of chiral molecules, particularly for natural products, have led to the wrong interpretation of chiral signature, which was later corrected. The results presented herein provide more insight into the widely used

exciton chirality method by reminding the scientific community that the interaction energy of the supramolecular assembly must also be considered while using the exciton chirality rule. The generalizations on the handedness of chiral supramolecular aggregates reported here based on the sign of CD spectra are indeed valuable for researchers working in the broad areas of chemistry and biology.

References

1. Harada, N.; Chen, S.-M. L.; Nakanishi, K., Quantitative definition of exciton chirality and the distant effect in the exciton chirality method. *J. Am. Chem. Soc.* **1975,** *97* (19), 5345-5352.
2. Davydov, A., *Theory of molecular excitons*. Springer: 2013.
3. Hochstrasser, R. M.; Kasha, M., Application of the exciton model to mono-molecular lamellar sytems. *Photochem. Photobiol.* **1964,** *3* (4), 317-331.
4. Kasha, M., Energy Transfer Mechanisms and the Molecular Exciton Model for Molecular Aggregates. *Radiat Res.* **2012,** *178* (2).
5. Thomas, R.; Kumar, J.; George, J.; Shanthil, M.; Naidu, G. N.; Swathi, R. S.; Thomas, K. G., Coupling of Elementary Electronic Excitations: Drawing Parallels Between Excitons and Plasmons. *J. Phys. Chem. Lett.* **2018,** *9* (4), 919-932.
6. Kasha, M., Molecular Excitons in Small Aggregates. In *Spectroscopy of the Excited State*, Di Bartolo, B.; Pacheco, D.; Goldberg, V., Eds. Springer US: Boston, MA, 1976; pp 337-363.
7. Harada, N.; Nakanishi, K., Optical rotatory power of the benzoate group. *J. Am. Chem. Soc.* **1968,** *90* (26), 7351-7352.
8. Harada, N.; Nakanishi, K.; Berova, N., Electronic CD Exciton Chirality Method: Principles and Applications. In *Comprehensive Chiroptical Spectroscopy*, Berova, N.; Polavarapu, P. L.; Nakanishi, K.; Woody, R. W., Eds. 2012; pp 115-166.
9. Blow, D. M., How Bijvoet Made the Difference: The Growing Power of Anomalous Scattering. In *Methods in Enzymology*, Academic Press: 2003; Vol. 374, pp 3-22.
10. Polavarapu, P. L., Molecular Structure Determination Using Chiroptical Spectroscopy: Where We May Go Wrong? *Chirality* **2012,** *24* (11), 909-920.
11. Polavarapu, P. L., *Chiroptical spectroscopy: fundamentals and applications*. Crc Press: 2016.
12. Jurinovich, S.; Guido, C. A.; Bruhn, T.; Pescitelli, G.; Mennucci, B., The role of magnetic–electric coupling in exciton-coupled ECD spectra: the case of bis-phenanthrenes. *Chem. Commun.* **2015,** *51* (52), 10498-10501.
13. Pescitelli, G., For a correct application of the CD exciton chirality method: the case of laucysteinamide A. *Mar. Drugs* **2018,** *16* (10), 388.

14. Covington, C. L.; Nicu, V. P.; Polavarapu, P. L., Determination of the Absolute Configurations Using Exciton Chirality Method for Vibrational Circular Dichroism: Right Answers for the Wrong Reasons? *J. Phys. Chem. A* **2015,** *119* (42), 10589-10601.
15. Polavarapu, P. L., Structural Analysis Using Chiroptical Spectroscopy: Insights and Cautions. *Chirality* **2016,** *28* (6), 445-452.
16. Swathi, K.; Sissa, C.; Painelli, A.; Thomas, K. G., Supramolecular chirality: a caveat in assigning the handedness of chiral aggregates. *Chem. Commun.* **2020,** *56* (59), 8281-8284.
17. Anzola, M.; Di Maiolo, F.; Painelli, A., Optical spectra of molecular aggregates and crystals: testing approximation schemes. *Phys. Chem. Chem. Phys.* **2019,** *21* (36), 19816-19824.
18. Yang, Y.; da Costa, R. C.; Fuchter, M. J.; Campbell, A. J., Circularly polarized light detection by a chiral organic semiconductor transistor. *Nature Photonics* **2013,** *7* (8), 634-638.
19. Frisch, M. J.; Trucks, G. W.; Schlegel, H. B.; Scuseria, G. E.; Robb, M. A.; Cheeseman, J. R.; Scalmani, G.; Barone, V.; Petersson, G. A.; Nakatsuji, H.; Li, X.; Caricato, M.; Marenich, A. V.; Bloino, J.; Janesko, B. G.; Gomperts, R.; Mennucci, B.; Hratchian, H. P.; Ortiz, J. V.; Izmaylov, A. F.; Sonnenberg, J. L.; Williams; Ding, F.; Lipparini, F.; Egidi, F.; Goings, J.; Peng, B.; Petrone, A.; Henderson, T.; Ranasinghe, D.; Zakrzewski, V. G.; Gao, J.; Rega, N.; Zheng, G.; Liang, W.; Hada, M.; Ehara, M.; Toyota, K.; Fukuda, R.; Hasegawa, J.; Ishida, M.; Nakajima, T.; Honda, Y.; Kitao, O.; Nakai, H.; Vreven, T.; Throssell, K.; Montgomery Jr., J. A.; Peralta, J. E.; Ogliaro, F.; Bearpark, M. J.; Heyd, J. J.; Brothers, E. N.; Kudin, K. N.; Staroverov, V. N.; Keith, T. A.; Kobayashi, R.; Normand, J.; Raghavachari, K.; Rendell, A. P.; Burant, J. C.; Iyengar, S. S.; Tomasi, J.; Cossi, M.; Millam, J. M.; Klene, M.; Adamo, C.; Cammi, R.; Ochterski, J. W.; Martin, R. L.; Morokuma, K.; Farkas, O.; Foresman, J. B.; Fox, D. J. *Gaussian 16 Rev. C.01*, Wallingford, CT, 2016.
20. Condon, E. U., Theories of Optical Rotatory Power. *Rev. Mod. Phys.* **1937,** *9* (4), 432-457.
21. Stephens, P. J.; Harada, N., ECD cotton effect approximated by the Gaussian curve and other methods. *Chirality* **2010,** *22* (2), 229-233.
22. Bialas, D.; Zhong, C.; Würthner, F.; Spano, F. C., Essential States Model for Merocyanine Dye Stacks: Bridging Electronic and Optical Absorption Properties. *J. Phys. Chem. C* **2019,** *123* (30), 18654-18664.

Chapter 4

Investigation of the chiroptical response from molecular assemblies of linear phenyleneethynylenes

4.1 Abstract

The unique optical properties of molecular aggregates are primarily dictated by the mutual orientation of the molecular transition dipole moments. Asymmetric or twisted arrangement of molecules (and more specifically of their transition dipoles) leads to the emergence of chiroptical properties in aggregates. In this work, phenyleneethynylene (PE) based molecular systems appended with D- and L-isomers of phenylalanine have been synthesized having electronic transitions in the 300-400nm spectral region. H-bonding between the carbonyl (C=O) and amide (N-H) bonds of phenylalanine is exploited to drive the chiral arrangement in a phenyleneethynylene based phenylalanine substituted molecular system. The observed chiroptical properties in aggregates suggest the formation of right- or left-handed organizations, according to the chirality of phenylalanine. Further, a joint experimental and theoretical investigation is reported to understand the influence of intermolecular interactions on chiroptical properties, particularly during the early stages of self-assembly. In this regard, the standard exciton approach has been successfully employed to explain the observation of a bisignated electronic circular dichroism signal in molecular systems.

4.2 Introduction

Chirality manifests in nature at a different level, from molecular level as in L-amino acids, D-sugar, to secondary structures of proteins, DNA, RNA, and nanoscale helices to macroscopic seashells and even galaxy.[1] The aggregation of molecular building blocks with or without chiral centres leads to asymmetric spatial stacking.

This results in the appearance of non-symmetry in extended scales like helical nanofibers; the phenomenon termed supramolecular chirality.[2] Supramolecular chirality can also be classified into two prominent families: (a) asymmetric arrangement of molecules employing non-covalent interactions; (b) host-guest inclusion complexes where chirality is transferred from one to the other. In the former case, it is not necessary that the individual molecule should possess stereocentre, while in the latter case, at least one component (host/guest) should be chiral. An overview of supramolecular chirality is reported in chapter 1.

The availability of multiple sophisticated methods to invoke a chiral response from a supramolecular system makes the area interesting to work with, especially to analyze the emergence of chiroptical properties. It is fascinating to note that almost always chirality of a supramolecular assembly is determined by the chiral sense of the individual molecules if it has one.[3] In the other cases, in the absence of a chirality centre on the molecular building block, the external chiral perturbing force, like chiral light[4] or a chiral solvent,[5] dictates the handedness of the resulting assemblies. Thus the 'local' chirality present in a molecule is translated to the 'global' chirality of supramolecular assemblies. Depending on the handedness of the aggregates formed, they are called *P*-helix or *M*-helix: *P*-helix for right-handed assembly and *M*-helix for left-handed assembly.[2, 6]

Supramolecular assemblies allow us to arrange a large number of molecules in a specific direction utilizing the non-covalent interactions between them. It was noted from the literature that molecules to be used as building blocks for a supramolecular assembly is often substituted with an alkyl/alkoxy group.[7] The main advantage of such a substitution is that it helps in the dissolution of the molecule in non-polar solvents. The non-polar nature of the alkyl chain comes in handy during the aggregation of polar π-conjugated molecules, especially in non-polar solvents like alkanes, methylcyclohexane, etc. In addition, having a longer alkyl chain increases the van der Waals interaction between the molecules upon self-assembling, leading to

more stabilized aggregates.[8] In the case of chiral aggregates, attaching a chiral alkyl chain is one of the popular strategies to impart chirality. Investigations of such assemblies, especially if the alkyl chain is attached to a hydrophilic moiety, provide insights into many phenomena in life systems due to their similarity to membranes and organelles constructed from lipid molecules.[9] For example, tetraphenylethylene derivative attached with alkyl chain through an amide bond self assembles to form chiral supramolecular nanotube in a series of solvent system like THF:acetonitrile, THF:methanol, methanol:water, etc.[10] In another report, a π-conjugated molecular moiety like C_{60}, C_{70} or azobenzene (solvophobic part) attached to long alkyl chains (solvophilic part) phase-separated at the nanoscale owing to the energetic mismatch of C_{60} moieties with n-alkanes to induce a solvophobic interaction in the n-alkane solvent.[8, 11] This results in the supramolecular organization into nanostructures. An instance of chiral supramolecular assembly is reported when a C_3-symmetrical oligo-phenyleneethynylene (OPE) chromophore is substituted with a chiral 3,7-dimethyloctyl group, and the molecule self-assembles in methylcyclohexane.[12] Studies suggest that the chain length of the alkyl groups also determines the stability of aggregates and, in some cases, the morphology of the resulting assemblies.[13] But, the influence of such substitution on the electronic properties of the molecule and assembly is not so well-explored.

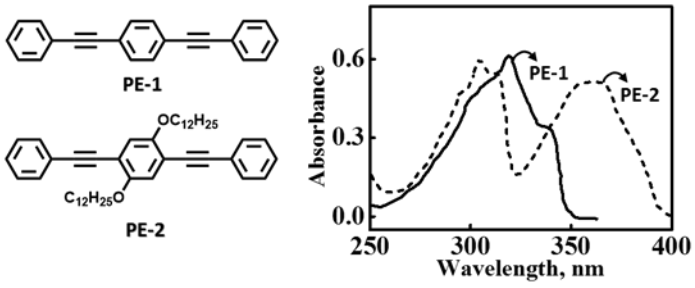

Figure 4.1: *Presented the schematic representation of the two phenyleneethynylene derivatives (**PE1** and **PE2**) and their respective absorption spectrum. When unsubstituted PE (solid line) showed only single absorption band, the alkoxy substituted (broken line) derivative showed two bands. Adapted with permission from Ref.[14] Copyright (2006) American Chemical Society.*

Earlier, a joint experimental and theoretical study focused on the photophysical properties of a series of PE molecules (see Figure 4.1) are carried out.[14] Experimentally, the alkoxy- substitution causes the appearance of an extra band in the absorption spectrum. The result is consistent irrespective of the length of the phenyleneethynylene molecule. Theoretical calculations using TD-DFT revealed that in the case of an unsubstituted molecule, the transition occurs due to HOMO-LUMO transition of 1,4-bis(phenylethynyl)-benzene. On the other hand, dialkoxy substitution in the 2,5-position of the phenyl ring alters its central π-π orbital interactions through the resonance interaction with lone pairs of oxygen in phenyleneethynylenes resulting in similar orbital features for HOMO and HOMO-1/HOMO-2, and the extra band occurs due to the transition from HOMO-1/HOMO-2 to LUMO. Thus, it was concluded that the presence of a heteroatom could indeed alter the electronic properties of the whole molecular system.[14]

Further, a dialkoxy-substituted chiral PE molecular system (Figure 4.2) is synthesized.[15] The absorption spectrum of the molecule in the molecularly dissolved form shows two bands, and both bands show a similar extinction coefficient. Combination of TD-DFT calculations and experimental fluorescence anisotropy, allowed the successfully estimation of the angle between the two transitions dipole moments. On aggregation of the molecule in methanol-water solvent system, absorption spectra again shows two bands.

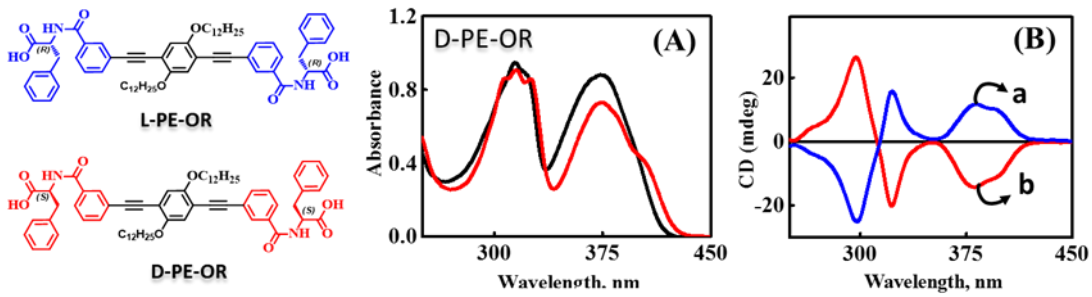

Figure 4.2: *Schematic representation of the phenylalanine conjugates of phenyleneethynylene derivatives substituted with alkoxy groups (D-PE-OR and L-PE-OR). (A) The absorption spectra of the compound in monomer (black trace) and aggregated state (red trace) is presented.*

(B) CD spectrum from the both isomers are also presented: red trace for D-PE-OR and blue trace for L-PE-OR. Adapted with permission from Ref.[15] Copyright (2018) American Chemical Society.

Interestingly, it is observed that the trend also gets translated to chiroptical properties as well. The CD spectrum of the molecular assemblies showed two CD features, of which the highest in energy (250-350nm) is bisignated, and the lowest in energy (350-400nm) is positive for **L-PE-OR** and negative for **D-PE-OR** (Figure 4.2). The chiroptical properties were explained using a generalized exciton model, invoking interactions between non-degenerate states. Such a modified exciton model became essential due to the presence of multiple transition dipole in the molecular system.[15]

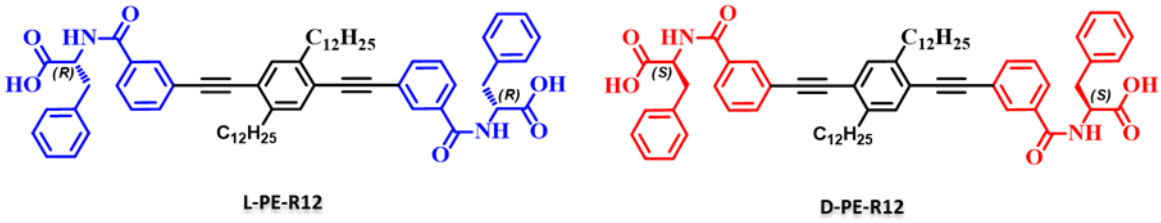

Chart 4.1: *Chiral Phenyleneethynylenes substituted with D- and L-isomers of phenylalanine at the -meta position of its terminal benzene ring and the dodecyl group is attached to the its central benzene ring.*

The objective of the work carried out herein is to investigate the nature of chiral response from the phenyleneethynylene assemblies on substituting the central benzene ring with alkyl groups. For this purpose, two chiral molecules are synthesized, namely **D-PE-R12** and **L-PE-R12,** by substituting an alkyl group (-$C_{12}H_{25}$) to the central benzene ring of the phenyleneethynylene system. Further, D- and L-phenylalanine are substituted to the meta-position of the chromophoric system so that the molecule has a chiral sense. The design strategy is based on the rationale that the molecular systems possess a hydrophobic chromophoric unit that can self-assemble in polar solvents. The functionalized amino acid groups provide helicity through various interactions, such as hydrogen bonding, leading to the formation of β-sheets.[16] By adopting various spectroscopic methods, the asymmetric organization of these molecular systems is explored and the role of interactions between the transition

dipoles on the origin of chiroptical properties. These aspects are further rationalized in terms of a simple and computationally cost-effective standard exciton model.

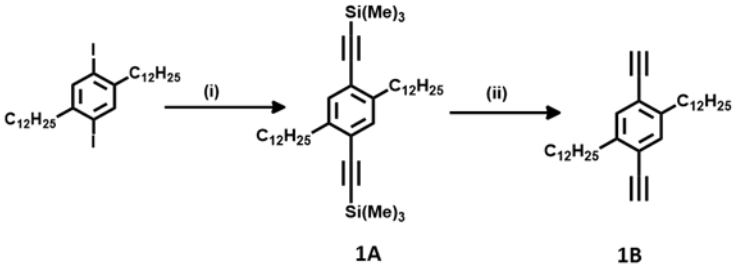

Scheme 4.1: *(i) $Pd(PPh_3)_2Cl_2$, TMSA, Et_3N, CuI, THF (ii) K_2CO_3, MeOH*

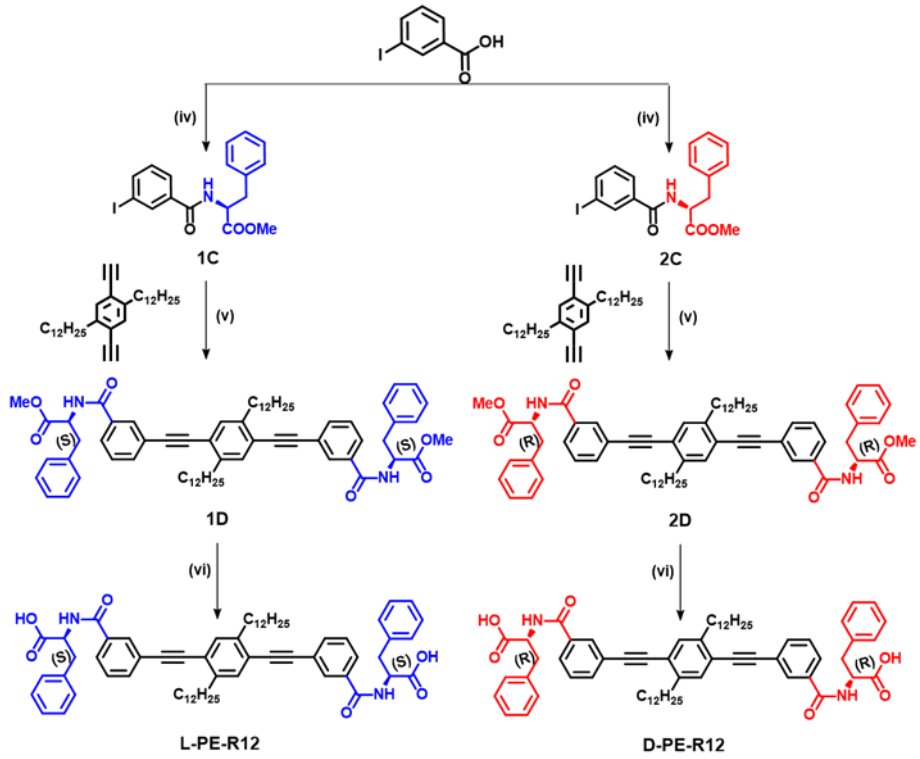

Scheme 4.2*: Synthetic route to the* ***D-*** *and* ***L-PE-R12****: (iv) D- Phenylalanine methyl ester hydrochloride, EDC, HOBT, N.N-diisopropylethylamine (DIPEA) ; (iv) L- Phenylalanine methyl ester hydrochloride, EDC, HOBT, DIPEA; (v) $Pd(PPh_3)_2Cl_2$, CuI, trimethylamine, PPh_3 ; (vi) LiOH, MeOH. The molecular systems are labeled with alphabetic extensions as D, PE, and R12 representing D-isomer, L-isomer, phenyleneethynylene unit, and alkyl substitutions.*

4.3 Results and Discussion

Synthesis of **D**- and **L-PE-R12** is reported in Section 4.5.

4.3.1 Photophysical properties of D/L-PE-R12

The optical spectra of **D**- and **L-PE-R12** in the region of 250-350 nm are governed by the chromophoric unit (PE), marginally perturbed by the phenylalanine substituents. Hence, both isomers show equivalent absorption spectral features in their molecularly dissolved forms in methanol (20 x 10^{-6} M) (trace a and c in Figure 4.3). The absorption and emission spectrum appears as a single band with partially resolved vibrational features (trace b and d in Figure 4.3). Thus it is observed that in the monomeric state, when alkoxy group is replaced by alkyl group in the phenylenenethynylene derivatives the number of absorption band reduces from two to one. These results are analogous with the previous observation that the unsubstituted 1,4-bis-(phenylethynyl) benzene shows a single absorption band, while two bands appear upon substituting the central benzene ring with dialkoxy groups.

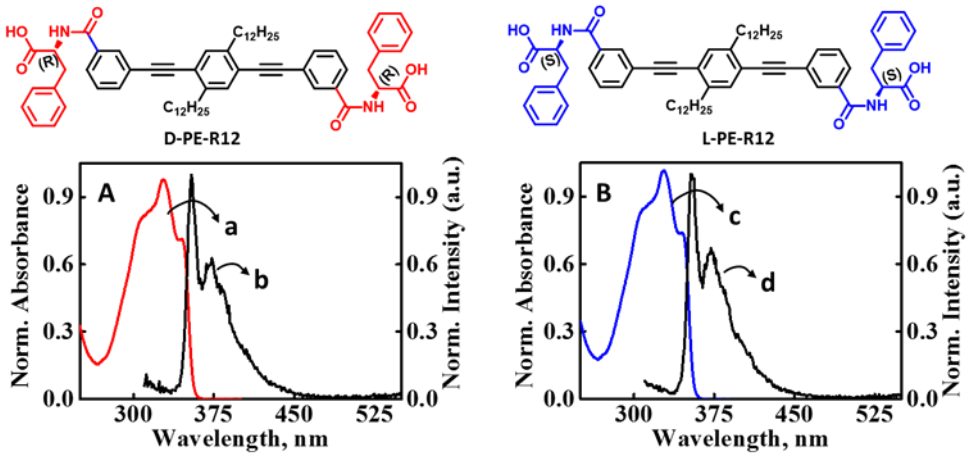

Figure 4.3: *Absorption and emission spectrum of* ***D-PE-R12*** *(A) and* ***L-PE-R12*** *(B) in their monomeric state, concentration used is 20 × 10-6 M in methanol. Absorption spectra of* ***D-PE-R12*** *is shown as blue trace (a) and* ***L-PE-R12*** *as red trace (c). Emission spectra of both isomers are shown as black trace, (b) for D-isomer and (d) for L-isomer.*

The λ_{max} of the structured absorption spectra is at 328 nm and the emission maxima is at 354 nm. Molar extinction coefficient is determined using Beer-Lambert's law and quantum yield is measured using relative method. The reference used is quinine hemisulphate in 0.5 M H_2SO_4 and excited at 330 nm.[17] Anisotropy studies were carried out in poly THF so that we could analyse the angular displacement between

absorption and emission transition dipoles. Poly THF being a highly viscous solvent suppresses the rotational diffusion. The excitation anisotropy studies showed that the anisotropy is flat in the excitation spectral region and the value is found out to be 0.36 (Figure 4.4), very close to the 0.4 limiting value of anisotropy, as expected when a single excited state is responsible for both the absorption and emission.

***Table 4.1**: Shows the photophysical properties of phenylalanine conjugated phenyleneethynylene derivatives in their monomeric form: concentration used is 20 × 10^{-4}M in methanol.*

Molecule	λ_{max}	λ_{em}	Extinction coefficient (ε) ($M^{-1}cm^{-1}$)	Relative quantum yield (ϕ_f)
D-PE-R12	328 nm	354 nm	5.35 × 10^4	0.39±0.02
L-PE-R12	328 nm	354 nm	5.3 × 10^4	0.40±0.02

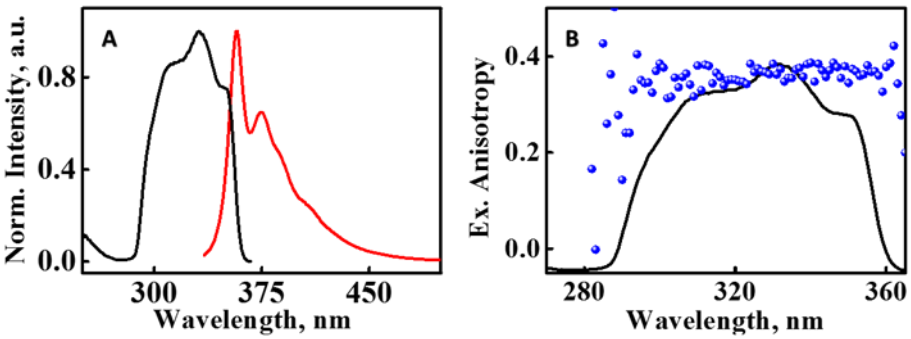

***Figure 4.4:** (A) excitation (black trace) and emission (red trace) spectra of **D-PE-R12** in polyTHF. (B) excitation anisotropy spectral profile (blue spheres) overlapped on the excitation spectrum of the molecule.*

4.3.2 TD-DFT Results

Table 4.2 collects transition wavelength, oscillator strength (f) and the three components of the transition dipole moments (D) for all transitions with λ>240 nm (for B3LYP the first 10 transitions are reported, for CAM-B3LYP and ωB97XD the first 5 transitions are reported). For the model molecule for **D/L-PE-R12**, only the lowest energy transition has a sizeable intensity, and is polarized along the main molecular axis (B_{1u} symmetry).

Table 4.2: *TD-DFT results in gas phase and in methanol.*

Solvent	**Gas phase**					**Methanol**				
Functional	**λ_{calc} (nm)**	**f**	**μ_x[a] (D)**	**μ_y[a] (D)**	**μ_z[a] (D)**	**λ_{calc} (nm)**	**f**	**μ_x[a] (D)**	**μ_y[a] (D)**	**μ_z[a] (D)**
B3LYP	360	1.89	-4.73	0	0	370	2.07	-5.01	0	0
	294	0	0	0	0	295	0	0	0	0
	280	0	0	-0.01	0	279	0	0	0.02	0
	274	0	0	0	0	273	0	0	0	0
	271	0	0	0	0	272	0	0	0	0
	270	0	0	0.06	0	271	0	0	0.05	0
	270	0	0	-0.01	0	271	0	0	0.20	0
	268	0	0	0	0	269	0	0	0	0
	248	0	0	0	0	247	0	0	0.01	0
	248	0.04	0	0.6	0	247	0.05	0	0.66	0
CAM-B3LYP	313	1.91	-4.44	0	0	319	2.09	-4.69	0	0
	251	0	0	0.03	0	254	0	0	0	0
	250	0	0	0	0	251	0	0	0.07	0
	243	0	0	0	0	242	0	0	0	0
	242	0	0	0	0	240	0	0	0	0
ωB97XD	310	1.92	-4.42	0	0	316	2.10	-4.67	0	0
	251	0	0	0.03	0	252	0	0	0	0
	249	0	0	0	0	251	0	0	-0.08	0
	243	0	0	0	0	242	0	0	0	0
	242	0	0	0	0	240	0	0	0	0

[a]x,y and z components of the transition dipole moment. [a]the two transitions are slightly red-shifted on moving from gas phase to MeOH, however no major effects are observed due to solvation, [b]x,y and z components of the transition dipole moment.

Hence, the single band observed in the absorption spectrum of the molecule is ascribed to the first transition calculated in TD-DFT. In comparison, for the alkoxy substituted PE derivative we observed that the presence of the two substituents lowers the symmetry from D_{2h} to C_{2h}. As a result, B_{1u} and B_{2u} states, mutually orthogonal in D_{2h} symmetry, are mixed up as B_u states in C_{2h} symmetry, acquiring both a sizeable intensity. Calculated transition energies are in reasonable agreement with experimental data. TD-DFT results obtained with all three functional gave similar result, the difference being that while B3LYP are slightly red-shifted compared to experiment, CAM-B3LYP and ωB97XD are slightly blue-shifted.

4.3.3 Solvent dependent properties of D/L-PE-R12

Self-assembly of the molecule is achieved by increasing the water (poor solvent) content in methanol. The hydrophobicity of the molecule brings them together and the presence of the D-/L-phenylalanine groups onto the phenyleneethynylene core guides the formation of a chiral supramolecular aggregate.[16] The aggregates are stable when the percentage composition of water in methanol is high, which is evident from the absorption, emission, and ECD studies. The **D-** and **L-PE-R12** molecular aggregates are stable in 70% (v/v) water in methanol but tend to precipitate upon further increasing the water content. As at this composition, aggregates formed are observed to be more stable and further studies are performed and reported at this solvent composition. On aggregation, a change in the absorption spectral profile with a marked difference in the relative intensities of the vibronic bands (Figure 4.5A) is observed. Even though the aggregates formed are H-type due to H-bonding between the amide linkages, the observed bathochromic shift on the aggregation maybe a result of the formation of higher order aggregates. In addition the emission spectrum also shows a change in the spectral feature and becomes broader with the appearance of an additional peak on aggregation. However, the excitation spectra measured by collecting the emission at the two λ_{max} showed similar spectral feature as absorption in Figure 4.5. The origin of the additional peak observed in emission is not clear, and will be a subject of more detailed investigations in the future. In Figure 4.5, the absorption, emission and CD spectra of aggregates at different concentration (ranging from 2 μM to 15 μM) are presented: from these spectra, it is evident that at low concentration (2 μM and 5 μM), aggregates are not properly formed and hence the spectral profile is similar to that of the monomer. On the opposite, at higher concentration (10 μM and 15 μM), the aggregates are well developed and marked difference in the spectral profile of absorption and emission spectra is clearly visible. Figure 4.5D shows the excitation spectra of chiral assembly of **L-PE-R12** collected at 423 nm (black trace) and 470 nm (red trace) which are the two

emission maxima. Further comparison of the absorption and emission spectral features with monomeric absorption and emission, absorption and emission of the **D-PE-R12** is provided in Figure 4.6A and C (blue trace). Interestingly, the aggregated alkoxy substituted PE derivatives also showed similar trend.

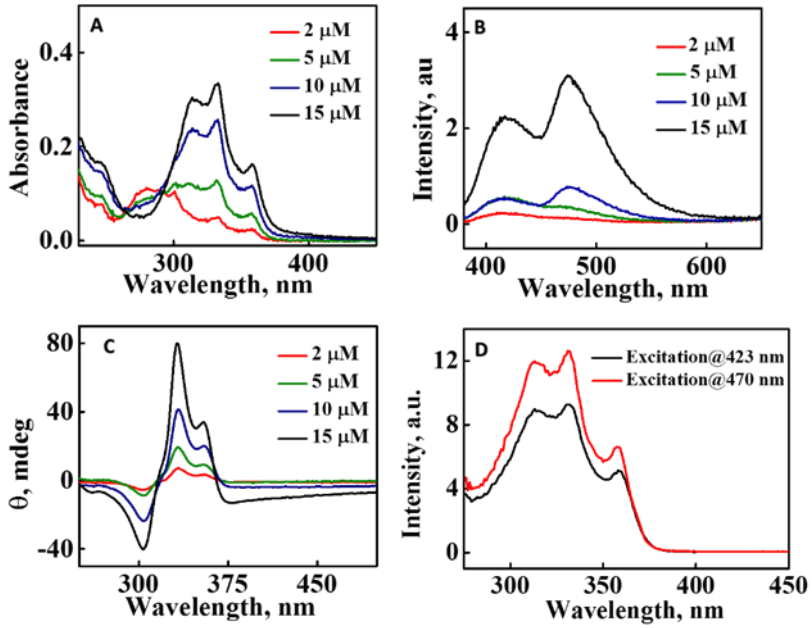

Figure 4.5: *(A) Absorption spectra, (B) emission spectra, (C) ECD spectra of* ***L-PE-R12*** *in the aggregated state with the concentration ranging from 2 μM – 15 μM. (D) shows the excitation spectra collected at 423 nm (black trace) and 470 nm (red trace) of* ***L-PE-R12*** *in aggregates state, which are the peaks of its emission spectrum.*

4.3.4 Chiroptical properties of D/L-PE-R12

ECD spectra of all the derivatives in methanol are fully silent in the 250-450 nm spectral region (Figure 4.8B), confirming that the chiral end groups hardly interact with the central phenyleneethynylene chromophoric unit. However, in the same spectral region, supramolecular assemblies of **D-** and **L-PE-R12** (Figure 4.6B) in 70% (v/v) water in methanol show distinct ECD signals with opposite sign. The ECD signals measured in this spectral region are therefore ascribed to the exciton-coupling of transition dipole moments on different molecules in the supramolecular assembly.[6] An exciton coupled ECD signal is observed in the region of chromophore absorption for both the isomers. Quite interestingly, the ECD spectrum of **D-** and **L-PE-R12** in

70% water in methanol appears as a single bisignated band (vibronically resolved) in the short-wavelength region (Figure 4.6B) unlike the alkoxy substituted derivative which showed two CD bands on aggregation.[15] The ECD spectrum of the L-PE-R12 has a positive band at 334 nm (g_{abs}= 8.5 ×10^{-3}) followed by a negative band at 305 nm (g_{abs}= -5.5×10^{-3}). On the other hand, its isomer, D-PE-R12 show a negative band at 334 nm followed by a positive band at 305 nm. The ECD spectra of **D-** and **L-PE-R12** in the far-UV region (200-240 nm), recorded in methanol and 70% (v/v) water in methanol are also presented in Figure 4.7. The ECD spectrum of the molecularly dissolved form of **D-** and **L-PE-R12** in methanol showed negative and positive signals, respectively (at 219 nm), originating from the chirality of the attached D/L-phenylalanine groups, respectively (Figure 4.7B). More interestingly, the characteristic ECD signals observed for **D-** and **L-PE-R12** in 70% (v/v) water in methanol, with distinct negative and positive couplets, signify the formation of β-sheet structures (Figure 4.7C).[18] The spectral profile of various secondary structures are presented as Figure 4.7A for comparison.[16, 18-19] The β-sheet structures in the aggregated states of **D-/L-PE-R12** are formed due to the H-bonding interaction between –C=O and –NH groups of adjacent molecules in the supramolecular assembly. The directionality in the twist of the chiral assembly is guided by the chirality of the D- and L- isomers of phenylalanine groups. It is reported that amide groups play a significant role in inducing twist in the supramolecular structures and in amplifying the chiral response.[20-22] Thus, far-UV ECD spectra provide unequivocal evidence on the role of amide groups in the formation of β-sheets.[18] The formation of chiral supramolecular systems is often explained based on a helical supramolecular geometry,[23-24] and the sign of ECD spectrum is used as a thumb-rule to assign their handedness.[6, 25] Since the helical assembly is guided by the amide functionalities, it is presumed that the interaction energy is positive, V>0 enabling the prediction of the handedness of assembly using rule.[26] Accordingly, we ascribe a left-handed (*M*-type) helical arrangement to **D-PE-R12** aggregates and right-handed (*P*-type) arrangement to **L-PE-R12** aggregates.

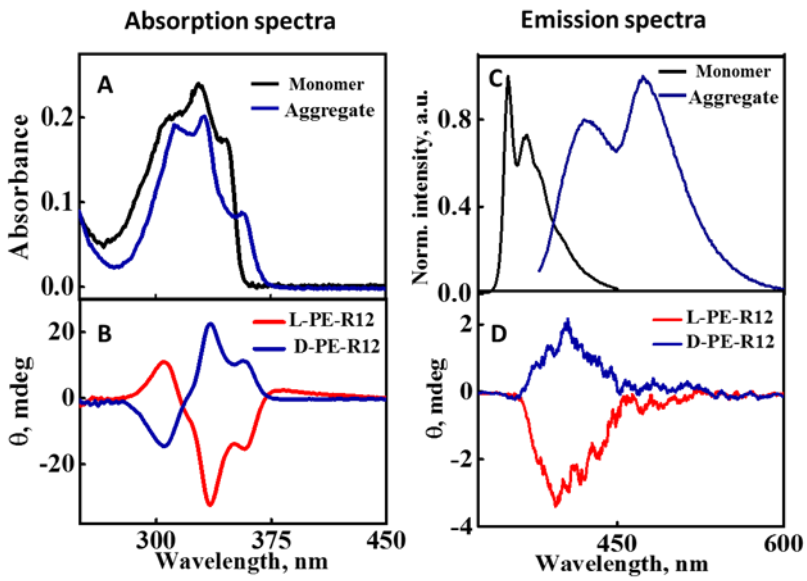

Figure 4.6: *(A) Absorption and (C) emission spectra of* ***D-PE-R12*** *in 70% (v/v) H_2O/MeOH solvent mixture (blue trace) is presented: for comparison, corresponding monomer spectrum (black trace) is also presented. Corresponding CD (B) and CPL (D) spectra of both isomer are also provided. D-isomer (red trace) shows positive chirality while L-isomer (blue trace) shows negative chirality in both techniques. The concentration used is 20 × 10^{-6} M.*

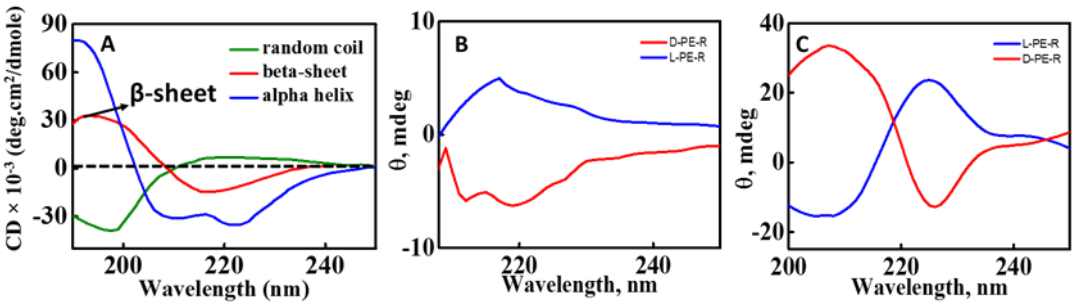

Figure 4.7: *(A) Provided the spectral profile of various secondary structure in the far UV-region. Presented the CD spectrum of monomer in methanol (B) and aggregate in 70% (v/v) H_2O/MeOH (C) where blue trace represents* ***L-PE-R12*** *and red trace represents* ***D-PE-R12****. (A) Adapted by permission from Ref.[18] Copyright (2007) Springer Nature.*

Since the chiral phenyleneethynylene derivatives exhibited reasonably good emissive profiles, we decided to measure the chiral emission from the aggregates. We observed that the aggregates of the isomers showed measurable chiral emission but the intensity was lower (Figure 4.6D). Interestingly, the CPL from the isomers showed opposite chirality and are mirror images of each other. The g_{lum} of the CPL signals from isomers are measured to be 7×10^{-3} which is in line with CPL dissymmetry factor for similar

organic systems. We further carried out a temperature-dependent study on both the isomers using CD spectroscopy. Results indicate that the chiral aggregates formed are thermally stable up to 60 °C (Figure 4.8). Even though there is a slight dip in the CD intensity on increasing the temperature, spectral feature are intact.

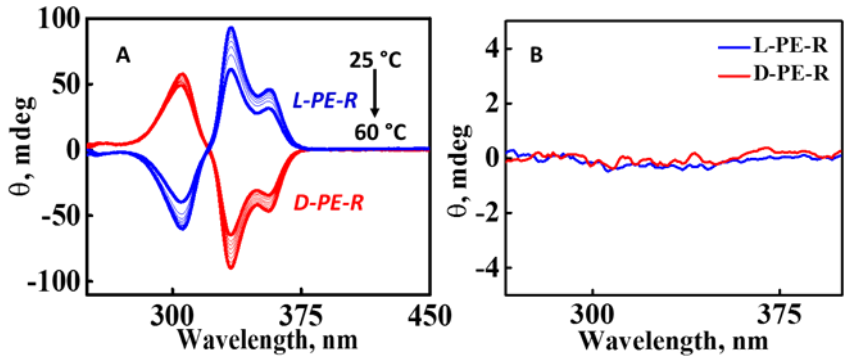

Figure 4.8: *Temperature dependent CD spectra of D-PE-R12 (red trace) and L-PE-R12 (blue trace) is presented. The CD spectra (B) of the both isomers of molecule in methanol (monomer) at concentration of 20 × 10⁻⁶ M is silent.*

4.3.5 Microscopic studies

Morphological analysis of the assembled chiral aggregates are carried out using scanning tunnelling microscopy (SEM).

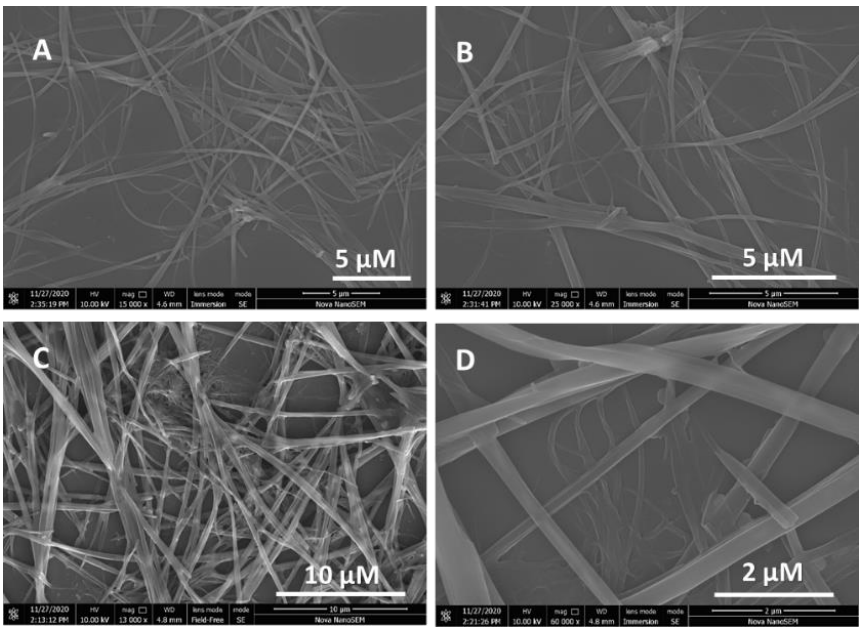

Figure 4.9: *SEM images of the aggregates are presented:* ***L-PE-R12*** *(A,B) and* ***D-PE-R12*** *(C,D) at a concentration of 20 × 10⁻⁶M in 70% (v/v) H₂O/MeOH.*

For this purpose, few drops of aggregates of **D/L-PE-R12** having a concentration of 20 × 10^{-6} M in 70% (v/v) water in methanol is dropcasted to a thoroughly cleaned silica wafers of ~ 0.5 × 0.5 cm size. The sample is left to dry overnight undisturbed and the measurements are carried out next day. The studies show that the aggregates have fibrous morphology (Figure 4.9).

4.3.6 Theoretical investigation of the properties of D/L-PE-R12

For the exciton model calculations (see Chapter 3 for details), the simplest chiral aggregate structure are considered wherein two molecules are organized as a helical dimer (Figure 4.10). Here the molecules are treated as the dipoles and properties are calculated using dipolar approximation as explained in Chapter 3. In an aggregate formed by **D-/L-PE-R12** molecules, since each molecule bears a single excitation in the spectral region of interest, N degenerate states are present. These degenerate states split by intermolecular interactions forming the exciton band. To rationalize the handedness of the molecular assemblies by **D-/L-PE-R12**, we constructed right-handed and left-handed assemblies in helicoidal model (V>0).[26] This is because of the assumption that the formation of molecular assemblies are driven by the H-bonding between the NH- and C=O amide linkages in the neighbouring molecules and hence the formed assemblies are H-type helices. Exciton model calculations are carried out by imposing the molecular transition energy and dipole moment as 3.96 eV and 11.3 D (these values are obtained after optimizing the ground state of the model molecule using TD- DFT calculations), respectively for a monomer and setting σ as 0.35 eV and the refractive index as 1.33, respectively. The tilt angle (θ) between the two monomers is set to 10°. ECD spectra are calculated using equations 3.16, allowing the sum run on all the N excitonic states (Figure 4.10).

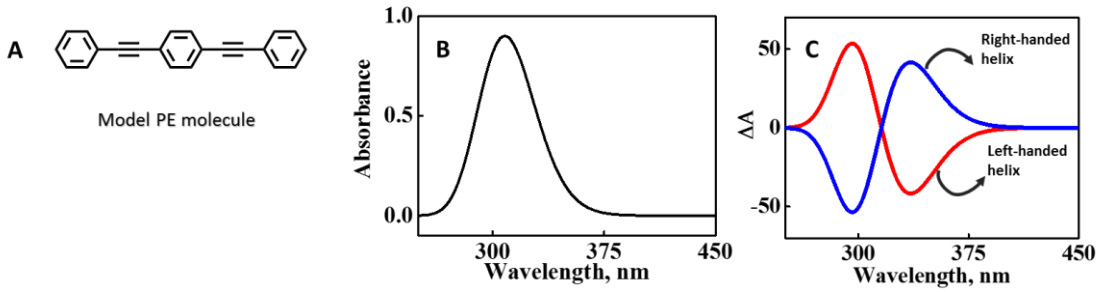

Figure 4.10: *(A) Schematic representation of the model molecule used for calculation. Theoretically calculated absorption spectrum (B) and CD spectra (blue for right-handed) and red for (left-handed) assemblies) of aggregates (C) using exciton model is presented.*

The absorption spectra of the aggregate, calculated by giving a Gaussian band shape as shown below is also provided:

$$A \propto \exp\left[-\left(\frac{\tilde{\nu}-\tilde{\nu}_i}{\sigma}\right)^2\right] \qquad (4.1)$$

where A is the absorbance of the molecule, $\tilde{\nu}_i$ is the wavenumber in nm^{-1} corresponding to the transition of interest, and σ is the standard deviation. From the exciton model results, it is evident that the D-isomers give rise to a left-handed assembly while the L-isomer gives right-handed assembly. As expected, the calculated ECD spectrum in Figure 4.10C shows a well-defined exciton couplet which matches with experimental results (Figure 4.6B). This helical geometry is compatible with the formation of β-sheets, but does not rationalize the weak red-shift observed in the absorption spectra of aggregates with respect to monomers (Figure 4.6A). This can be ascribed to various intermolecular interactions resulting from the assembly of helices as bundles as observed in SEM images.

4.4 Conclusions

In conclusion, the chiroptical properties of a set of helical assemblies, where the molecule have single excitation (**D-/L-PE-R12**; Chart 4.1) are investigated and comparison have been made to their alkoxy substituted counterparts. This comparison helps to understand the modification in electronic properties brought

about by alkyl/alkoxy substitution. By replacing alkoxy group with an alkyl group, one absorption band disappears.

Secondary structure of the assemblies as revealed by the CD spectra in the far UV-region discloses the influence of H-bonding through amide bonds in dictating the chirality of the assemblies. The alkyl/alkoxy-substitution strongly influences the chiroptical properties of aggregates. In the alkyl-substituted derivatives a single exciton couplet is observed in the same spectral region of the low-energy absorption band, while a more complicate CD spectrum is observed in aggregates of alkoxy substituted molecule, due to the presence of two transitions which are very close in energy. Theoretical investigation using exciton model and supported by TD-DFT calculations successfully confirmed the experimental results. While the alkoxy-substituted derivatives demanded a generalized exciton model to explain the chiroptical properties, to account for the presence of two excited state close in energy, for alkyl substituted derivatives, the standard exciton model is deemed good to analyze the properties. Furthermore, the insights gained are useful for the design of supramolecular and nanoscopic materials with tailored chiroptical properties having potential applications in chiral sensing, synthesis, and catalysis.

4.5 Materials and Methods

All solvents used for the synthesis are purchased from commercial sources and used as such without much purification. All the precursors for the synthesis of D/L-PE-R12 is purchased from Sigma Aldrich. Silica gel of 200-400 mesh size is used to perform flash column chromatography. Appropriate eluent is selected with the help of TLC prior to column chromatography by trial and error method. Intermediate compounds are purified by passing through recycling HPLC manufactured by Japan Analytical Industry Co., Ltd. All melting points are uncorrected and determined using Stuart SMP30 melting point apparatus. IR spectra are recorded on Shimadzu IR prestige-21 FT-IR spectrophotometer as KBr pellets in the case of solids. 1H and 13C NMR spectra are recorded on Bruker Avans 500 MHz DPX spectrometer

using 1,1,1,1-tetramethyl silane (TMS) as an internal standard. Elemental analysis is carried out on Elementar vario MICRO cube Elemental Analyser. Electronic absorption spectra are recorded using quartz cuvette of 1 cm path length on a Shimadzu UV-3600 Vis-NIR Spectrophotometer. Steady state fluorescence spectra are recorded on Horiba Jobin Yvon Fluorimeter equipped with thermostat peltier cell holder, in a quartz cuvette of 1 cm path length. Circular Dichroism (CD) analyses are done on JASCO J-815 CD spectropolarimeter having peltier controlled thermostatic cell holder, in a quartz cuvette of 1 cm path length. Fluorescence anisotropy spectra of **D-PE-R12** are collected on a Fluormax-3 Horiba Jobin Yvon spectrofluorometer equipped with Glan-Thompson automatic polarizers (single channel L-format). PolyTHF at room temperature is selected as appropriate solvents to avoid the depolarization of the fluorescence signal due to molecular motion during the excited-state lifetime measurements (polyTHF at room temperature is highly viscous).

4.5.1 Synthesis and characterization

Phenyleneethynylene derivatives (Chart 4.1) are synthesized via palladium catalyzed Heck-Cassar-Sonagashira-Hagihara cross-coupling reactions[27] and amide coupling[28] is achieved using EDC/HOBT to attach phenylalanine. Scheme 4.1 shows the stepwise synthesis of 1,4-didodecyl-2,5-diethynylbenzene from 1,4-didodecyl-2,5-diiodobenzene while scheme 4.2 shows the synthesis of **D-PE-R-12** and **L-PE-R12** from 3-iodobenzoic acid. The intermediate compounds, **1D** and **2D** are further purified using HPLC.

Synthesis of 1A: A pressure tube (100 mL) is evacuated, and N_2 is passed. A solution of 1,4-didodecyl-2,5-diiodobenzene (6 g, 9mmol), CuI (0.34 g, 1.8 mmol), $Pd(PPh_3)_2Cl_2$ (1.26 g, 1.8 mmol) in dry trimethylamine (50 mL) and dry THF (35 mL) is added. The reaction mixture is raised to a temperature of 60 °C and added trimethylsilylacetylene (3.5 mL, 27 mmol) to the flask under N_2 flow. The reaction mixture is stirred overnight. After the completion of reaction, the excess solvent is removed under pressure and resulting residue is dissolved in $CHCl_3$ followed by a

flash column chromatography. Further, the excess solvent is again removed under reduced pressure and the residue obtained is chromatographed over silica (100-200 mesh) using a hexane as eluent to yield 3.9 g of 1A (71%) as white solid. mp 74-75 °C; ^{1}H NMR ($CDCl_3$, 500 MHz): δ 6.88 (s, 2H, Ar), 2.74 (t, J = 7.65 Hz, 4H, aliphatic), 1.63-1.50 (m, 4H, aliphatic), 1.32-1.16 (m, 36H, aliphatic), 0.79 (t, J = 6.8 Hz, 6H, aliphatic), 0.27 (s, 18H, $SiCH_3$).

Synthesis of 1B: To a solution of 1A (4 g, 6.59 mmol) in dry THF (30 mL), a mixture of methanol (60 mL) and dry potassium carbonate (4.55 g, 32.94 mmol) is added and stirred for 4 h in a 250 mL two-neck RB flask. The solvent is evaporated; the residue is poured into water and extracted with chloroform. The organic layer is repeatedly washed with water (3 x 25 mL) and dried over anhydrous Na_2SO_4. Evaporation of solvent yielded 2.4 g (81 %) of 1B as a pale yellow solid. mp 75-77 °C; ^{1}H NMR ($CDCl_3$, 300 MHz): δ 6.82 (s, 2H, Ar), 2.74 (t, J = 7.65 Hz, 4H, aliphatic), 3.36 (s, 2H, acetylenic), 1.63-1.50 (m, 4H, aliphatic), 1.32-1.16 (m, 36H, aliphatic), 0.79 (t, J = 6.8 Hz, 6H, aliphatic)

Synthesis of 1C, 2C: Under N_2 atmosphere, to a mixture of 3-iodobenzoic acid and D/L-phenylalanine methyl ester hydrochloride (500 mg, 2 mmol) in 4 mL THF, 1-ethyl-3-(dimethylaminopropylamine)carbodiimide hydrochloride (EDCI.HCl) (462 mg, 2.42 mmol), hydroxybenzotriazole (HOBT) (326 mg, 2.42 mmol) in 1.5 mL N,N-diisopropylethylamine are added and stirred for 24 h at room temperature. Then the reaction mixture is poured into cold water and extracted with ethyl acetate. After repeatedly washed with water, organic layers are combined and dried over anhydrous Na_2SO_4. After removal of the solvent under reduced pressure the crude product is purified by column chromatography over silica gel (100-200 mesh) using ethyl acetate/hexane (1:4) as eluent to obtain a white solid of 1C/2C both with ~70% yield. mp 1C (94 °C) and 2C (96 °C). ^{1}H NMR (500 MHz, $CDCl_3$, TMS): δ 7.98 (s, 1H, aromatic), 7.76-7.74 (m, 1H, aromatic), 7.58-7.56 (m, 1H, aromatic), 7.25-7.17 (m, 3H, aromatic), 7.09-7.04 (m, 3H, aromatic), 6.45 (d, J = 7.3 Hz, 1H, NH), 5.01-4.97 (m, 1H,

CH), 3.70 (s, 3H, OCH_3), 3.25-3.12 (m, 2H, CH2). ^{13}C NMR (125 MHz, $CDCl_3$, TMS): δ 171.94, 165.31, 140.69, 136.21, 135.88, 135.71, 130.26, 129.32, 128.70, 127.32, 126.08, 94.32, 53.62, 52.53, 37.86. Anal. Calcd for $C_{17}H_{16}INO_3$: C, 49.90; H, 3.94; I, 31.01; N, 3.42; O, 11.73. Found for 2C: C, 49.95; H, 3.95; N, 3.43.

Synthesis of 1D, 2D: A mixture of 1,4-didodecyl-2,5-diethynylbenzene (300 mg, 0.60 mmol) and 1C/2C (546 mg, 1.34 mmol), CuI (12 mg, 0.06 mmol), $Pd(PPh_3)_2Cl_2$ (43 mg, 0.06 mmol), triphenylphosphine (32 mg, 0.12 mmol) was added to a degassed solution of triethylamine (20 mL), and the mixture was stirred at room temperature for 24 h. The reaction mixture was diluted with chloroform and passed through a short flash column. After removal of the solvent under reduced pressure, the crude product was purified by column chromatography over silica gel (100-200 mesh) using chloroform/hexane (1:3) as an eluent. The product was further purified by HPLC to obtain white solid of 1D/2D both with~50% yield. mp 122-124 °C; IR (KBr) νmax: 3312 cm-1, 2212 cm-1, 1740 cm-1, 1640 cm-1, 1535 cm-1. ^1H NMR (500 MHz, $CDCl_3$, TMS): δ 7.80 (s, 2H, aromatic), 7.61-7.58 (m, 4H, aromatic), 7.35 (t, J = 7.75 Hz, 2H, aromatic), 7.31 (s, 2H, aromatic), 7.25-7.17 (m, 4H, aromatic), 7.07 (d, J = 6.9 Hz, 4H, aromatic), 6.52 (d, J = 7.5 Hz, 2H, NH), 5.05-5.01 (m, 2H, CH), 3.71 (s, 3H, OCH_3) 3.26-3.15 (m, 4H, CH2), 2.74 (t, J = 7.65 Hz, 4H, aliphatic), 1.63-1.50 (m, 4H, aliphatic), 1.32-1.16 (m, 36H, aliphatic), 0.79 (t, J = 6.8 Hz, 6H, aliphatic). ^{13}C NMR (125 MHz, CDCl3, TMS): δ 171.97, 166.06, 142.37, 135.76,134.56,134.29, 132.52, 130.01, 129.36, 128.76, 128.66, 127.27, 126.69, 124.16,122.43, 92.90, 89.49, 53.62, 52.49, 37.94, 34.07, 31.92, 30.61, 29.70, 29.69, 29.66, 29.63, 29.60, 29.53, 29.36, 22.69, 14.12. Anal. Calcd for $C_{68}H_{84}N_2O_6$: C, 79.65; H, 8.26; N, 2.73; O, 9.36 Found for 1D: C, 80.31; H, 8.691; N, 2.17.

Synthesis of **D-PE-R12**, **L-PE-R12**: To a solution of 1D/2D (155 mg, 0.15 mmol) in THF (3 mL), LiOH.H2O (31 mg, 0.73 mmol), MeOH (3.8 mL) were added. The mixture was refluxed for 5 h. Then reaction mixture was quenched using 5% aqueous citric acid and extracted with ethyl acetate to yield **D-PE-R12/L-PE-R12** both with ~80% yield. mp 206-208 °C; IR (KBr) νmax: 3315 cm^{-1}, 2213 cm^{-1}, 1712 cm^{-1}, 1639 cm^{-1}, 1528 cm^{-1}. ^1H

NMR (500 MHz, DMSO, TMS): δ 12.80 (s, 2H, COOH), 8.86 (d, J = 8.5 Hz, 2H, NH), 7.98 (s, 2H, aromatic), 7.83 (d, J = 7.8 Hz, 2H, aromatic), 7.68 (d, J = 7.75 Hz, 2H, aromatic), 7.53 (t, J = 7.8 Hz, 2H, aromatic), 7.48 (s, 2H, aromatic), 7.33-7.25 (m, 8H, aromatic), 7.18 (t, J = 7.25 Hz, 2H, aromatic), 4.66-4.62 (m, 2H, CH), 3.23-3.05 (m, 4H, CH2), 2.82-2.79 (t, J = 7.35 Hz, 4H, aliphatic), 1.67-1.63 (m, 4H, aliphatic), 1.34-1.15 (m, 36H, aliphatic), 0.81 (t, J = 6.85 Hz, 6H, aliphatic). ^{13}C NMR (125 MHz, DMSO, TMS): δ 178.23, 170.64, 147.36, 143.35, 139.68, 134.25, 133.37, 131.56, 127.57, 127.17, 98.65, 93.67, 59.47, 41.51, 38.40, 36.46, 35.25, 34.18, 34.15, 34.11, 34.07, 33.93, 33.86, 33.78, 27.27, 19.13. Anal. Calcd for $C_{66}H_{80}N_2O_6$: C, 79.48; H, 8.08; N, 2.81; O, 9.63. Found for **D-PE-R12**: C, 78.05; H, 7.957; N, 2.58.

4.5.2 TD-DFT calculations

Gaussian 16 suite[29] of programs is employed to calculate optimized ground state geometries and excited state energies and transition dipole moments. For simplicity, the calculations are performed on an unsubstituted PE chromophoric unit (Figure 4.9A). Optimized geometries of molecule are obtained using density functional theory (DFT) method in gas phase and methanol in the polarizable continuum model approximation (PCM). 6-31G(d) is chosen as basis set, and different functional are tested (B3LYP, CAM-B3LYP and ωB97XD). Excited states are calculated at the time dependent DFT (TD-DFT) level.

References

1. Albano, G.; Pescitelli, G.; Di Bari, L., Chiroptical properties in thin films of π-conjugated systems. *Chem. Rev.* **2020,** *120* (18), 10145-10243.
2. Liu, M.; Zhang, L.; Wang, T., Supramolecular Chirality in Self-Assembled Systems. *Chem. Rev.* **2015,** *115* (15), 7304-7397.
3. Langeveld-Voss, B. M. W.; Janssen, R. A. J.; Christiaans, M. P. T.; Meskers, S. C. J.; Dekkers, H. P. J. M.; Meijer, E. W., Circular Dichroism and Circular Polarization of Photoluminescence of Highly Ordered Poly{3,4-di[(S)-2-methylbutoxy]thiophene}. *J. Am. Chem. Soc.* **1996,** *118* (20), 4908-4909.
4. Castriciano, M. A.; Gentili, D.; Romeo, A.; Cavallini, M.; Scolaro, L. M., Spatial control of chirality in supramolecular aggregates. *Sci. Rep.* **2017,** *7*, 44094.

5. Jin, Y.-J.; Kim, H.; Kim, J. J.; Heo, N. H.; Shin, J. W.; Teraguchi, M.; Kaneko, T.; Aoki, T.; Kwak, G., Asymmetric Restriction of Intramolecular Rotation in Chiral Solvents. *Cryst. Growth Des.* **2016,** *16* (5), 2804-2809.
6. Harada, N.; Nakanishi, K.; Berova, N., Electronic CD Exciton Chirality Method: Principles and Applications. In *Comprehensive Chiroptical Spectroscopy*, Berova, N.; Polavarapu, P. L.; Nakanishi, K.; Woody, R. W., Eds. 2012; pp 115-166.
7. Nakanishi, T., Supramolecular soft and hard materials based on self-assembly algorithms of alkyl-conjugated fullerenes. *Chem. Commun.* **2010,** *46* (20), 3425-3436.
8. Hollamby, M. J.; Karny, M.; Bomans, P. H. H.; Sommerdjik, N. A. J. M.; Saeki, A.; Seki, S.; Minamikawa, H.; Grillo, I.; Pauw, B. R.; Brown, P.; Eastoe, J.; Möhwald, H.; Nakanishi, T., Directed assembly of optoelectronically active alkyl–π-conjugated molecules by adding n-alkanes or π-conjugated species. *Nat. Chem.* **2014,** *6* (8), 690-696.
9. Ouyang, G.; Liu, M., Self-assembly of chiral supra-amphiphiles. *Mater. Chem. Front.* **2020,** *4* (1), 155-167.
10. Anuradha; La, D. D.; Al Kobaisi, M.; Bhosale, S. V., Right handed chiral superstructures from achiral molecules: self-assembly with a twist. *Sci. Rep.* **2015,** *5* (1), 15652.
11. Schenning, A. P. H. J.; George, S. J., Phases full of fullerenes. *Nat. Chem.* **2014,** *6* (8), 658-659.
12. Wang, F.; Gillissen, M. A. J.; Stals, P. J. M.; Palmans, A. R. A.; Meijer, E. W., Hydrogen Bonding Directed Supramolecular Polymerisation of Oligo(Phenylene-Ethynylene)s: Cooperative Mechanism, Core Symmetry Effect and Chiral Amplification. *Chem. Eur. J.* **2012,** *18* (37), 11761-11770.
13. Huo, P.; Xue, L.-J.; Li, Y.-H.; Chen, T.; Yu, L.; Zhu, Q.-Y.; Dai, J., Effects of alkyl chain length on film morphologies and photocurrent responses of tetrathiafulvalene-bipyridinium charge-transfer salts: a study in terms of structures. *CrystEngComm* **2016,** *18* (16), 2894-2900.
14. James, P. V.; Sudeep, P. K.; Suresh, C. H.; Thomas, K. G., Photophysical and Theoretical Investigations of Oligo(p-phenyleneethynylene)s: Effect of Alkoxy Substitution and Alkyne−Aryl Bond Rotations. *J. Phys. Chem. A* **2006,** *110* (13), 4329-4337.
15. Kar, S.; Swathi, K.; Sissa, C.; Painelli, A.; Thomas, K. G., Emergence of Chiroptical Properties in Molecular Assemblies of Phenyleneethynylenes: The Role of Quasi-degenerate Excitations. *J. Phys. Chem. Lett.* **2018,** *9* (16), 4584-4590.
16. Reches, M.; Gazit, E., Casting Metal Nanowires Within Discrete Self-Assembled Peptide Nanotubes. *Science* **2003,** *300* (5619), 625.
17. Brouwer, A. M., Determination of the photoluminescence quantum yield of dilute dye solutions. *Pure Appl. Chem.* **2013,** *85* (10), 2005-2026.
18. Greenfield, N. J., Analysis of the kinetics of folding of proteins and peptides using circular dichroism. *Nat. Protoc.* **2006,** *1* (6), 2891-2899.

19. Anslyn, E. V.; Dougherty., D. A., *Modern physical organic chemistry*. University science books.: 2006.
20. Palmans, A. R. A.; Meijer, E. W., Amplification of Chirality in Dynamic Supramolecular Aggregates. *Angew. Chem. Int. Ed.* **2007,** *46* (47), 8948-8968.
21. Venkata Rao, K.; Miyajima, D.; Nihonyanagi, A.; Aida, T., Thermally bisignate supramolecular polymerization. *Nat. Chem.* **2017,** *9* (11), 1133-1139.
22. Kim, T.; Mori, T.; Aida, T.; Miyajima, D., Dynamic propeller conformation for the unprecedentedly high degree of chiral amplification of supramolecular helices. *Chem. Sci.* **2016,** *7* (11), 6689-6694.
23. Korevaar, P. A.; Grenier, C.; Markvoort, A. J.; Schenning, A. P. H. J.; de Greef, T. F. A.; Meijer, E. W., Model-driven optimization of multicomponent self-assembly processes. *Proc. Natl. Acad. Sci. U.S.A.* **2013,** *110* (43), 17205.
24. Zhao, X.; Schanze, K. S., Meta-Linked Poly(phenylene ethynylene) Conjugated Polyelectrolyte Featuring a Chiral Side Group: Helical Folding and Guest Binding. *Langmuir* **2006,** *22* (10), 4856-4862.
25. Berova, N.; Bari, L. D.; Pescitelli, G., Application of electronic circular dichroism in configurational and conformational analysis of organic compounds. *Chem. Soc. Rev.* **2007,** *36* (6), 914-931.
26. Swathi, K.; Sissa, C.; Painelli, A.; Thomas, K. G., Supramolecular chirality: a caveat in assigning the handedness of chiral aggregates. *Chem. Commun.* **2020,** *56* (59), 8281-8284.
27. Bunz, U. H. F., Poly(aryleneethynylene)s: Syntheses, Properties, Structures, and Applications. *Chem. Rev.* **2000,** *100* (4), 1605-1644.
28. Bodanszky, M.; Bodanszky, A., Activation and coupling. In *The Practice of Peptide Synthesis*, Springer: 1984; pp 87-150.
29. Frisch, M. J.; Trucks, G. W.; Schlegel, H. B.; Scuseria, G. E.; Robb, M. A.; Cheeseman, J. R.; Scalmani, G.; Barone, V.; Petersson, G. A.; Nakatsuji, H.; Li, X.; Caricato, M.; Marenich, A. V.; Bloino, J.; Janesko, B. G.; Gomperts, R.; Mennucci, B.; Hratchian, H. P.; Ortiz, J. V.; Izmaylov, A. F.; Sonnenberg, J. L.; Williams; Ding, F.; Lipparini, F.; Egidi, F.; Goings, J.; Peng, B.; Petrone, A.; Henderson, T.; Ranasinghe, D.; Zakrzewski, V. G.; Gao, J.; Rega, N.; Zheng, G.; Liang, W.; Hada, M.; Ehara, M.; Toyota, K.; Fukuda, R.; Hasegawa, J.; Ishida, M.; Nakajima, T.; Honda, Y.; Kitao, O.; Nakai, H.; Vreven, T.; Throssell, K.; Montgomery Jr., J. A.; Peralta, J. E.; Ogliaro, F.; Bearpark, M. J.; Heyd, J. J.; Brothers, E. N.; Kudin, K. N.; Staroverov, V. N.; Keith, T. A.; Kobayashi, R.; Normand, J.; Raghavachari, K.; Rendell, A. P.; Burant, J. C.; Iyengar, S. S.; Tomasi, J.; Cossi, M.; Millam, J. M.; Klene, M.; Adamo, C.; Cammi, R.; Ochterski, J. W.; Martin, R. L.; Morokuma, K.; Farkas, O.; Foresman, J. B.; Fox, D. J. *Gaussian 16 Rev. C.01*, Wallingford, CT, 2016.

List of Publications

1. Kar, S.; Swathi, K.; Sissa, C.; Painelli, A.; Thomas, K. G., Emergence of Chiroptical Properties in Molecular Assemblies of Phenyleneethynylenes: The Role of Quasi-degenerate Excitations. *J. Phys. Chem. Lett.* **2018,** *9*, 4584-4590.

2. Swathi, K.; Sissa, C.; Painelli, A.; George Thomas, K., Supramolecular chirality: a caveat in assigning the handedness of chiral aggregates. *Chem. Commun.* **2020**, *56*, 8281-8284.

3. Shahana Nizar, N. S. S., M; Swathi, K.; Cissa, C.; Painelli, A.; Thomas, K. G., Emergent chiroptical properties in supramolecular and plasmonic assemblies. *Chem. Soc. Rev* **2021**, xx, xx (Manuscript submitted).

Acknowledgements

I have great pleasure in extending my sincere and heartfelt gratitude to Prof. K. George Thomas and Prof. Cristina Sissa and Prof. Anna Painelli, my supervisors, for giving me support and valuable guidance at all stages of my work, leading to the successful completion of the graduate programme.

I would also like to express my immense gratitude to the Director of IISER-TVM and University of Parma for providing me all the basic amenities to carry out the research work and financial funding during this period.

I also extend my sincere thanks to Prof. Enrico Dalcanale, Co-ordinator of Doctoral Programme as well as all the faculty members at the School of Chemistry, IISER-TVM, for their inspiration and aid during this time.

I also express my wholehearted gratitude to Francesco Di Maialo, Prof. Francesca Terenziani, Dr. Anoop Thomas, Dr. Reshmi Thomas, Dr. Hemna Fathima, Sanoop Somasundaran and Dr. Shyamala, for their constant motivation, care and outstanding ideas which enabled me to carry out the research to completion. I am also grateful to Dr. Murali, and Vighnesh, whose advice and support enable me to complete the project. I am extremely thankful to Dr. Sabnam, Elizabeth, Reshma, Devika, Aiswarya, Ajaykumar, Rema and Sangeeth without whose support, inspiration and resourcefulness this research work would not be a reality. I always cherish the friendship we shared. I like to extend my gratitude to all the other members of Anna's group at UNIPR and KGT's group at IISER TVM for their constant motivation and help at urgent hours. I also want to convey my regards to Dr. Asha Pankajakshan for our time together in Italy.

I also conveys my deepest gratitude to the technical staff of IISER TVM, Mr. Adarsh, Mr. Nibith and Mr. Aneesh for helping me in completing some sophisticated experiments.

I also wants to thank my best friend since childhood days, Haripriya. B. Menon for her constant companionship and inspiration. I am also grateful to Dr. Bincy Babu and

Smitha Sajeev for their understanding, trust and motivation. They are in a way the reason for me to join for Ph.D.!

Above all, I also express my deep felt gratitude to my family, especially my parents, brother, Mithun, my aunts: Devika and Smitha and others as well as my friends for their constant motivation, love, and understanding during this period.

I am also obliged to the Dual-Degree program between the IISER TVM and University of Parma which enabled me to spend time in Italy.

Origin of DNA-Induced Circular Dichroism in a Minor-Groove Binder

Author: Nanna Holmgaard List, Jérémie Knoops, Jenifer Rubio-Magnieto, et al

Publication: Journal of the American Chemical Society

Publisher: American Chemical Society

Date: Oct 1, 2017

PERMISSION/LICENSE IS GRANTED FOR YOUR ORDER AT NO CHARGE

This type of permission/license, instead of the standard Terms & Conditions, is sent to you because no fee is being charged for your order. Please note the following:

- Permission is granted for your request in both print and electronic formats, and translations.
- If figures and/or tables were requested, they may be adapted or used in part.
- Please print this page for your records and send a copy of it to your publisher/graduate school.
- Appropriate credit for the requested material should be given as follows: "Reprinted (adapted) with permission from (COMPLETE REFERENCE CITATION). Copyright (YEAR) American Chemical Society." Insert appropriate information in place of the capitalized words.
- One-time permission is granted only for the use specified in your request. No additional uses are granted (such as derivative works or other editions). For any other uses, please submit a new request.

If credit is given to another source for the material you requested, permission must be obtained from that source.

BACK CLOSE WINDOW

Chirality Transfer in Coassembled Organogels Enabling Wide-Range Naked-Eye Enantiodifferentiation

Author: Bingbing Yue, Liyuan Yin, Wandong Zhao, et al
Publication: ACS Nano
Publisher: American Chemical Society
Date: Nov 1, 2019

PERMISSION/LICENSE IS GRANTED FOR YOUR ORDER AT NO CHARGE

This type of permission/license, instead of the standard Terms & Conditions, is sent to you because no fee is being charged for your order. Please note the following:

- Permission is granted for your request in both print and electronic formats, and translations.
- If figures and/or tables were requested, they may be adapted or used in part.
- Please print this page for your records and send a copy of it to your publisher/graduate school.
- Appropriate credit for the requested material should be given as follows: "Reprinted (adapted) with permission from (COMPLETE REFERENCE CITATION). Copyright (YEAR) American Chemical Society." Insert appropriate information in place of the capitalized words.
- One-time permission is granted only for the use specified in your request. No additional uses are granted (such as derivative works or other editions). For any other uses, please submit a new request.

If credit is given to another source for the material you requested, permission must be obtained from that source.

BACK CLOSE WINDOW

Photophysical and Theoretical Investigations of Oligo(p-phenyleneethynylene)s: Effect of Alkoxy Substitution and Alkyne−Aryl Bond Rotations

Author: P. V. James, P. K. Sudeep, C. H. Suresh, et al

Publication: The Journal of Physical Chemistry A

Publisher: American Chemical Society

Date: Apr 1, 2006

PERMISSION/LICENSE IS GRANTED FOR YOUR ORDER AT NO CHARGE

This type of permission/license, instead of the standard Terms & Conditions, is sent to you because no fee is being charged for your order. Please note the following:

- Permission is granted for your request in both print and electronic formats, and translations.
- If figures and/or tables were requested, they may be adapted or used in part.
- Please print this page for your records and send a copy of it to your publisher/graduate school.
- Appropriate credit for the requested material should be given as follows: "Reprinted (adapted) with permission from (COMPLETE REFERENCE CITATION). Copyright (YEAR) American Chemical Society." Insert appropriate information in place of the capitalized words.
- One-time permission is granted only for the use specified in your request. No additional uses are granted (such as derivative works or other editions). For any other uses, please submit a new request.

If credit is given to another source for the material you requested, permission must be obtained from that source.

BACK CLOSE WINDOW

Emergence of Chiroptical Properties in Molecular Assemblies of Phenyleneethynylenes: The Role of Quasi-degenerate Excitations

Author: Sabnam Kar, K. Swathi, Cristina Sissa, et al

Publication: Journal of Physical Chemistry Letters

Publisher: American Chemical Society

Date: Aug 1, 2018

PERMISSION/LICENSE IS GRANTED FOR YOUR ORDER AT NO CHARGE

This type of permission/license, instead of the standard Terms & Conditions, is sent to you because no fee is being charged for your order. Please note the following:

- Permission is granted for your request in both print and electronic formats, and translations.
- If figures and/or tables were requested, they may be adapted or used in part.
- Please print this page for your records and send a copy of it to your publisher/graduate school.
- Appropriate credit for the requested material should be given as follows: "Reprinted (adapted) with permission from (COMPLETE REFERENCE CITATION). Copyright (YEAR) American Chemical Society." Insert appropriate information in place of the capitalized words.
- One-time permission is granted only for the use specified in your request. No additional uses are granted (such as derivative works or other editions). For any other uses, please submit a new request.

BACK CLOSE WINDOW

SPRINGER NATURE LICENSE TERMS AND CONDITIONS

Dec 28, 2020

This Agreement between Mrs. Swathi Swathi ("You") and Springer Nature ("Springer Nature") consists of your license details and the terms and conditions provided by Springer Nature and Copyright Clearance Center.

License Number	4977721447831
License date	Dec 28, 2020
Licensed Content Publisher	Springer Nature
Licensed Content Publication	Nature Protocols
Licensed Content Title	Using circular dichroism spectra to estimate protein secondary structure
Licensed Content Author	Norma J Greenfield
Licensed Content Date	Jan 25, 2007
Type of Use	Thesis/Dissertation
Requestor type	non-commercial (non-profit)
Format	print and electronic
Portion	figures/tables/illustrations
Number of figures/tables/illustrations	1
High-res required	no
Will you be translating?	no
Circulation/distribution	1 - 29
Author of this Springer Nature content	no
Title	Emergence of Chirality in Phenyleneethynylene Based Molecular Assemblies: Experimental and Theoretical Study
Institution name	IISER Thiruvananthapuram
Expected presentation date	Dec 2020
Portions	Fig 1A
Requestor Location	Mrs. Swathi Swathi IISER Thiruvananthapuram Thiruvananthapuram, 695551 India Attn: Mrs. Swathi Swathi
Total	**0.00 USD**
Terms and Conditions	

Springer Nature Customer Service Centre GmbH
Terms and Conditions

This agreement sets out the terms and conditions of the licence (the **Licence**) between you and **Springer Nature Customer Service Centre GmbH** (the **Licensor**). By clicking 'accept' and completing the transaction for the material (**Licensed Material**), you also confirm your acceptance of these terms and conditions.

1. Grant of License

1. 1. The Licensor grants you a personal, non-exclusive, non-transferable, world-wide licence to reproduce the Licensed Material for the purpose specified in your order only. Licences are granted for the specific use requested in the order and for no other use, subject to the conditions below.

1. 2. The Licensor warrants that it has, to the best of its knowledge, the rights to license reuse of the Licensed Material. However, you should ensure that the material you are requesting is original to the Licensor and does not carry the copyright of another entity (as credited in the published version).

1. 3. If the credit line on any part of the material you have requested indicates that it was reprinted or adapted with permission from another source, then you should also seek permission from that source to reuse the material.

2. Scope of Licence

2. 1. You may only use the Licensed Content in the manner and to the extent permitted by these Ts&Cs and any applicable laws.

2. 2. A separate licence may be required for any additional use of the Licensed Material, e.g. where a licence has been purchased for print only use, separate permission must be obtained for electronic re-use. Similarly, a licence is only valid in the language selected and does not apply for editions in other languages unless additional translation rights have been granted separately in the licence. Any content owned by third parties are expressly excluded from the licence.

2. 3. Similarly, rights for additional components such as custom editions and derivatives require additional permission and may be subject to an additional fee. Please apply to Journalpermissions@springernature.com/bookpermissions@springernature.com for these rights.

2. 4. Where permission has been granted **free of charge** for material in print, permission may also be granted for any electronic version of that work, provided that the material is incidental to your work as a whole and that the electronic version is essentially equivalent to, or substitutes for, the print version.

2. 5. An alternative scope of licence may apply to signatories of the STM Permissions Guidelines, as amended from time to time.

3. Duration of Licence

3. 1. A licence for is valid from the date of purchase ('Licence Date') at the end of the relevant period in the below table:

Scope of Licence	Duration of Licence
Post on a website	12 months
Presentations	12 months
Books and journals	Lifetime of the edition in the language purchased

4. Acknowledgement

4. 1. The Licensor's permission must be acknowledged next to the Licenced Material in print. In electronic form, this acknowledgement must be visible at the same time as the figures/tables/illustrations or abstract, and must be hyperlinked to the journal/book's homepage. Our required acknowledgement format is in the Appendix below.

5. Restrictions on use

5. 1. Use of the Licensed Material may be permitted for incidental promotional use and minor editing privileges e.g. minor adaptations of single figures, changes of format, colour and/or style where the adaptation is credited as set out in Appendix 1 below. Any other changes including but not limited to, cropping, adapting, omitting material that affect the meaning, intention or moral rights of the author are strictly prohibited.

5. 2. You must not use any Licensed Material as part of any design or trademark.

5. 3. Licensed Material may be used in Open Access Publications (OAP) before publication by Springer Nature, but any Licensed Material must be removed from OAP sites prior to final publication.

6. Ownership of Rights

6. 1. Licensed Material remains the property of either Licensor or the relevant third party and any rights not explicitly granted herein are expressly reserved.

7. Warranty

IN NO EVENT SHALL LICENSOR BE LIABLE TO YOU OR ANY OTHER PARTY OR ANY OTHER PERSON OR FOR ANY SPECIAL, CONSEQUENTIAL, INCIDENTAL OR INDIRECT DAMAGES, HOWEVER CAUSED, ARISING OUT OF OR IN CONNECTION WITH THE DOWNLOADING, VIEWING OR USE OF THE MATERIALS REGARDLESS OF THE FORM OF ACTION, WHETHER FOR BREACH OF CONTRACT, BREACH OF WARRANTY, TORT, NEGLIGENCE, INFRINGEMENT OR OTHERWISE (INCLUDING, WITHOUT LIMITATION, DAMAGES BASED ON LOSS OF PROFITS, DATA, FILES, USE, BUSINESS OPPORTUNITY OR CLAIMS OF THIRD PARTIES), AND
WHETHER OR NOT THE PARTY HAS BEEN ADVISED OF THE POSSIBILITY OF SUCH DAMAGES. THIS LIMITATION SHALL APPLY NOTWITHSTANDING ANY FAILURE OF ESSENTIAL PURPOSE OF ANY LIMITED REMEDY PROVIDED HEREIN.

8. Limitations

8. 1. ***BOOKS ONLY:***Where **'reuse in a dissertation/thesis'** has been selected the following terms apply: Print rights of the final author's accepted manuscript (for clarity, NOT the published version) for up to 100 copies, electronic rights for use only on a personal website or institutional repository as defined by the Sherpa guideline (www.sherpa.ac.uk/romeo/).

8. 2. For content reuse requests that qualify for permission under the STM Permissions Guidelines, which may be updated from time to time, the STM Permissions Guidelines supersede the terms and conditions contained in this licence.

9. Termination and Cancellation

9. 1. Licences will expire after the period shown in Clause 3 (above).

9. 2. Licensee reserves the right to terminate the Licence in the event that payment is not received in full or if there has been a breach of this agreement by you.

Appendix 1 — Acknowledgements:

For Journal Content:
Reprinted by permission from [**the Licensor**]: [**Journal Publisher** (e.g. Nature/Springer/Palgrave)] [**JOURNAL NAME**] [**REFERENCE CITATION** (Article name, Author(s) Name), [**COPYRIGHT**] (year of publication)

For **Advance Online Publication papers:**
Reprinted by permission from [**the Licensor**]: [**Journal Publisher** (e.g. Nature/Springer/Palgrave)] [**JOURNAL NAME**] [**REFERENCE CITATION** (Article name, Author(s) Name), [**COPYRIGHT**] (year of publication), advance online publication, day month year (doi: 10.1038/sj.[JOURNAL ACRONYM].)

For Adaptations/Translations:
Adapted/Translated by permission from [**the Licensor**]: [**Journal Publisher** (e.g. Nature/Springer/Palgrave)] [**JOURNAL NAME**] [**REFERENCE CITATION** (Article name, Author(s) Name), [**COPYRIGHT**] (year of publication)

Note: For any republication from the British Journal of Cancer, the following credit line style applies:

Reprinted/adapted/translated by permission from [**the Licensor**]: on behalf of Cancer Research UK: : [**Journal Publisher** (e.g. Nature/Springer/Palgrave)] [**JOURNAL NAME**] [**REFERENCE CITATION** (Article name, Author(s) Name), [**COPYRIGHT]** (year of publication)

For **Advance Online Publication** papers:
Reprinted by permission from The [**the Licensor**]: on behalf of Cancer Research UK: [**Journal Publisher** (e.g. Nature/Springer/Palgrave)] [**JOURNAL NAME**] [**REFERENCE CITATION** (Article name, Author(s) Name), [**COPYRIGHT**] (year of publication), advance online publication, day month year (doi: 10.1038/sj.[JOURNAL ACRONYM])

For Book content:
Reprinted/adapted by permission from [**the Licensor**]: [**Book Publisher** (e.g. Palgrave Macmillan, Springer etc) [**Book Title**] by [**Book author**(s)] [**COPYRIGHT**] (year of publication)

Other Conditions:

Version 1.3

Questions? customercare@copyright.com or +1-855-239-3415 (toll free in the US) or +1-978-646-2777.